
Observing sea ice thickness variability in the Laptev Sea and the implications for the Transpolar Drift system

Dissertation submitted by

Hans JAKOB Belter

in partial fulfilment of the requirements
for the degree of

Doctor of Natural Sciences (Dr. rer. nat.)

to

Faculty 1
Physics and Electrical Engineering
University of Bremen

Colloquium: January 12, 2021



- Supervisor: Dr. Thomas Krumpen
[**Alfred Wegener Institute**, Helmholtz Centre for
Polar and Marine Research, Bremerhaven]
1. Reviewer: Prof. Dr. Christian Haas
[**Alfred Wegener Institute**, Helmholtz Centre for
Polar and Marine Research, Bremerhaven]
[**University of Bremen**]
2. Reviewer: Prof. Dr. Torsten Kanzow
[**Alfred Wegener Institute**, Helmholtz Centre for
Polar and Marine Research, Bremerhaven]
[**University of Bremen**]

This dissertation was written at the Sea Ice Physics section of the Alfred Wegener Institute, Helmholtz Centre for Polar and Marine Research, Bremerhaven.

Abstract

The Arctic sea ice cover is strongly connected to the global climate system and therefore not only subject to internal variability but also in a phase of significant change related to the ongoing increase in global mean surface temperatures. The most important parameters to monitor and describe sea ice are its areal extent, thickness, and motion. While reliable, long-term satellite measurements of sea ice concentration, which is used to derive the area covered by sea ice, exist since the late 1970s, sea ice thickness and motion data sets of comparable quality and length are currently not available.

The overarching goal of this dissertation is to contribute to the improvement of sea ice thickness observations and to understand and quantify the impact of ongoing sea ice thickness changes and variability in the most important regions of sea ice formation on the overall Arctic sea ice budget. To achieve that, the first study presented in this dissertation focuses on extending the knowledge about sea ice thickness variability in the Laptev Sea by developing a new method to derive sea ice thickness time series from moored sonars. It is shown that daily mean sea ice thickness time series can be inferred from basic, moored upward-looking Acoustic Doppler Current Profilers. This adaptive approach allows to revisit data sets from past mooring deployments in the Laptev Sea and exploit them to extend the available sea ice thickness records and close observational gaps in a region that, due to its limited accessibility, is vastly under-sampled.

These new data sets are the basis for the validation of multiple satellite sea ice thickness products, including the longest available one introduced by the European Space Agency, which provides Arctic-wide sea ice thickness since 2002. It is shown that in the first-year ice dominated Laptev Sea the investigated satellite products provide the most frequently occurring (modal) rather than the mean sea ice thickness. This important discovery allows for a better interpretation of the available satellite records, especially for the investigation of sea ice volume transports, and underlines their deficiencies in representing dynamically deformed sea ice.

Based on the knowledge gained in the Laptev Sea, the final study presented in this dissertation follows the Arctic sea ice life cycle from the regions of ice formation along the Transpolar Drift towards Fram Strait and analyses whether sea ice thickness anomalies induced in the source regions of Arctic sea ice propagate to the central Arctic Ocean and beyond. More specifically, it is investigated which particular processes are potentially responsible for the induced anomalies in the source regions and whether their signals persist until the end of the Transpolar Drift. In the absence of a single-source Arctic-wide, high temporal and spatial resolution sea ice thickness data product, this final part promotes the combination of different techniques and tools for the investigation of this complex Arctic climate parameter. At the center of the investigation is an extended long-term electromagnetic induction sounding-based sea ice thickness time series, which shows a general thinning and decreasing age of sea ice at the end of the Transpolar Drift between 2001 and 2020. Due to its length, this unique time series also permits to put ice thickness measurements conducted during the Multidisciplinary drifting Observatory for the Study of Arctic Climate (MOSAiC) expedition into the historical context. Lagrangian ice tracking and modelling of thermodynamic sea ice growth along the pathways of Arctic

sea ice reveal a potential preconditioning effect of observed increases in upward ocean heat fluxes in the eastern Arctic, termed Atlantification, that decelerates sea ice growth.

The presented efforts are an important contribution to the better understanding of Arctic sea ice thickness variability and change and can be seen as starting points for more targeted analyses of the driving mechanisms behind them. In addition, the acquisition, validation, and extension of sea ice thickness observations provide the basis for more detailed sea ice modelling, which will improve not only the monitoring but also the prediction of Arctic sea ice thickness changes in the future.

Contents

Abstract	I
Nomenclature	V
Abbreviations	V
Symbols	VII
1 Introduction	1
1.1 Arctic sea ice and its role in the Earth’s climate system	1
1.2 Objectives and outline of this dissertation	4
2 Sea ice – Theoretical background	7
2.1 Sea ice thickness distribution	7
2.1.1 Thermodynamic components	7
2.1.2 Dynamic components	10
2.1.3 Sea ice thickness distribution in the Arctic	11
2.2 Key measurement techniques	13
2.2.1 Upward-Looking Sonar	14
2.2.2 Electromagnetic induction sounding	16
2.2.3 Satellite remote sensing	18
2.2.4 Conclusion	21
3 Sea ice draft from upward-looking Acoustic Doppler Current Profilers: an adaptive approach, validated by Upward-Looking Sonar data	23
3.1 Introduction	24
3.2 Data and Methods	26
3.2.1 Data processing	27
3.3 Results	33
3.4 Discussion	36
3.4.1 Open water detection	37
3.4.2 Tilt and beamwidth bias	37
3.4.3 Sound speed correction	38
3.4.4 Uncertainty estimates	39
3.4.5 ULS versus ADCP-derived ice draft	41
3.5 Conclusions	42
4 Satellite-based sea ice thickness changes in the Laptev Sea from 2002 to 2017: comparison to mooring observations	45
4.1 Introduction	46
4.2 Data and methods	49
4.2.1 Sonar-based ice draft measurements	49
4.2.2 Satellite data	50
4.2.3 Data limitations	52
4.3 Results	53

4.3.1	ESA CCI-2 Laptev Sea SIT	53
4.3.2	Validation of CCI-2 products	54
4.4	Discussion	59
4.4.1	Comparability of satellite and sonar measurements	59
4.4.2	Stability of the CCI-2 SIT CDR	60
4.4.3	Taymyr 2013/2014 case	61
4.5	Conclusion	63
5	From the Laptev Sea to the Fram Strait – Life cycle of Arctic sea ice	67
6	Interannual variability in Transpolar Drift ice thickness and potential impact of Atlantification	71
6.1	Introduction	72
6.2	Data and methods	75
6.2.1	EM sea ice thickness measurements	75
6.2.2	Sea ice pathways and source regions	76
6.2.3	Thermodynamic sea ice model	77
6.2.4	Shipborne sea ice thickness observations	78
6.3	Results and Discussion	78
6.3.1	Processes driving interannual SIT variability between 2001 and 2018	78
6.3.2	Possible impact of Atlantification on SIT in 2016	81
6.3.3	Interpretation of sea ice surveys from the MOSAiC year	85
6.3.4	Comparison to Russian shipborne SIT observations	86
6.4	Conclusion	88
7	Conclusion and outlook	93
	Appendix	101
	List of Figures	103
	List of Tables	105
	References	107
	Acknowledgements	125
	Curriculum vitae	127
	Statement/Erklärung	131

Nomenclature

Abbreviations

AARI	Arctic and Antarctic Research Institute
ADCP	Acoustic Doppler Current Profiler
AEM	Airborne electromagnetic induction instrument
AOI	Area of interest
ARTIST	Arctic radiation and turbulence interaction study
ASSIST	Arctic Shipborne Sea Ice Standardization Tool
AW	Atlantic Water
AWI	Alfred Wegener Institute, Helmholtz Centre for Polar and Marine Research
BMBF	Bundesministerium für Bildung und Forschung
BT	Bottom track
CCI-2	Climate Change Initiative Phase 2
CDR	Climate data record
CERSAT	Center for Satellite Exploitation and Research
CO	MOSAiC Central Observatory
CRISTAL	Copernicus Polar Ice and Snow Topography Altimeter
CS2	CryoSat-2
CS2SMOS	Merged weekly CS2 and SMOS sea ice thickness data record
DN	MOSAiC Distributed Network
DNR	Combined CO and DN regions (wider area around the MOSAiC floe)
ECMWF	European Centre for Medium-Range Weather Forecasts
EASE	Equal Area Scalable Earth
EM	Electromagnetic induction
ENVISAT	Environmental Satellite
ERA	ECMWF Re-Analysis
ESA	European Space Agency
FDD	Freezing degree days
FYI	First-year ice

GEM	Ground-based electromagnetic induction instrument
IBCAO	International Bathymetric Chart of the Arctic Ocean
ICESat-2	Ice, Cloud, and land Elevation Satellite 2
IPCC	Intergovernmental Panel for Climate Change
IPS	Ice Profiling Sonar
MOSAiC	Multidisciplinary drifting Observatory for the Study of Arctic Climate
MYI	Multi-year ice
NAOSIM	North Atlantic Arctic Ocean Sea Ice Model
NSIDC	National Snow and Ice Data Center
OSISAF	Ocean and Sea Ice Satellite Application Facility
PDF	Probability Density Function
QUARCCS	Quantifying Rapid Climate Change in the Arctic: regional feedbacks and large-scale impacts
RFBR	Russian Foundation for Basic Research
RMSE	Root Mean Square Error
RV	Research vessel
SIC	Sea ice concentration
SIT	Sea ice thickness
SMOS	Soil Moisture and Ocean Salinity
SSM/I	Special Sensor Microwave/Imager
STK	Shipborne television complex
SYI	Second-year ice
ULS	Upward-Looking Sonar
VAL	Sonar-derived satellite validation data

Symbols

β	Sound speed correction factor
D	Vertical spacing between ULS pressure and range sensor [m]
d	Sea ice draft [m]
η	Instrument depth [m]
F	Ocean heat flux [W m^{-2}]
f	Thermodynamic ice growth/decay function
g	Local gravitational acceleration [m s^{-2}]
$\frac{\Delta H}{\Delta t}$	Ice growth rate [m s^{-1}]
H_{ice}	Sea ice thickness [m]
H_{snow}	Snow thickness [m]
h_i	Distance EM device to air-snow/ice interface [m]
h_w	Distance EM device to ice-water interface [m]
i	Number of ADCP beams
ITD	Ice thickness distribution
κ_{ice}	Thermal conductivity of ice [$2 \text{ W m}^{-1}\text{K}^{-1}$]
κ_{snow}	Thermal conductivity of snow [$0.33 \text{ W m}^{-1}\text{K}^{-1}$]
L	Latent heat of fusion [$3 \cdot 10^8 \text{ J m}^{-3}$]
p_{uls}	Pressure at ULS [hPa]
p_{atm}	Pressure at sea surface [hPa]
Φ	Redistribution function
ϕ	ADCP instrument tilt [$^\circ$]
ρ	Density of seawater [kg m^{-3}]
r	Range [m]
σ_d	Uncertainty of hourly mean sea ice draft from ADCP [m]
$\sigma_{r\phi}$	Uncertainty of tilt-corrected ADCP range [m]
σ_z	Uncertainty of ADCP-derived instrument depth [m]
T_0	Temperature at the ice-water interface [-1.86°C]
T_{surf}	Sea surface temperature [$^\circ\text{C}$]

t	Time
θ	ULS instrument tilt [°]
\vec{v}	Ice drift velocity
x	Location
z	Derived quasi-depth of ADCP [m]

1 Introduction

1.1 Arctic sea ice and its role in the Earth's climate system

The Arctic is one of the key regions of interest in the Earth's complex and variable climate system. Global changes in climate-relevant parameters, like the increase in global mean surface air temperature, are amplified in the Arctic (Chapman and Walsh, 1993). In the recent decades, the Arctic mean surface air temperature anomaly has been nearly two to three times higher than the global mean (Hansen et al., 2010; Screen and Simmonds, 2010; Pithan and Mauritsen, 2014), which continues to have vast implications for one of the Arctic's key components – sea ice.

Sea ice forms when seawater freezes. Due to its low density compared to seawater, sea ice floats at the interface between ocean and atmosphere and, together with the above snow cover, forms an insulating layer for the exchange of heat, mass, and momentum between the two climate components (McPhee, 2017). Due to the reflective surfaces of sea ice and snow, sea ice is an important component of the surface energy budget. Therefore, changes in the composition of sea ice and its areal extent can have major implications for the exchange of energy at the ocean surface. One example is the ice-albedo feedback first discussed by Budyko (1969), which describes a positive feedback mechanism induced by changes in the fraction of solar radiation reflected by the ice-covered ocean surface, known as albedo. Simplified, a reduction of sea ice area exposes more of the comparably dark ocean surface to the atmosphere. The albedo of the surface reduces and more solar radiation is absorbed, which subsequently leads to more warming of the ocean surface layer. This induced warming leads to sea ice melt, further reduction of the area covered by sea ice and even more energy-uptake by the ocean (Hall, 2004).

With the upper part of the ice cover protruding above the water level (ice freeboard) and the lower part being submerged into the water (ice draft), sea ice is exposed to influences from, but also interacts with, the atmosphere above and the ocean below. Sea ice impacts surface ocean properties and stratification through freshwater release during melt and brine rejection in the upper ocean layer during sea ice formation. The changes in upper ocean density resulting from sea ice formation and melt contribute to the thermohaline ocean circulation, which is an integral part of the global ocean circulation (Rahmstorf, 2003). These few processes are single examples of the much more complex effects and interactions sea ice has on and with the Arctic climate system and show why it is considered a valuable indicator for variability of the Arctic climate but also ongoing global climate change.

One of the most common parameters used to describe sea ice is its areal coverage. Based on sea ice concentration data, regions covered by ice are described using sea ice area and extent. While sea ice area is a measure for the actual area covered by ice (km^2), sea ice extent refers to gridded fields of data and whether single grid cells are considered ice-covered or not. Commonly, grid cells with sea ice concentrations of at least 15% are

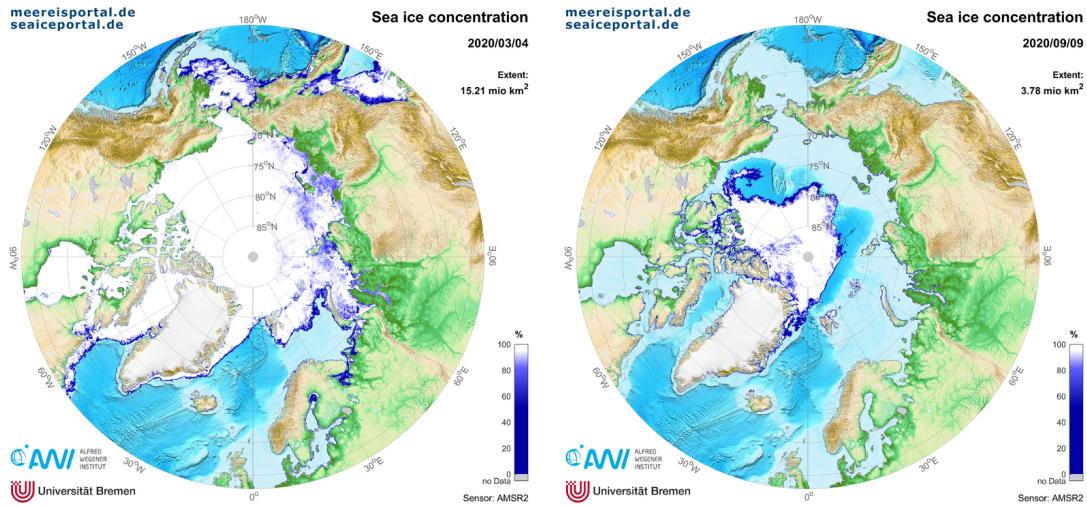


Figure 1.1: AMSR-2 sea ice concentration data (Spreen et al., 2008) from the days of maximum extent on March 4, 2020 (left) and minimum extent on September 9, 2020 (right) obtained from www.seaiceportal.de (accessed October 2020).

considered ice-covered and the entire grid cell contributes to the total sea ice extent. Therefore, the value of sea ice extent is usually higher than the area value.

Since the year 2000, Arctic sea ice covers between 14 and 16×10^6 km² at its maximum extent in winter (Comiso et al., 2017) including the whole central Arctic Ocean and most parts of the adjacent seas (example for March, 2020 in Fig. 1.1 (left)). During the summer melt season, the ice edge retreats to the central Arctic Ocean and sea ice covers only between 3.5 and 8×10^6 km² (Comiso et al., 2017) when it reaches its minimum extent in September (example for September, 2020 in Fig. 1.1 (right)). The region covered by sea ice during the extent minimum in summer marks the permanent ice zone. It consists of sea ice that has survived at least one melt season and is therefore considered multi-year ice (MYI). The seasonal ice zone is defined as the area of ocean between the permanent ice zone and the boundary of the sea ice extent maximum. It is partly covered by ice during the year and dominated by first-year ice (FYI, ice that has not survived a full melt season).

Solely observing sea ice extent only allows for a differentiation between ice covered and open water areas. Combining observations of sea ice extent, thickness, and motion are required to describe overall changes of the Arctic sea ice mass balance. The consideration of the temporal development of the most important sea ice parameters, extent and thickness, indicates a connection to observed trends in global surface air temperatures. The overall area covered by sea ice is reducing in all months (Cavalieri and Parkinson, 2012; Comiso et al., 2017; Stroeve and Notz, 2018), while sea ice in general is thinning (Kwok, 2018). Due to the impact of sea ice on the surface energy and mass budgets, continuous decline in extent and thinning will increase the direct interaction between atmosphere and ocean with major implications for the entire Arctic ecosystem.

The predicted total summer sea ice loss is projected to change not only the Arctic, but also the global climate system severely (Stroeve et al., 2012; Overland and Wang, 2013; Overland et al., 2019). According to the Intergovernmental Panel for Climate Change (IPCC), these climatic changes will also have extensive socioeconomic impacts in the Arctic (Larsen et al., 2014). Besides new possibilities for economic diversification, shipping, forestry, and tourism, which are considered positive impacts, the loss in sea ice cover and permafrost may cause damage to all kinds of infrastructure used and built in the Arctic and impact the livelihoods of indigenous communities (Larsen et al., 2014).

In the context of global climate change, the discussions about observed trends in sea ice extent and thickness mostly refer to changes on an Arctic-wide scale. However, a more detailed analysis of the Arctic sea ice cover reveals that strong regional and seasonal variability exists (Haas, 2017). Therefore, observations of sea ice have to meet the expectation of the highest possible resolution on both temporal and spatial scales to monitor this variability. While satellite observations provide reliable, year-round, long-term sea ice extent and concentration records, sea ice thickness records of comparable length and quality are not available to this date. Satellite sea ice thickness records cover a much shorter period than sea ice extent and concentration records, are available only during the winter season, and have mostly been validated in regions dominated by MYI. Considering the trend towards thinner and younger sea ice dominating the Arctic (Kwok, 2018), it is eminently important that satellite sea ice thickness data sets are continued, extended to the summer season, and validated for FYI-dominated regions.

One of these FYI-dominated regions is found in the eastern Arctic and especially in the Laptev Sea (Reimnitz et al., 1994). The Laptev Sea is considered one of the most important source regions of Arctic sea ice (Rigor et al., 2002; Hansen et al., 2013). The prevailing offshore-directed winds transport newly formed ice away from the shelf seas, exposing vast areas of open water to the cold atmosphere, which leads to more ice formation in the shallow waters (Timokhov, 1994; Krumpfen et al., 2013). This makes the Laptev Sea a region of major interest for the long-term development of Arctic sea ice. The ice transported northward from the Siberian coast is incorporated into the Transpolar Drift system, which acts as a conveyor belt moving ice across the central Arctic Ocean towards the Fram Strait (Rigor et al., 2002). This prevailing ice drift regime across the Arctic Ocean was already observed and used by Fridtjof Nansen during his Fram drift expedition from 1893 to 1896 (Nansen, 1897). At the end of the Transpolar Drift, most of the ice exits the Arctic Ocean through the Fram Strait and melts as it progresses southward. The Fram Strait therefore poses another area of major interest for sea ice thickness observations in the Arctic. Ice reaching the Fram Strait and its vicinity carries integrated signals of the mechanisms acting on the ice along its journey through the Arctic Ocean (Hansen et al., 2013) and analysing and understanding its variability improves the understanding of the complex interactions between the ice and the atmosphere as well as the ocean.

In light of the ongoing reduction of sea ice extent and thickness, investigating changes in these regions of interest may give insight into the reasons for the observed Arctic-wide change. Due to its location and comparably good accessibility, the Fram Strait has been the destination for numerous research expeditions and multiple long-term sea

ice thickness data sets exist (Hansen et al., 2013; Renner et al., 2014; Krumpen et al., 2016). Unfortunately, observations of sea ice thickness in the Laptev Sea are sparse and continuous long-term records used for the analysis of interannual variability and satellite data validation are non-existent. However, influences altering the thickness of sea ice are far-reaching on both temporal and spatial scales and in order to fully comprehend their impact, it is important to follow the full life cycle of sea ice, from ice formation until its disintegration and melt. Due to the limitations of sea ice thickness measurement techniques and temporary inaccessibility of regions of major interest, observing sea ice step by step along its pathway through the Arctic remains a challenge. It is therefore vitally important to combine different observational methods and additional tools to monitor and understand the variability of Arctic sea ice as accurately and detailed as possible.

1.2 Objectives and outline of this dissertation

The overarching goal of this dissertation is to determine the impact ongoing changes and variations in sea ice thickness in the regions of sea ice formation have on the overall Arctic sea ice budget. To achieve that, it is necessary not only to observe sea ice thickness reliably and with high temporal and spatial resolution but also in the regions mostly affected by these changes. This dissertation supports the development of continuous, long-term, and large-scale sea ice thickness data records through three main foci: the development and adaptation of known measurements principles to generate new sea ice thickness data sets; the application of these data sets to validate existing sea ice thickness records from satellites; and the analysis of available and newly acquired data records to improve the understanding of observed ice thickness variability in regions representative for different stages of sea ice development.

Chapter 2 gives a general summary of sea ice in the Arctic and the mechanisms that lead to changes in its thickness. It also introduces different methods of measuring sea ice thickness, their advantages and disadvantages, and focuses on the three methods that are essential for the studies presented in this dissertation.

This dissertation includes three separate studies that were conducted to fulfil three main objectives. The **first objective** of the presented dissertation is:

To develop a new method to derive sea ice thickness data sets that extend back in time long enough to be used for the validation satellite sea ice thickness products and to allow the investigation of interannual sea ice thickness variability in the FYI-dominated Laptev Sea.

Chapter 3 presents a study describing the development and validation of an adaptive method to extend mooring-based observations of sea ice draft in the Laptev Sea. Initially, measurements from two moored Upward-Looking Sonars (ULSs), specifically designed for measuring sea ice, are processed to provide sea ice draft time series from 2013 to 2015. Due to the temporal limitations of these time series, different approaches are analysed to extend the available two-year data set. Multiple studies have shown that upward-looking Acoustic Doppler Current Profilers (ADCPs), using sonar-based methods similar to ULSs to derive ocean currents and sea ice drift velocities, can also be used to derive sea ice draft (Shcherbina et al., 2005; Banks et al., 2006; Bjoerk et al., 2008; Hyatt et al., 2008). These

previous approaches relied on integrated or external pressure sensors to derive instrument depth of the ADCP, which is one of the most important components of the processing chain from sonar-based measurements of range (distance from the instrument to the ice-water interface) to sea ice draft values. The approach described in Chapter 3 shows that instrument depth can be inferred from default measurements of ADCPs operated in bottom track mode. Based on this approach, daily mean sea ice draft time series can be generated from ADCPs even when they are not equipped with a reliable pressure sensor.

While ULSs have only been deployed from 2013 to 2015, ADCPs were deployed over much longer time periods in the Laptev Sea. Following the method developed in Chapter 3, old ADCP data archives from the Laptev Sea are investigated to exploit data sets potentially useful for the derivation of sea ice draft. Building upon this newly acquired data archive, the **second objective** is:

To validate satellite sea ice thickness data in the Laptev Sea. Based on the reliability of these satellite records, the goal is to investigate interannual ice thickness variability in the Laptev Sea.

Chapter 4 presents the comparison of sea ice draft time series derived from ADCP and ULS measurements from moorings distributed over the entire Laptev Sea with different satellite sea ice thickness products based on the European Space Agency's (ESA) Climate Change Initiative Phase 2 (CCI-2) sea ice thickness climate data record (CDR). The acquired sonar-based validation data record provides data from 2003 to 2016 and is compared to gridded and orbit ESA CCI-2 sea ice thickness data and the merged CryoSat-2 (CS2) and Soil Moisture and Ocean Salinity (SMOS) satellite data from 2002 to 2017. Following this validation, the newly acquired insights are used to interpret satellite-derived sea ice thickness changes in the Laptev Sea.

Chapter 5 gives a short summary of the results and most important insights from the data investigation and validation of Chapters 3 and 4. It also shifts the focus from the Laptev Sea to the Fram Strait, where sea ice thickness observations were conducted using electromagnetic induction (EM) sounding to investigate sea ice thickness variability at the end of the Transpolar Drift. The analysis of this additional long-term data set, based on a different measurement technique, is carried out to fulfil the **third objective** of this dissertation, which is:

To investigate the preconditioning effect of sea ice thickness variability in the source regions of Arctic sea ice on Arctic-wide ice thickness and especially on the thickness of sea ice exiting the Arctic through the Fram Strait.

Chapter 6 presents the study on pathways of Arctic sea ice. Sea ice thickness variability is investigated at the main exit gate of Arctic sea ice – the Fram Strait. Lagrangian tracking reveals that about 65% of sea ice reaching Fram Strait originates from the Laptev Sea. The study further investigates the reasons for the observed interannual variability and connects observed thinning north of the Fram Strait to oceanic influences exposed to the ice already in the Laptev Sea. Connecting the main region of Arctic sea ice formation to sea ice shortly before it leaves the Arctic Ocean and melts, helps reconstruct the life cycle of Arctic sea ice, the mechanisms forming and changing it, and supports the prediction of

future changes in a global climate system that is subject to a continuous transformation process.

The concluding Chapter 7 summarises the key findings of this dissertation and provides an outlook towards future scientific studies that can build on and complement the presented work.

Remark

Chapters 3, 4 and 6 present published and submitted papers which were compiled with contributions from the mentioned co-authors. All three papers are included in an unaltered form which leads to minor variations in style, language, tenses, and abbreviations throughout this dissertation. Summaries of the contributions of the respective authors are given at the beginning of each of these chapters.

2 Sea ice – Theoretical background

The simplified description of the ice-albedo feedback (Chapter 1) shows the relevance of ice-covered and ice-free areas for the surface energy budget in the Arctic Ocean (Fig. 2.1). However, especially when it comes to the albedo of the ice surface, it is too simplistic to only consider the existence or absence of ice. Snow-covered ice provides the highest albedo (0.8 to 0.9), while snow-free ice is slightly darker (0.5 to 0.7), and freshly formed young ice is almost transparent, which results in a surface albedo close to that of the dark ocean (Curry et al., 1995). In this context, sea ice thickness is relevant as well. Thinner ice allows a larger fraction of solar energy to be absorbed by the ice or penetrate through to the underlying ocean (Nicolaus et al., 2012; Katlein et al., 2019). To predict and monitor what this increased energy input to the ocean means for primary productivity (Assmy et al., 2017), ocean heat deposition (Perovich et al., 2007; Pinker et al., 2014), and future development of sea ice in general, it is vital to observe sea ice thickness reliably. To comprehend the role and distribution of sea ice thickness in the Arctic, it is essential to understand how sea ice forms and how its thickness changes.

This chapter summarises how sea ice grows, evaluates processes changing its thickness, and describes its general distribution. It also provides information about different ice thickness measurement techniques, what they measure, and how to interpret and utilise the available data to investigate past, present, and future changes and variability in Arctic sea ice thickness.

2.1 Sea ice thickness distribution

The temporal development of sea ice thickness distribution, $\partial ITD/\partial t$, is governed by three processes that are given by (Thorndike et al., 1975):

$$\frac{\partial ITD}{\partial t} = - \underbrace{\frac{\partial}{\partial H_{ice}}(f \cdot ITD)}_I - \underbrace{div(\vec{v} \cdot ITD)}_{II} + \underbrace{\Phi}_{III}, \quad (2.1)$$

with f being the function for thermodynamic increase/decrease in ice thickness (H_{ice}), which depends on the location (x) and the time (t), represented in term I . Combining for the dynamic component of sea ice growth are the divergence in the ice drift velocity ($\vec{v}(x, t)$), which describes the advection of sea ice (term II), and the redistribution function (Φ), which describes mechanical deformation (term III).

2.1.1 Thermodynamic components

Seawater freezes at approximately -1.9°C . The cold atmosphere cools the ocean surface, which gradually increases the density of the surface waters. As seawater approaches its freezing point, it penetrates downwards in the water column and is replaced by less dense, warmer water that is subsequently cooled by the atmosphere. This vertical mixing

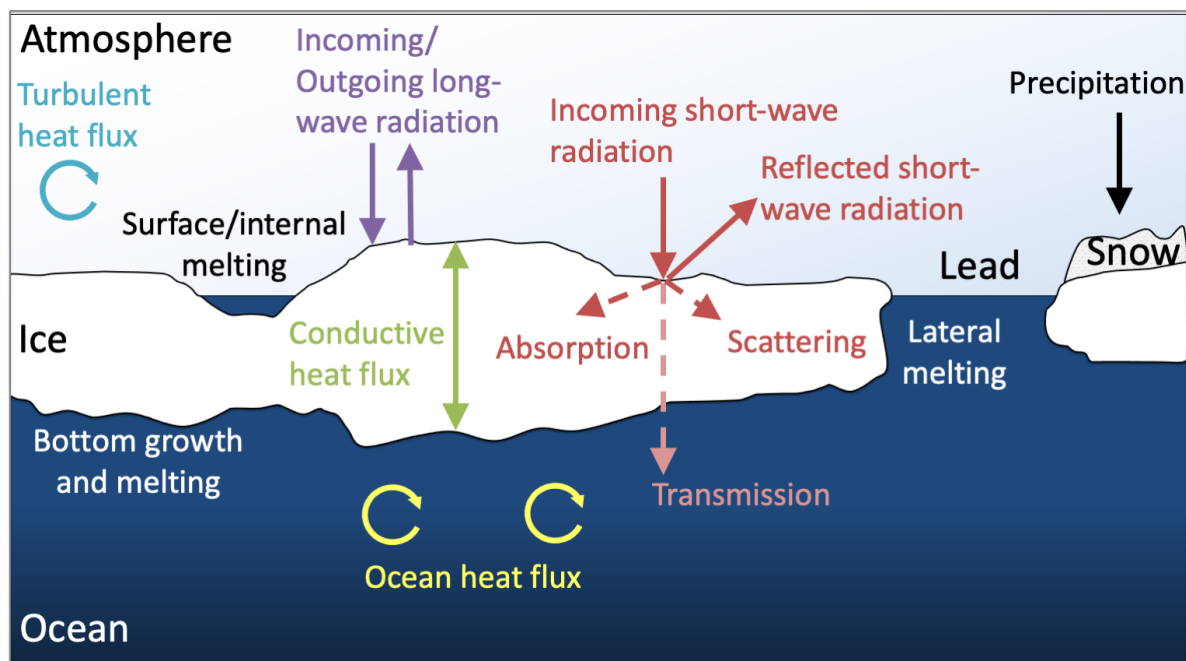


Figure 2.1: Schematic showing relevant mechanisms of sea ice thermodynamics (adapted from Perovich and Richter-Menge (2009); Leppäranta (2011)). Sea ice grows and melts forced by heat exchange with the atmosphere and the ocean and by radiation. Growth and melt occur at the upper and lower boundaries and in the ice interior (Leppäranta, 2011).

reaches down to the halocline, which is the boundary layer between lower density surface and warm and saline deeper waters (Cottier et al., 2017). Depending on the atmospheric conditions, sea ice begins to grow as a thin layer in calm conditions, or as loose ice crystals (frazil ice) moving in the turbulent surface layer in windy conditions. Once the surface layer calms, frazil ice crystals consolidate to a solid layer. As sea ice continues to grow, congelation ice crystals form at the ice-water interface (Leppäranta, 2011).

During the ice formation process, sea salt ions are rejected from the crystals and form brine at the ice-water interface (Petrich and Eicken, 2017). When ice growth continues, brine pockets can become enclosed into the newly formed ice, significantly altering the physical properties of the ice cover (Maykut and Untersteiner, 1971). Additional ice impurities influencing the physical properties of sea ice include incorporations of gases, organic matter, sediments, and pollutants (Rigor and Conoly, 1997; Dethleff et al., 2000; Damm et al., 2018).

The growth rate of sea ice is determined by the energy balances at the sea ice bottom and surface (Fig. 2.1), which are coupled by conductive heat fluxes through the snow and ice layers (Petrich and Eicken, 2017). Sea ice forms an insulating layer at the ocean surface, limiting the exchange of heat between ocean and atmosphere. In general, sea ice growth at the bottom requires the surface air temperature to be below the freezing point of seawater and the conductive heat flux from the warmer ocean through the ice and to the atmosphere to be larger than the ocean heat input from below (Maykut and

Untersteiner, 1971; Petrich and Eicken, 2017). As sea ice grows thicker, the insulating effect of the ice cover increases. It takes longer to transport heat from the ocean to the atmosphere, which is required to maintain the seawater freezing point and form ice at the ice-water interface (Leppäranta, 2011). Hence, the rate of growth at the ice bottom is not only dependent on the physical properties of the inhomogeneous ice cover but also on its thickness.

The accumulation of snow on sea ice drastically increases the insulating effect of the ice cover. The thermal conductivity of snow is approximately one order of magnitude lower than that of sea ice and although snow only accounts for a small fraction of the total mass of sea ice, it further reduces its growth rate (Petrich and Eicken, 2017). Snow can also contribute to sea ice growth at the ice surface. Different types of ice form at the surface when snow is infiltrated by liquid water from precipitation, surface melt, or flooding and refreezes. Since flooding is the most common mechanism to form ice from snow, thick snow covers are required to submerge the ice into the ocean. Snow covers sufficiently thick to initiate this process are uncommon in the central Arctic and mostly occur in low-latitude seas on the northern hemisphere and in the Antarctic (Leppäranta, 2011). However, recent studies have found that the impact of snow-ice on sea ice growth in the central Arctic may be increasing as more frequent storms bring heavy precipitation to the thinning central Arctic ice cover (Merkouriadi et al., 2017; Provost et al., 2017).

Ultimately, thermodynamic sea ice growth is limited. Based on the thickness and the composition of the snow and ice cover, the conductive heat fluxes from the ocean to the

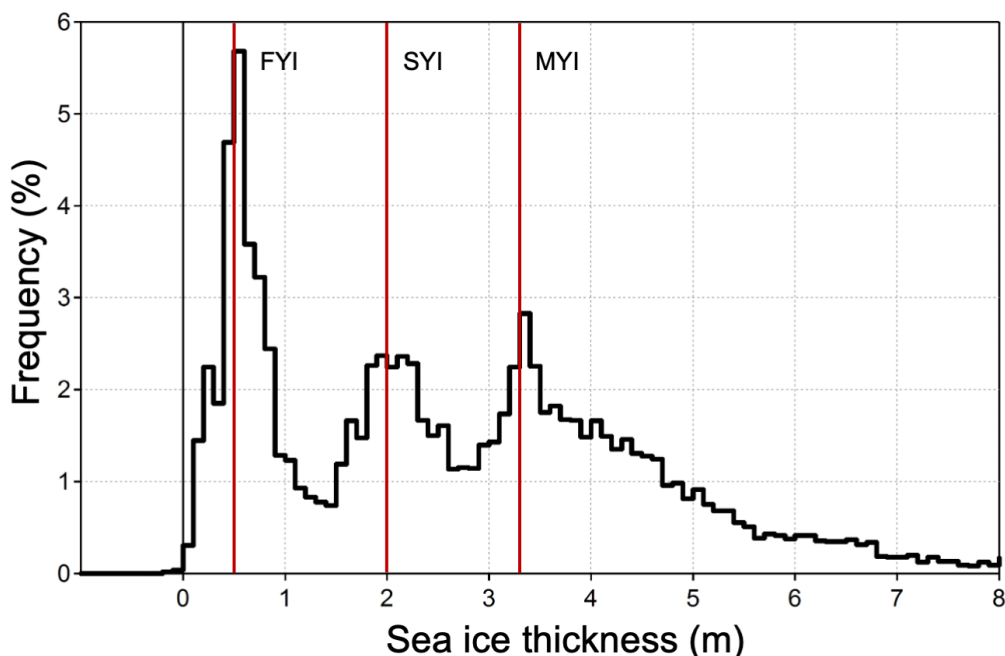


Figure 2.2: Example of sea ice thickness distribution measured in the Beaufort Sea in April 2008 (Hendricks, 2009). The three apparent modes indicate thicknesses of thermodynamically grown sea ice: first-year ice (FYI, 0.5 m), second-year ice (SYI, approximately 2 m) and multi-year ice (MYI, 3.3 m).

atmosphere are reduced, which slows the thermodynamic ice growth until an equilibrium thickness is reached (Maykut and Untersteiner, 1971; Leppäranta, 2011). Theoretical estimates by Maykut and Untersteiner (1971) indicate that the equilibrium thickness of undeformed MYI can reach values between 3 and 4 m.

The second thermodynamic influence on ice thickness is melt, which, in general, occurs due to four different processes (Fig. 2.1). Solar and atmospheric heat fluxes lead to melting of snow and ice at the surface. In cases where the solar radiation is absorbed in the ice, it causes internal melting processes. When ocean heat fluxes exceed the conductive fluxes from the ocean to the atmosphere, sea ice starts to melt at the ice-water interface (bottom melt) or laterally at the ice edges in leads (Leppäranta, 2011).

Figure 2.2 shows an example of the sea ice thickness distribution measured in the Beaufort Sea in April 2008 (Hendricks, 2009). The distribution displays the frequency of occurrence of different ice thickness values. The most frequently occurring thickness value (mode) is considered to be a measure for thermodynamically grown ice (Rabenstein et al., 2010; Haas, 2017). Three distinct modes are visible, indicating thermodynamically grown FYI (0.5 m), second-year ice (SYI, ice that has survived one summer melt season, approximately 2 m), and MYI (3.3 m). However, the example also shows the occurrence of ice thickness values considerably larger than the theoretical equilibrium thickness, which are the result of dynamic, and more specifically ice deformation processes.

2.1.2 Dynamic components

Dynamic effects on sea ice thickness can be divided into two main mechanisms (Fig. 2.3). While divergence and advection are described by term II in Equation 2.1, the mechanical deformation of sea ice following convergence is given by the redistribution function, Φ (term III).

The divergence of the ice cover is the result of the prevailing wind fields and, to a lesser degree, ocean currents (Sprenn et al., 2011). As long as ice motion is not prevented by obstacles or coastlines, sea ice drifts at approximately 1 to 2% of the mean wind speed (Sprenn et al., 2011). However, multiple studies have shown that Arctic sea ice drift velocities are increasing (Sprenn et al., 2011; Itkin and Krumpfen, 2017), which is attributed to the general thinning of Arctic sea ice (Rampal et al., 2009), but also to the positive trend in wind stress caused by a shift in storm tracks (Hakkinen et al., 2008). Divergence in the ice cover generates small openings, leads, and polynyas. Open water is exposed to the cold atmosphere and new ice forms. The removal of sea ice of a certain thickness by divergence results in zero thickness or a thin ice signal in the overall ice distribution (Haas, 2017). Regions where the continuous generation of open water areas leads to most of the Arctic's sea ice formation are found on the shallow shelves of the Russian Arctic and specifically in the Laptev and East Siberian Sea. The prevailing wind fields transport newly formed ice northward and away from the coast, which opens large areas of open water where new ice can be formed (Timokhov, 1994; Krumpfen et al., 2013).

The redistribution function, Φ , describes the deformation of sea ice in response to convergence (negative divergence) in the sea ice cover. Especially thin ice is susceptible to being transformed into thicker ice by deformation (Haas, 2017). Depending on the initial thickness and physical properties of the ice that is deformed, fracture mechanics,

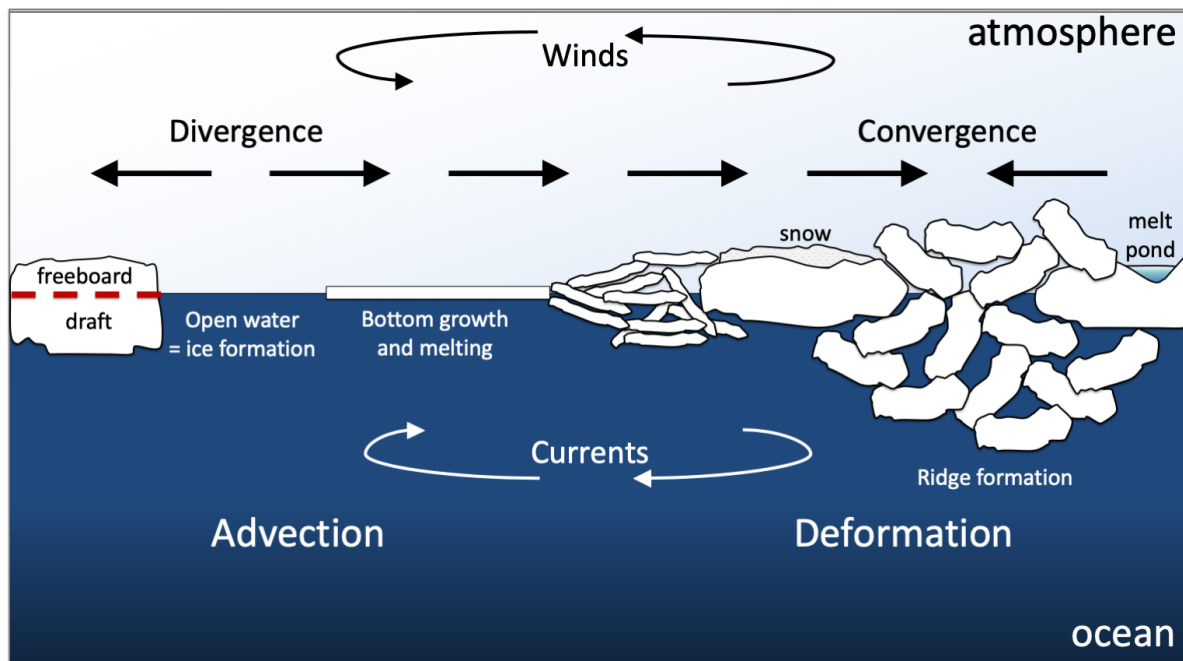


Figure 2.3: Schematic of the dynamic influences on the development of the sea ice thickness distribution (adapted from Haas and Druckenmiller, 2009). Sea ice thickness varies considerably and depends on various atmospheric and oceanic factors including wind, ocean currents, and sea and air surface temperatures (Meier and Haas, 2012).

the snow and ice interfaces, the energy of the deformation, and the scales on which these processes occur, sea ice deformation generates a wide range of thicknesses (Haas, 2017). Mechanical changes in ice thickness are asymmetric, which means ice thickness increases mechanically but decreases only thermodynamically by melt (Leppäranta, 2011), or by the advection of thinner ice to the specific region. The influence of deformation on the temporal development of the ice thickness distribution is the most challenging to quantify. While thermodynamic ice growth is represented by the mode, the grade of deformation determines the tail of the overall thickness distribution and therefore governs its mean.

2.1.3 Sea ice thickness distribution in the Arctic

Changes in sea ice thickness at any given location and time are the result of a combination of the above-mentioned thermodynamic and dynamic processes. However, due to the large-scale atmospheric and oceanic circulation patterns in the Arctic, individual regions are dominated by either deformed MYI or thermodynamically grown younger ice (Zhang et al., 2000). The persistent atmospheric high pressure system over the Beaufort Sea is the main driver of the anticyclonic (clockwise) Beaufort Gyre and the Transpolar Drift system (Rigor et al., 2002, Fig. 2.4). Offshore-directed winds from the Siberian coast push newly formed, thin ice northward where it is incorporated into the Transpolar Drift. This process leads to continuous ice formation on the shallow Russian shelves and a dominance of thermodynamically grown young sea ice in this region (Krumpfen et al., 2013). Ice not

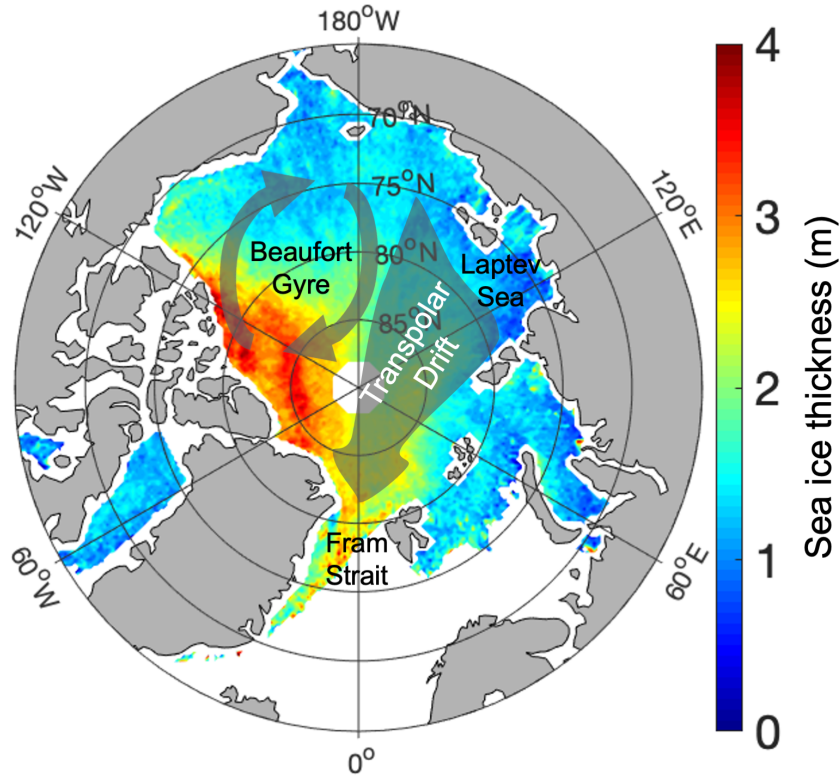


Figure 2.4: January to April 2020 mean sea ice thickness from the ESA CCI-2 climate data record (Hendricks et al., 2018a), superimposed by schematics of the general Arctic sea ice drift patterns.

exiting the Arctic through Fram Strait is pushed towards the northern coast of Greenland and the Canadian Archipelago where it piles up and strongly increases its thickness mainly through deformation processes (Kwok and Cunningham, 2015). Most of this ice continues to circulate within the Beaufort Gyre and is usually much older and thicker than the ice passing along the Transpolar Drift (Rigor et al., 2002, Fig. 2.4).

The strength of both large-scale circulation regimes, the Beaufort Gyre and the Transpolar Drift, is governed by the general wind-driven Arctic Ocean circulation and can be linked to the Arctic Oscillation (AO), which is described by surface level pressure anomalies over the Northern Hemisphere and especially the central Arctic Ocean (Thompson and Wallace, 1998). A positive AO phase is characterised by a negative surface pressure anomaly over the central Arctic Ocean, while a negative AO phase shows a positive pressure anomaly. The more cyclonic (counter-clockwise) motion of sea ice during a positive AO phase leads to increased transports of sea ice from the Russian shelves and a fast Transpolar Drift (Rigor et al., 2002). According to Rigor et al. (2002), the increasing ice formation in the Russian Arctic, a faster Transpolar Drift, and a coincidental slowing of sea ice motion in the Beaufort Gyre result in less ridging and recirculation of sea ice and should contribute to the thinning of sea ice during a positive AO phase. During a negative AO phase, ice from the Beaufort Gyre gets transported towards the eastern Arctic

much faster than during a positive AO phase. Due to the strengthened Beaufort Gyre circulation the ice exiting Fram Strait tends to be thicker than during a positive AO phase (Rigor et al., 2002). However, there is an ongoing debate whether the AO is the correct mechanism to describe variations in the general wind-driven Arctic Ocean circulation and the ensuing variations in sea ice drift speeds (Hakkinen et al., 2008; Rampal et al., 2009; Spreen et al., 2011; Vihma et al., 2012).

Independent of the origin of observed variations in sea ice drift speeds, the dominant processes changing sea ice thickness, and the variations in the general circulation of sea ice in the Arctic, individual regions can be dominated by thermodynamically grown or dynamically deformed sea ice. Since the processes changing sea ice thickness strongly impact the physical properties of the respective ice, different measurement techniques are more suitable in different regions and for certain ice types than others.

2.2 Key measurement techniques

The large-scale distribution of sea ice thickness is one of the integral parameters for monitoring changes in the Arctic sea ice cover. Sea ice thickness varies strongly on local scales and its vertical extent is comparably small, which requires highly sensitive and accurate measurement techniques (Eicken et al., 2014). Beside the possibility of manually drilling sea ice to measure its thickness, most of the measurement techniques applied are indirect methods. This means that parameters related to the ice thickness are measured and sea ice thickness is inferred from these measurements (Haas, 2017). The most common methods used to measure or infer sea ice thickness, their limitations, and their main areas of application are presented in greater detail in the following. The most relevant methods for the studies presented in this dissertation are given a more detailed description in separate subsections.

The most accurate and direct way of measuring ice thickness is manually drilling the ice from the surface and measuring its thickness with a gauge (Haas and Druckenmiller, 2009). This method allows for the simultaneous observation of all thickness components: ice freeboard and draft (combining for ice thickness), as well as snow thickness (Haas, 2017). While the accuracy of measuring ice thickness by drilling holes is unmatched, it is only possible in regions the observer can access. Once the observer is on the ice, it is tedious work and takes a lot of time. The enormous effort required limits the spatial extent of the measurements and restricts the validity of the results to a small area. A collection of ice thickness values measured with a drill is usually biased towards thicker ice, as very thin ice is hardly accessible on foot. Hence, manual drilling is mainly done to validate larger-scale measurements (Haas, 2017).

During shipborne expeditions, Arctic sea ice thickness is usually observed visually during the transit through the ice (recently based on the Arctic Shipborne Sea Ice Standardization Tool, ASSIST/IceWatch protocol introduced by Hutchings, 2018). Ice fragments broken by a passing ship usually turn sideways against the hull and their thickness can be estimated visually or even with camera systems (Chapter 6). However, visual ice thickness measurements date back to the early 20th century and continue to be an integral part of Russian ice charting efforts managed by the Arctic and Antarctic Research

Institute (AARI). Sea ice thickness information is limited to the route of the ship and biased towards thinner ice that is easier to navigate.

Different configurations of autonomous measurement stations equipped with thermistor chains can infer sea ice thickness while drifting with the ice. Once the chain and its closely spaced thermistors are solidly frozen into the ice, vertical temperature profiles are measured. The vertical temperature gradients are very different in snow and ice and absent in the water and air columns close to the respective interfaces due to the differing thermal conductivities of the relevant layers. Using a satellite link to transfer the data, this technique allows for very accurate distinction of the interfaces between air, snow, ice, and water in quasi real-time. However, it is very limited spatially as it provides a point measurement and follows the drift path of a single ice floe. In addition, these thermistor buoys provide only thermodynamic changes of sea ice thickness and are prone to break during deformation events (Eicken et al., 2014).

2.2.1 Upward-Looking Sonar

Upward-Looking Sonars (ULSs) are the primary source of long-duration sea ice draft data with high temporal resolution (Ross et al., 2016). They emit short pulses of acoustic energy in narrow beams and at frequencies of up to 2 Hz (Ross et al., 2016). The return signals are detected and the delay times between emitted and detected signal are precisely measured and converted into the distance between the instrument and the reflecting ice surface (range, Fig. 2.5). Additional information about the depth of the instrument underneath the water surface are required to derive sea ice draft. Usually ULS moorings are equipped with pressure sensors to record contemporary pressure data at the instrument. In combination with surface pressure information, these data records provide accurate distances between the instrument and the water surface. Taking sound velocity in seawater, possible current and tide-induced instrument tilts, and beamwidth biases into account, range is subtracted from the instrument depth to obtain sea ice draft (Ross et al., 2016, the relevant equations are provided in Chapter 3). Sea ice thickness can be inferred from the draft time series using a constant ratio between thickness and draft determined from drilling (Vinje and Finnekasa, 1986) or by assuming hydrostatic equilibrium. Following Archimedes' principle, hydrostatic equilibrium assumes that the forces acting downward (gravity) and upward (buoyancy) on the observed ice are equally strong, which keeps the ice in a balanced position at the ocean surface. Based on this balance and information about snow depth and the densities of ice and snow, sea ice thickness can be derived (Eicken et al., 2014).

While all types of sonars are technically usable to derive sea ice draft, the Ice Profiling Sonar (IPS) was specifically designed for the application of deriving sea ice draft from acoustic data. IPSs have been mounted to submarines (Bourke and Garret, 1987; Rothrock and Wensnahan, 2007) or oceanographic moorings (Fukamachi et al., 2003; Hansen et al., 2013; Krishfield et al., 2014; Behrendt et al., 2015) in both the Arctic and Antarctic. Other sonar-based instruments, such as Acoustic Doppler Current Profilers (ADCPs), have also been used to derive sea ice draft time series (Shcherbina et al., 2005; Banks et al., 2006; Hyatt et al., 2008).

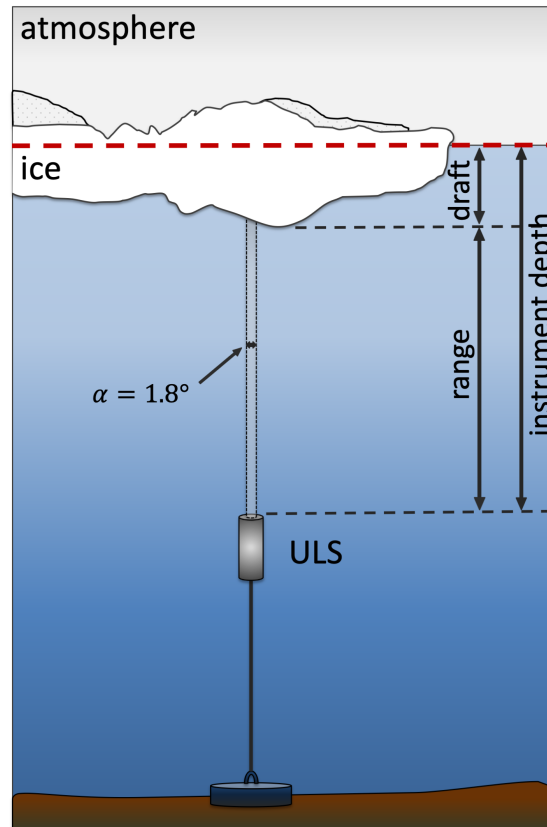


Figure 2.5: Schematic of the measurement principle of upward-looking, or ice profiling sonars (adapted from (Ross et al., 2016)). The two-way travel time of the acoustic signal emitted from the ULS and reflected at the ice-water interface is calculated into distance between ULS and ice (range) and subtracted from the distance of the instrument to the air-water interface (instrument depth) to determine sea ice draft.

Submarine-mounted ULSs allow for long-range sea ice thickness transects in the regions where the submarines are operating and usually have to be corrected for seasonal variability in order to be compared to other data sets (Rothrock and Wensnahan, 2007). Moored ULSs on the other hand provide continuous time series for single locations and for several years (Ross et al., 2016). State of the art IPSs are even deployed with a second mooring equipped with an upward-looking ADCP. Combining ice draft time series from the ULS and drift data from the ADCP allows for the derivation of spatial sea ice thickness series and detailed investigations of sea ice volume transports, especially when multiple ULS/ADCP mooring pairs are deployed along transects across known sea ice pathways (Hansen et al., 2013). However, the use of moorings is dependent on ice-free conditions during deployment and recovery, which limits their application to the seasonal ice zones, and data can not be obtained in real-time (see summary box for an overview of pros and cons of moored sonars).

Pros and cons: moored Upward-Looking Sonar

Method: indirect**Accuracy:** up to 0.05 m**Component measured:** draft**Advantages:**

- high temporal resolution
- year-round coverage
- thickness distribution of passing ice

Disadvantages:

- spatially limited
- battery-powered
- data access only after recovery
- deployment/recovery only in ice-free conditions

2.2.2 Electromagnetic induction sounding

In contrast to ULS measurements of sea ice draft from below the ice, electromagnetic induction (EM) sounding is applied from above the sea ice and snow surface. The EM method takes advantage of different electrical conductivities of the investigated layers and was first applied for geophysical exploration (Kovacs et al., 1987). The EM device is equipped with a transmitter coil, which generates a primary electromagnetic field that penetrates through the low-conductivity ice and snow layers almost unaffectedly (Kovacs et al., 1987). While the conductivity of ice and snow ranges from 0 to 50 milli-Siemens per metre (mS m^{-1}), seawater conductivities typically reach values between 2400 and 2700 mS m^{-1} (Haas et al., 1997). These values are highly dependent on the season and, in the case of the conductivity of sea ice, on the physical properties of the sampled ice (Haas et al., 1997). The penetrating primary electromagnetic field induces electric eddy currents in the seawater. The induced eddy currents generate a secondary field which penetrates upwards. The receiver coil in the EM device records the total electromagnetic field (primary and secondary field) and their differences in phase and amplitude (Kovacs et al., 1987; Hendricks, 2009). The proportionality between the strength of the secondary field and the distance from the coils to the conductive seawater surface is used to calculate the distance between the EM device and the ice-water interface, h_w (Keller and Frischknecht, 1966, Kovacs et al., 1987, Haas et al., 1997, Fig. 2.6 a)). Additional factors, such as signal frequency and coil orientation and spacing, also affect the received secondary EM signal (Haas, 2017). Due to the fact that the amplitude of the secondary field decreases exponentially with increasing distance between the conductive seawater surface and the receiver coil, state of the art EM devices used for ice thickness sampling are commonly operated at heights less than 20 m above the sea ice surface (Haas et al., 2009). These restrictions allow for two possible measurement setups that require different approaches to derive ice thickness.

The first setup uses ground-based EM devices (GEM), commonly built into a light-weight sledge, that are located directly on the ice or snow cover (offset between EM device

and surface has to be known) and effectively infer the distance between the air-ice and ice-water interface, the total ice thickness (Haas et al., 1997). The second setup uses airborne EM devices (AEM), that are towed from either a helicopter, fixed-wing aircraft (Kovacs et al., 1987; Multala et al., 1996), or even mounted to the bow of a ship (Haas, 1998) and infer the distance from their position to the ice-water interface (h_w). Radar or laser altimeters integrated into EM devices measure the distance from the instrument to the air-ice interface, h_i (Kovacs et al., 1987; Haas et al., 2009). This distance is subtracted from the EM-derived distance between the AEM and the ice-water interface to derive sea ice thickness (Fig. 2.6). Both the ground-based and the airborne approach therefore provide total sea ice thickness, including ice thickness, H_{ice} , and the thickness of the snow cover, H_{snow} .

GEM measurements are obtained on foot or using snowmobiles, which limits the areal extent of the measurements significantly. However, parallel ground measurements of snow depth along the GEM surveys, using instruments such as the Magna Probe (Sturm and Holmgren, 2018), allow for reliable ice thickness data from these ground-based measurements. The spacing between individual measurements is dependent on the survey speed and the instrument configuration (Haas et al., 1997). For both of the approaches, it is important to ensure a large-enough distance between the EM device and any metallic parts to avoid disturbance of the EM field by other highly conductive media (commonly, a couple of meters for the GEM and approximately 60 m for the AEM). In addition to the spatial limitations, ice thickness distributions inferred from GEM measurements usually lack information about thin ice due to the limitations of sampling it on foot (Haas, 2004).

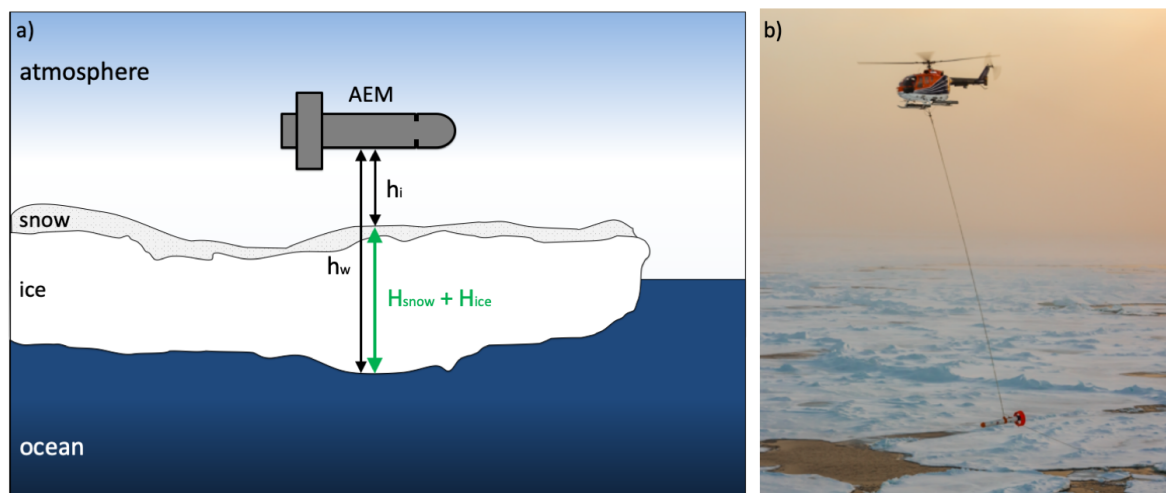


Figure 2.6: a) Schematic of the measurement principle of an airborne electromagnetic induction sounding (AEM) instrument (adapted from (Haas et al., 2009)). Total sea ice thickness (snow + ice thickness) is calculated from EM measurement inferred distance between the EM device and the ice-water interface, h_w , and the laser altimeter measured distance between the EM device and the ice/snow surface, h_i . b) Airborne EM device (EM Bird) towed by a RV Polarstern helicopter in the Arctic (photo by Stefan Hendricks, Alfred Wegener Institute).

AEM measurements require considerable extra effort compared to the GEM measurements. Pilots have to fly the aircraft at very low altitudes to ensure that the distance between the AEM and the ice cover does not exceed 20 m. As for the GEM, towing the EM device is done to prevent interference from any conductive metal parts, but also to ensure safe flying altitudes for the aircraft. The airborne approach provides a significant increase in areal coverage compared to the ground-based setup but has a much larger footprint of two to four times the altitude of the EM device. Measurements are averaged over this footprint area, which is one of the reasons the maximum sea ice thickness is underestimated within each footprint (Eicken et al., 2014). While the EM-derived total thickness is within 0.1 m of drill hole measurements over level ice, it underestimates total ice thickness over deformed ice by approximately 40 to 50% (Pfaffling et al., 2007; Haas et al., 2009). Especially ridged ice consisting of ice blocks and connecting hollow spaces filled with seawater prevent accurate measurements of ridge keels (Haas et al., 2009). In this context, improvements in EM sounding methods and especially the use of multi-channel sensors, which allow the detection of internal and bottom layers in different ice structures, are actively investigated to reduce the uncertainty over sea ice consisting of layers with different physical properties (Hunkeler et al., 2015; Haas, 2017).

Like moored ULSs, EM devices provide sea ice thickness distributions. However, EM-derived distributions are independent of sea ice motion and sampling is only dependent on weather conditions and the observer's preferences. EM data are available immediately after sampling but lack the accuracy over ridged ice that is achieved using moored ULSs (see summary box for pros and cons of EM sounding).

Pros and cons: airborne and ground-based EM sounding

Method: indirect

Accuracy: 0.1 m (level ice)

Component measured: total thickness (ice + snow)

Advantages:

- areal coverage (AEM)
- accuracy over level ice
- thickness distribution over sampled area

Disadvantages:

- areal coverage (GEM)
- underestimation of deformed ice
- bias towards thicker ice (GEM)
- limited by weather and accessibility
- temporal coverage

2.2.3 Satellite remote sensing

Recent developments in satellite remote sensing of sea ice have resulted in a variety of open-access satellite sea ice thickness products (Sallila et al., 2019). Satellite retrievals of sea ice thickness are based on two main measurement principles. Active satellite remote sensing uses the active emission of an electromagnetic signal from the satellite and the

recording of the respective reflected or backscattered signal from the ice and ocean surface to derive a sea ice related parameter that can be converted into sea ice thickness (Spren and Kern, 2017). Passive satellite remote sensing of sea ice thickness is carried out using radiometry, which uses the fact that the Earth itself emits electromagnetic radiation. These received radiative signals are used to infer sea ice thickness (Spren and Kern, 2017). Since the 1990s, various different configurations of altimeters (active) and radiometers (passive) have been deployed with satellites, with altimetry being the most commonly applied method for the derivation of various satellite sea ice thickness products today (Sallila et al., 2019).

The focus of the study presented in Chapter 4 is on the validation and application of the longest available satellite sea ice thickness data set, which consists of combined data from two different satellite altimetry missions. The following section will therefore present a basic summary of the application of satellite altimetry for the derivation of sea ice thickness but also touch on the radiometric approach, to introduce the second satellite sea ice thickness product investigated. This second product combines the advantages of active and passive satellite remote sensing for an improved satellite sea ice thickness product.

Satellite altimeters used to derive sea ice thickness measure different forms of the fraction of the ice that protrudes from the ocean – freeboard. The determination of freeboard is strongly dependent on and requires knowledge of the physical properties of snow, ice, their respective surfaces, and the sea surface height. Due to the comparably large footprints of the used altimeters, the correct determination of sea surface height over almost closed ice covers is challenging. Open water areas, required to detect the sea surface, usually occur on comparably small spatial scales that can not be resolved (Spren and Kern, 2017) and available mean sea surface height data sets have to be used instead (Sallila et al., 2019). Like the determination of the sea surface height, deriving the height of the snow surface is achieved using different approaches and data sets (Sallila et al., 2019). While some configurations of radar altimeters that are assumed to fully penetrate the snow cover provide ice freeboard, others together with laser altimeters determine the height of the total freeboard, including snow and ice freeboard (Spren and Kern, 2017). As summarised in Sallila et al. (2019), the most commonly used products rely on different algorithms and assumptions to detect the desired interface and sea surface height (Kwok et al., 2009; Laxon et al., 2013; Kurtz et al., 2014; Ricker et al., 2014; Tilling et al., 2018). However, the strong annual changes in the physical properties of ice and snow even prevent the detection of these interfaces completely during periods of surface melt (Ricker et al., 2017; Hendricks and Ricker, 2019a). This is why satellite altimeter sea ice thickness data are usually only available for the winter months, when the air-snow or snow-ice interface can be detected. Once freeboard is determined, it is converted into sea ice thickness. Like for the above-mentioned ULS calculations, this conversion is based on the assumption of hydrostatic equilibrium and auxiliary information of snow and ice density and snow depth (Spren and Kern, 2017). While the ULS-based method to derive sea ice thickness utilises the submerged larger fraction of ice, the draft, for the conversion to sea ice thickness, the altimeter approaches use the smaller fraction, freeboard. Due to the small freeboard/thickness ratio even small errors in freeboard strongly effect the accuracy

of the final sea ice thickness estimate (Eicken et al., 2014). It is therefore vitally important to acquire reliable information of snow and ice density and snow depth that is not only required for the determination of freeboard but also for the conversion of freeboard into sea ice thickness. Since snow depth and snow and ice densities are not routinely measured, current satellite sea ice thickness products have to rely on assumptions and estimates for these parameters, which increases the uncertainty of the final sea ice thickness product even further (Spren and Kern, 2017; Hendricks and Ricker, 2019b).

The above-mentioned longest available satellite-derived sea ice thickness climate data record is a product of the European Space Agency’s (ESA) Climate Change Initiative Phase 2 (CCI-2). Combining radar altimeter-derived sea ice thickness data from the Environmental Satellite (ENVISAT, Hendricks et al., 2018c) and from CryoSat-2 (CS2, Hendricks et al., 2018a), this product provides monthly mean sea ice thickness from 2002 onwards. The initial daily orbit data is interpolated to a 25 km resolution grid. However, due to the limitations of freeboard retrieval during ice and snow melt and the resulting high moisture content at the ice surface, data is only available from October through April (Ricker et al., 2017; Hendricks and Ricker, 2019a).

The second data product utilised here is a merged product combining CS2 altimeter-derived sea ice thickness and radiometer-derived sea ice thickness from the Soil Moisture and Ocean Salinity (SMOS) satellite (Ricker et al., 2017). SMOS sea ice thickness is derived using radiometer measurements of the thermal microwave radiation emitted by a closed ice cover during freezing conditions (Kaleschke et al., 2010). This passive remote sensing method relies on the fact that different media possess different radiative properties. In terms of sea ice thickness derivation, the different radiative properties of seawater and sea ice of different thicknesses are utilised (Spren and Kern, 2017). The specific parameter observed by the SMOS radiometer is the surface brightness temperature, which is dependent on ice and seawater temperatures and their respective emissivities (Kaleschke et al., 2010). It has been shown that the SMOS ice thickness retrieval algorithm, based on a combined thermodynamic and radiative transfer model, is best suited to retrieve sea ice thickness values of ice thinner than 0.5 m (Kaleschke et al., 2012; Tian-Kunze et al., 2014). While uncertainties of SMOS sea ice thickness are lower over thin ice compared to radar altimeter retrievals, uncertainties increase exponentially for ice thicker than 0.5 m (Tian-Kunze et al., 2014). The complementarity of the relative uncertainties of CS2 and SMOS sea ice thickness shown by Kaleschke et al. (2015) was used by Ricker et al. (2017) to develop a merged sea ice thickness product (CS2SMOS). This merged product not only reduces sea ice thickness uncertainties by prioritising the lower uncertainty data set but also increases the temporal resolution of satellite-derived sea ice thickness data from monthly to weekly (Ricker et al., 2017).

For the satellite sea ice thickness validation study presented in Chapter 4, the ESA CCI-2 radar altimetry-based and the merged CS2SMOS product are selected, as they provide the longest available record and the highest temporal resolution of the available gridded sea ice thickness products, respectively. Despite the improvement in temporal resolution provided by the merged CS2SMOS product, temporal coverage is one of the main limitations of satellite-derived sea ice thickness data in general. Both data products only provide data from October through April with no sea ice thickness data available

during the Arctic summer season. Additionally, these data products provide gridded averages of sea ice thickness (Ricker et al., 2017; Hendricks and Ricker, 2019a,b). Sea ice thickness distributions especially on scales smaller than their 25×25 km grids are not available and thermodynamic and dynamic thickness changes that occur on these small spatial and short temporal scales are not represented at all. The uncertainty of the gridded mean values of sea ice thickness are given for each grid point (Hendricks and Ricker, 2019a) and vary substantially for different regions and months. As an example, the Arctic-wide average of ESA CCI-2 sea ice thickness uncertainty is approximately 0.65 m (in April, see summary box for pros and cons of satellite remote sensing).

Pros and cons: satellite remote sensing

Method: indirect

Uncertainty: satellite product specific
e.g. ESA CCI-2: 0.65 m (Arctic mean April)

Component measured:
freeboard (altimeter), brightness temperature (SMOS)

Advantages:

- Arctic-wide data
- weekly resolution
(merged CS2SMOS)

Disadvantages:

- temporal resolution
- temporal coverage
(no summer data)
- small-scale features not resolved
- high uncertainty

2.2.4 Conclusion

The comparison of ULS, EM and satellite-based methods to derive sea ice thickness shows the requirement for further development and improvement of sea ice thickness measurements. Each of these methods has at least one characteristic that is superior to other methods and more suitable for specific applications. However, no method currently available provides sufficient spatial resolution and Arctic-wide coverage paired with high temporal resolution and year-round coverage to observe the complex changes of sea ice thickness and its distribution comprehensively. In the absence of an overall sufficient sea ice thickness data set, it is necessary to improve and combine data from different measurement techniques and regions and find solutions to connect these data sets. Therefore, the studies within this dissertation aim to contribute to the extension of existing data sets and the improvement of satellite sea ice thickness products but also combine available data, models, and additional tools for the investigation of ongoing sea ice thickness changes and variability in the Arctic.

3 Sea ice draft from upward-looking Acoustic Doppler Current Profilers: an adaptive approach, validated by Upward-Looking Sonar data

Currently under review at *Cold Regions Science and Technology*

Belter, H. J.¹, T. Krumpfen¹, M. A. Janout¹, E. Ross², and C. Haas¹

¹*Alfred Wegener Institute, Helmholtz Centre for Polar and Marine Research, Bremerhaven, Germany*

²*ASL Environmental Sciences Inc.*

Author contributions

HJB processed the 2014/2015 ULS data and together with MAJ developed the method to derive sea ice draft from upward-looking ADCP data. HJB also conducted the statistical analysis and comparison of ULS and ADCP-derived draft and wrote the manuscript. TK, MAJ and CH provided guidance and important comments during the writing, editing, and review of the manuscript. Apart from their contributions to the writing of the manuscript MAJ deployed and recovered the ADCP and ULS moorings and ER processed the 2013/2014 ULS data. ER also provided support during data processing.

Abstract

Moored upward-looking Acoustic Doppler Current Profilers (ADCPs) can be used to observe sea ice draft. While previous studies relied on the availability of auxiliary pressure sensors to measure the instrument depth of the ADCP, we present an adaptive approach that infers instrument depth from ADCP bottom track (BT) mode measurements of error velocity and range. The ADCP-derived ice draft time series are validated with data from adjacent Upward-Looking Sonar (ULS) moorings. We demonstrate that this method can be used to obtain daily mean sea ice draft time series that, on average, are within 20% of ULS-derived draft time series. ULS and ADCP ice draft time series were observed by four moorings in the Laptev Sea and show correlations between 0.7 and 0.9. This new approach is not a substitute for high-frequency, high-precision ULS measurements of ice draft but it provides a low-cost opportunity to derive daily mean ice draft time series accessing existing ADCP data that was not used for that purpose so far. This method has the potential to close data gaps and extend existing ice draft time series in all ice-covered regions and supports the validation of sea ice thickness products from satellite missions such as CryoSat-2, SMOS or ENVISAT.

3.1 Introduction

Upward-Looking Sonars (ULS) are the primary source for high-resolution and long-duration time series of sea ice draft (Ross et al., 2016). They sample at high frequencies (up to 0.5 Hz) using a single narrow vertical beam and have been used for quite some time in several ice-covered regions around the world (Fukamachi et al., 2003; Hansen et al., 2013; Krishfield et al., 2014; Behrendt et al., 2015; Janout et al., 2016; Fukamachi et al., 2017). In regions where ULS data is not available or funding constraints prohibited the deployment of ULSs, upward-looking Acoustic Doppler Current Profiler (ADCP) records have been utilised to derive sea ice draft information (Shcherbina et al., 2005; Banks et al., 2006; Hyatt et al., 2008; Bjoerk et al., 2008).

In the world oceans, ADCPs are primarily used to measure current velocity profiles. When operated in bottom track (BT) mode such setups allow measurements of ice drift velocities that are commonly used to complement ULS measurements of sea ice draft (Ross et al., 2016; Fukamachi et al., 2017). As suggested by Visbeck and Fischer (1995) a combination of ADCPs and precise pressure sensors to determine the instrument depth also allows the derivation of sea ice draft. However, compared to standard ULS systems the inherent instrument setup of upward-looking ADCPs, with larger beamwidth and default beam angles to the vertical, leads to larger uncertainties of the derived sea ice draft values. This is the case even if the instrument depth is precisely known from pressure measurements and correction terms are applied to overcome the ADCPs deficiencies (Visbeck and Fischer, 1995; Shcherbina et al., 2005; Hyatt et al., 2008). Consequently, ice draft derivations based on ADCP BT data are less common and simply a mean to overcome ULS data gaps.

One region that is lacking long-term ULS ice draft measurements is the Laptev Sea in the Eastern Arctic Ocean (Fig. 3.1). The Laptev Sea is considered to be a key source region of Arctic sea ice (Rigor et al., 2002; Hansen et al., 2013; Krumpfen et al., 2013,

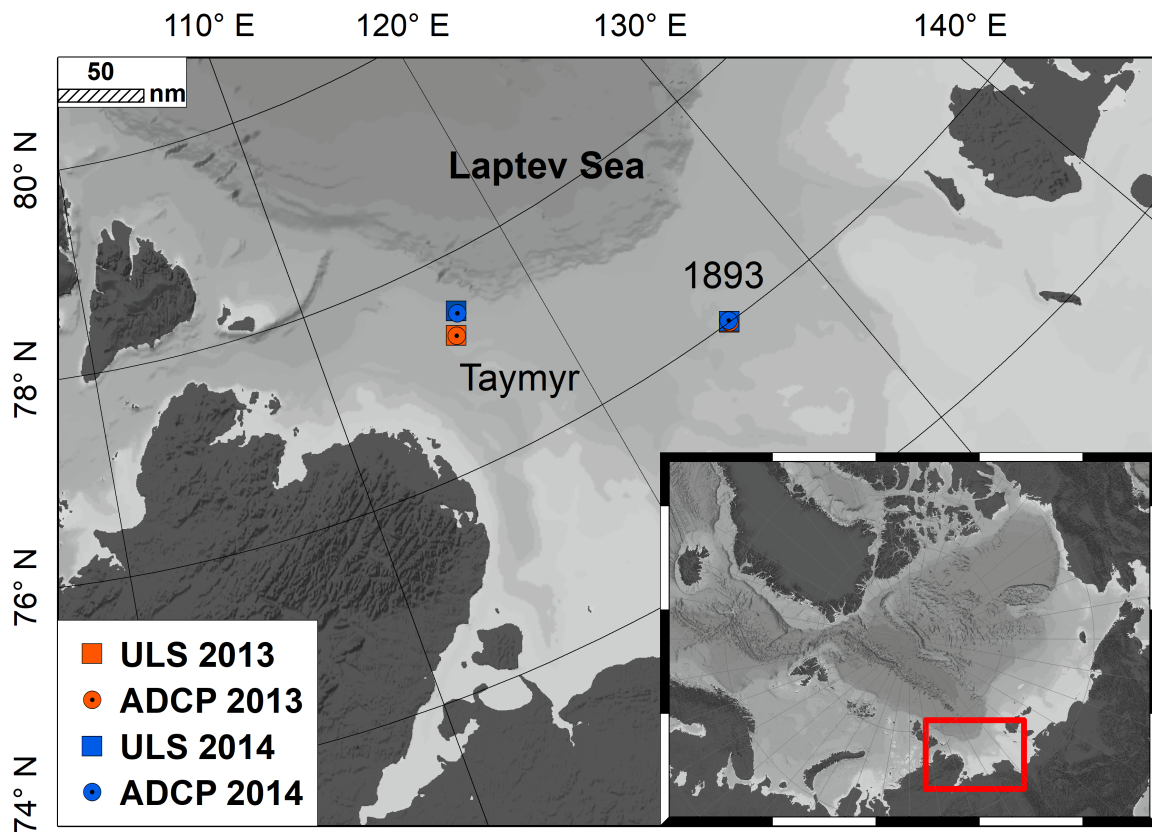


Figure 3.1: Map of the Laptev Sea showing the 2013/2014 (orange) and 2014/2015 (blue) Upward-Looking Sonar (ULS, squares) mooring sites. An additional mooring holding an upward-looking Acoustic Doppler Current Profiler (ADCP, circles) was deployed close to each ULS mooring.

2019). From October through June the Laptev Sea is covered mostly by first-year ice (Reimnitz et al., 1994; Bareiss and Goergen, 2005). Sea ice is formed in polynyas on the shallow shelves (water depths between 15 and 200 m) and continuously transported north towards the central Arctic Ocean by the prevailing offshore-directed winds (Timokhov, 1994; Krumpfen et al., 2013). Despite the importance of the region for the formation of Arctic sea ice, long-term in situ measurements of sea ice draft are not available. ULS measurements for scientific purposes were only carried out for two years (2013-2015) within the framework of the Russian-German research cooperation 'Laptev Sea Systems'. As the access to this region is very limited and further ULS moorings have not been deployed over the past few years, high-resolution long-duration ice draft measurements are sparse. Oceanographic moorings with upward-looking ADCPs on the other hand, were operated in the Laptev Sea over much longer time periods (2003-2016)(Janout and Lenn, 2014). However, unlike for previous studies (Shcherbina et al., 2005; Banks et al., 2006; Hyatt et al., 2008; Bjoerk et al., 2008) the available ADCP data was not complemented by reliable auxiliary pressure data to determine instrument depth. Therefore, the extension

of the available ULS-based sea ice draft time series was not possible in the Laptev Sea so far.

In order to overcome the lack of ice draft data in this important source region of Arctic sea ice, we present an adaptive approach to derive ice draft time series from ADCP data that is not based on additional pressure data to determine instrument depth. This new approach builds on previous techniques to derive ice draft from ADCPs but its validation relies on the availability of coincidental ULS moorings. The ULS measurements provide reliable reference data for the ice draft derivation from ADCPs, which was not available to previous studies (Shcherbina et al., 2005). Similar to Hyatt et al. (2008), we provide the means to utilise more available ADCP data records to extend ice draft time series in regions where no other data is available rather than a substitute for combined ULS and ADCP measurements of ice draft.

Access to the available long-term ADCP data in the Laptev Sea allows an extension of existing ULS-based ice draft time series. This extended time series will support upcoming efforts to investigate seasonal and interannual sea ice thickness variability in this vital source region of Arctic sea ice that were not possible until now. Furthermore, these data sets provide unique in situ validation data for sea ice thickness products based on satellite missions such as CryoSat-2, SMOS or ENVISAT.

3.2 Data and Methods

Two ULSs of the type Ice Profiling Sonar 5 (420 kHz, manufactured by ASL Environmental Sciences) were deployed in the Laptev Sea in September 2013. In addition, two moorings with upward-looking Teledyne RDI Workhorse 300 kHz Sentinel ADCPs were deployed in the vicinity of the ULS moorings (for distances see Table 3.1) over the same time period (Fig. 3.1). All four devices were recovered in September 2014. Both ULS and one ADCP were redeployed until September 2015. The other ADCP was exchanged and the entire mooring newly deployed until September 2015 as well.

Initially, the ADCPs were deployed to provide complementary ice drift velocity data to the obtained ULS draft data. The combination of ULS draft and ADCP ice drift data allows the conversion of sea ice draft time series into quasi-spatial series. Spatial series of ice draft are used for detailed characterizations of keel shapes and other ice features (Ross et al., 2016) as well as the estimation of ice volume fluxes. Despite their differing purposes, both systems, ULS and ADCP, are built to determine distances between transducer and

Table 3.1: Distances between ADCP and ULS mooring at the stations 1893 and Taymyr for the two sampling periods (2013-2014 and 2014-2015).

	2013/2014	2014/2015
Station		
1893	0.33 km	0.99 km
Taymyr	0.35 km	2.85 km

reflecting surfaces or scattering particles from the two-way travel time of their emitted and reflected acoustic signal which allows the computation of ice draft. However, the specific configuration of the ULS, with one narrow vertical beam, makes it the primary mooring-deployed device for this task. The high-precision ULS measurements provide an excellent reference for the validation of our approach to derive sea ice draft from ADCP data. For this study we analysed a total of four ULS/ADCP data sets from two different locations and time periods (Fig. 3.1).

3.2.1 Data processing

Upward-Looking Sonar

The Laptev Sea ULSs were deployed at water depths between 43 and 78 m (instrument depths between 14 and 23 m) and operated with a single vertical beam (beamwidth 1.8°) at a sampling frequency of 1 Hz for range (distance from device to ice-water interface) and $1/60$ Hz for auxiliary data (instrument tilt, pressure and temperature at instrument depth). Sea ice draft (d) was calculated as the difference between instrument depth (η) and distance to the ice-water interface:

$$d = \eta - \beta \cdot r \cdot \cos\theta, \quad (3.1)$$

where β is a calibration factor (ASL, 2017) for the corrected speed of sound in seawater relative to the initially assumed value used when decoding the raw range data, r is the ULS-measured range and θ is the total instrument tilt from the vertical (ASL, 2017). The continuous instrument depth time series was computed as follows:

$$\eta = \left(\frac{p_{uls} - p_{atm}}{\rho g} \right) - \Delta D, \quad (3.2)$$

where p_{uls} is the ocean pressure at instrument depth as measured by the ULS. Surface pressure, p_{atm} , was taken from the ECMWF ERA-Interim (6 h sea level pressure) reanalysis product, ρ is the seawater density, g is the local gravitational acceleration and ΔD is the vertical spacing between ULS pressure and range sensor (ASL, 2017). The 2013-2014 (13/14) data sets were processed by ASL Environmental Sciences Inc., while the 2014-2015 (14/15) data sets were processed by the authors using the ASL Ice Profiling Sonar Processing Toolbox (ASL, 2017).

The resulting data sets provide high-frequency ice draft time series for the two locations in the Laptev Sea (Fig. 3.1). According to Ross et al. (2016) the theoretical error of ULS-derived ice drafts is within 0.05 m. This error estimate is based on the accuracy and precision of the range measurements, pressure, tilt and temperature sensors. However, errors may accumulate during the individual processing steps due to errors inherent in air pressure data, sound speed estimates, instrument tilt, false targets (like bubbles and biota), signal spikes, beamwidth and footprint effects and wave penetration into the ice (Hansen et al., 2013). A detailed description of the individual processing steps and possible uncertainties can be found in the Ice Profiling Sonar Processing Toolbox User's Guide (ASL, 2017) and in Hansen et al. (2013).

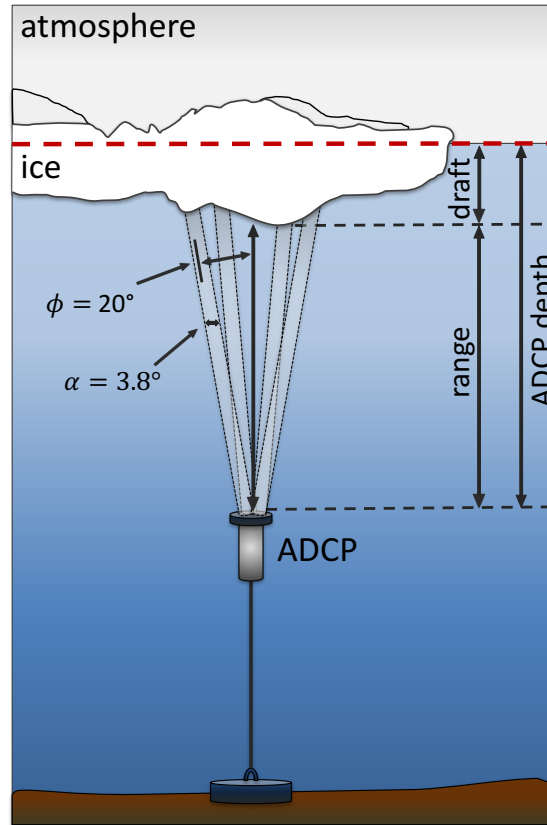


Figure 3.2: Simple schematic of a moored upward-looking Acoustic Doppler Current Profiler.

Acoustic Doppler Current Profiler

The moored ADCPs sampled in bottom track (BT) mode at a frequency of 1/60 Hz. However, the raw data output provides hourly values that were calculated as an ensemble average over 60 values. Measurements in BT mode are characterized by longer transmit pulses compared to water tracking mode that is used to profile the water column (Teledyne RDI, 2011). Additionally, the signal echoes are processed differently (for a detailed explanation see Teledyne RDI (2011)). The ADCPs measured with four different beams, each with a 3.8° beamwidth. By default, the beams were mounted at an angle of 20° to the vertical (Fig. 3.2). BT range to the boundary above was measured by each one of the four beams and the final values were corrected for the 20° mounting angle internally by the ADCP. Prior to further processing, we also corrected for instrument tilts (roll and pitch) that resulted from mooring movement and were not accounted for by the ADCP internally. Fig. 3.3 shows the tilt magnitudes for the four ADCP data sets.

The uncertainty of the measured range is correlated to the instrument depth and amounts to about $\pm 1\%$ of the total measured range for the current setup. For the depth ranges of the ADCPs used for this study, the BT mode range uncertainty is between ± 0.3 and ± 0.5 m (Teledyne RDI, 2011).

The derivation of ice draft records from ADCP data is based on the same processing steps used to compute draft from ULSs (Eq. 3.1). However, since the ADCPs primary purpose was to measure velocity fields, it was not configured to measure ice draft with the same accuracy as the ULS. Previous studies (Shcherbina et al., 2005; Hyatt et al., 2008; Bjoerk et al., 2008) on ice draft derivation from ADCP data applied a number of correction terms in order to obtain ice draft time series. All these studies relied on pressure sensors that were deployed with or integrated into the ADCPs. The additional pressure sensor proved vital for an accurate determination of instrument depth. However, older ADCPs are not necessarily equipped with these additional sensors. This is true for the ADCPs that were deployed in the Laptev Sea. The presented approach to derive ice draft from upward-looking ADCPs adapts to the lack of auxiliary pressure data and determines instrument depth using only the BT mode data output provided by the ADCP.

Instrument depth is deduced from BT mode measurements of surface and error velocity. BT error velocity quantifies the difference in vertical velocity as measured by any two opposite ADCP beams (Belliveau et al., 1990), meaning that it provides a measure of the consistency of the velocity measurements at the reflecting surface from the four beams. Belliveau et al. (1990) found that error velocities also provide an indication of either ice-covered or open water conditions. Error velocities and horizontal surface velocities were steady and close to zero during permanent ice cover and became rather noisy when open water prevailed (Belliveau et al., 1990; Bjoerk et al., 2008). Hyatt et al. (2008) used windowed variances of vertical and error velocities to distinguish between open water

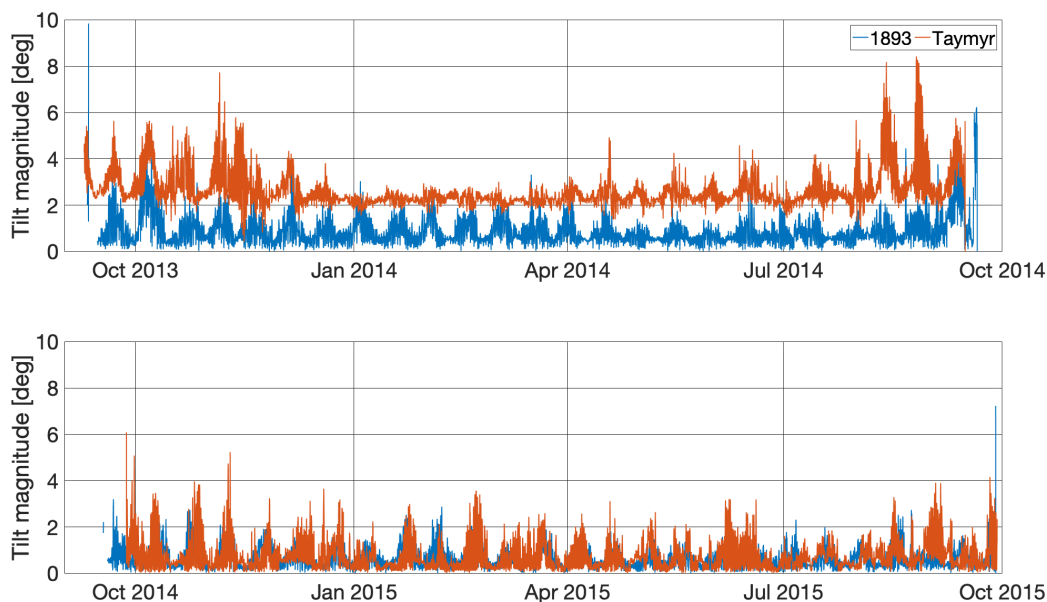


Figure 3.3: Tilt magnitude calculated from roll and pitch data from the ADCP. Top (bottom) panel shows tilt time series for stations 1893 (blue) and Taymyr (orange) for the period from 2013 to 2014 (2014 to 2015).

and ice-covered conditions. Since the open water surface is rather variable and strongly influenced by winds, it is valid to assume that four beams measuring four different areas (Fig. 3.2) are likely to detect inhomogeneities in the velocity field. The ADCPs used here were deployed at depths between 34 and 46 m which resulted in a minimum (maximum) distance between measurements of two opposing beams of approximately 25 m (33.5 m) at the surface. These distances between measurements from the four beams arise only due to the default 20° angle between the individual beams from the vertical. With higher velocities and noisy signals during open water periods the error velocity is bound to increase, indicating inhomogeneous surface velocities. The ADCPs were configured to save flag values in the error velocity output file in cases where error velocities exceeded a threshold value of 1 m/s.

Following these assumptions, we consider error velocity flag values a definitive measure for open water conditions. Unlike Hyatt et al. (2008) we require this information for the detection of ADCP instrument depth rather than to determine sea ice concentration.

Based on the detection of open water from the error velocity flag values we consider all BT range values during open water periods to provide the distance between the ADCP and the water surface - the instrument depth. Figure 3.4 shows an example of all open water range values from a single beam of the ADCP deployment at the Taymyr station in 13/14. In general the instrument depth is strongly influenced by surface gravity waves and tidal amplitudes, as well as vertical movement of the ADCP due to mooring blowdown in strong currents. Figs. 3.3 and 3.4 confirm mooring movement and the variability of the instrument depth throughout the sampling period.

During winter the central Laptev Sea is characterised by a closed ice cover. Accordingly, leads and open water areas that are detected using the error velocity almost exclusively occur during freeze up, melt and ice-free periods (Fig. 3.4). Moreover, periods of open water that occurred during winter are difficult to detect due to the ADCPs comparably long sampling interval of 1 min and the internal averaging to hourly values. Narrow openings in the ice were simply not resolved or averaged out. Without any open water records during the ice-covered period the determination of a continuous instrument depth time series, like with the high-frequency ULS measurements, is not possible with our ADCP approach. We therefore determine a constant instrument depth for the entire sampling period for each ADCP time series. In order to account for offsets between the four ADCP beams we determine a constant 'quasi-depth' for each beam individually by finding the most frequent (modal) BT range value during open water periods (Fig. 3.4).

With limited knowledge about water column properties and the long sampling interval we rely on sound speed estimates based on the ADCPs temperature measurements and the assumption of constant salinity (measured at mooring deployment) between the ADCP and the water surface throughout the sampling period (Teledyne RDI, 2011). Following these assumptions and limitations for the derivation of ice draft and instrument depth from an ADCP with no internal pressure sensor Eq. 3.1 is reduced to:

$$d_i = z_i - r_i \cdot \cos\phi, \quad (3.3)$$

where i is the number of beams (four in this case), z is the quasi-depth based on the most frequently occurring BT range value during open water periods, r is the BT range and

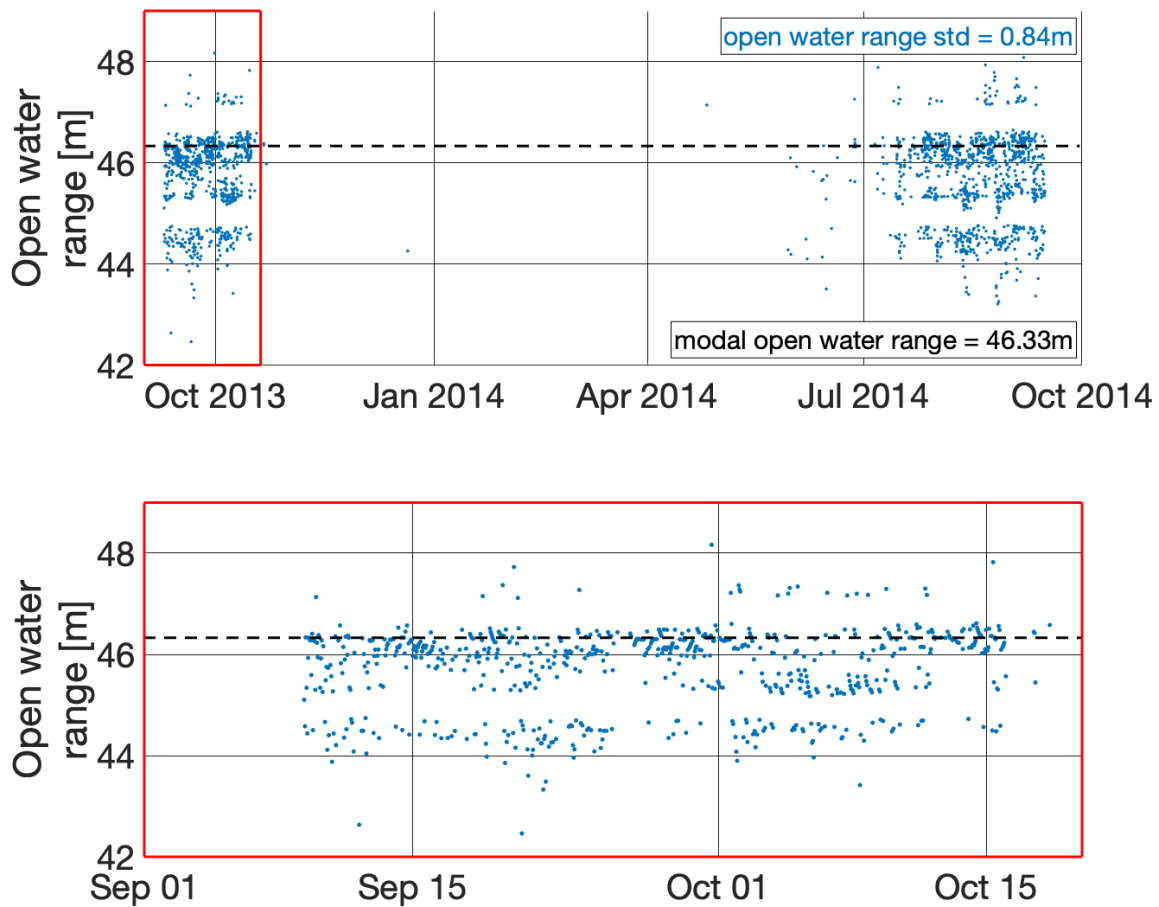


Figure 3.4: Open water range values from beam 2 of the Taymyr-13/14 ADCP are shown in blue (top panel). Bottom panel shows the image section of the top panel for the period from Sep. 1 until Oct. 20, 2013. The black dashed line indicates the beam 2 instrument quasi-depth determined from the most frequent open water range value (derived from distribution with 0.01 m bins). This depth was considered the constant depth throughout the sampling period and used to calculate the beam 2 sea ice draft time series.

ϕ is the tilt of the ADCP. Eq. 3.3 is applied to each beam individually resulting in four separate sea ice draft time series per ADCP.

Since we account for possible offsets between the four beams, in theory, the four draft time series ought to be very similar. However, as mentioned before the default mounting angle between the individual beams led to the measurement of four different areas of ice. After accounting for possible offsets between the beams the final step before averaging over the four beams is to determine whether individual beams or their data output are erroneous. In this context, we consider physical mechanisms (e.g. tilting of a beam that is not accounted for) that act on individual beams that otherwise performed

as expected. In order to identify erroneous data from individual beams we calculate the percentage of negative ice draft values throughout the entire sampling period from each beam. In reality, negative draft values are non-existent but due to our instrument depth assumptions and the limitations of this method they can occur especially during freeze up, melt and ice-free periods. Hence, depending on the length of the transition time between ice-free and ice-covered periods the percentage of negative draft values changes. We average the percentages over the four beams and calculate their standard deviation. Too high a percentage of negative draft values of one beam compared to the other three is an indication for erroneous data from that beam. We therefore exclude data from beams with a percentage of negative draft values that is outside of one standard deviation of all beams. The exclusion of data from one or more beams occurred only once for the four ULS/ADCP data set pairs. Averaging over all remaining beams yields one ice draft time series for each ADCP with a sampling interval of 1 h.

Values recorded during open water periods and remaining negative draft values are excluded and daily mean ice drafts are calculated. Averaging the draft time series to daily mean values is necessary due to the noisiness in the data and the uncertainty that is introduced to the hourly draft values by our estimate of constant instrument depth. Daily mean draft values are calculated for all days with a minimum number of 12 (half the data recorded per day) 'good' draft values. This threshold prevents that daily mean values are distorted by outliers during days with long or frequent open water periods. ULS reference time series are averaged to daily mean values as well. Apart from minimizing the noise of the final ADCP-derived sea ice draft time series the averaging to daily mean values improves the comparability of the ULS and ADCP-derived data sets.

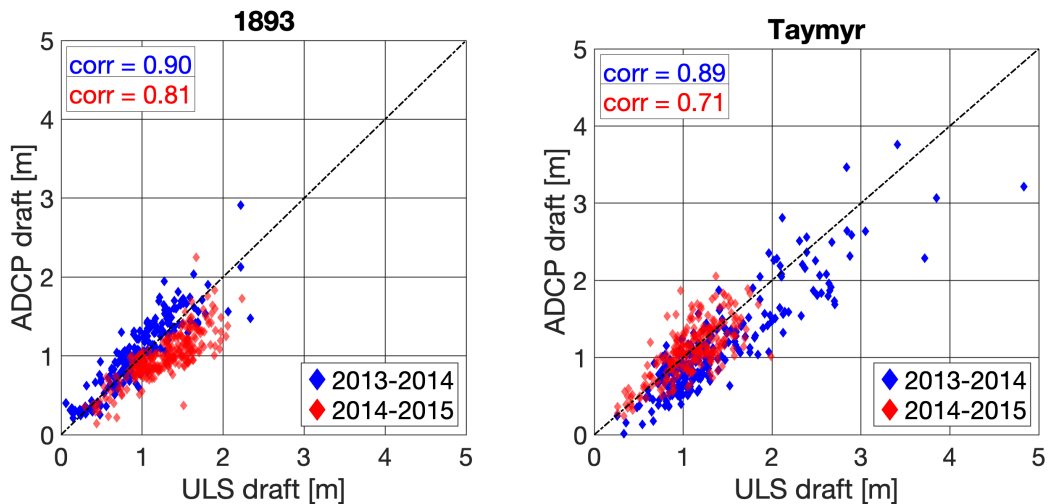


Figure 3.5: ULS and ADCP-derived daily mean sea ice draft comparison from the 1893 (left) and Taymyr (right) stations. Blue (red) markers indicate data from the 2013-2014 (2014-2015) sampling period. Values (corr) show Pearson correlation coefficients between ULS and ADCP-derived sea ice draft for the respective station and sampling period. Correlation coefficients are significant at the 99% confidence level for all four ULS/ADCP data pairs.

3.3 Results

In contrast to previous studies on ice draft derivation from upward-looking ADCPs (Shcherbina et al., 2005) we are able to compare ADCP-derived daily mean ice draft to reference time series based on ULS data. However, it has to be noted that ULS and ADCP were deployed using two different moorings some distance apart. In theory, the two moorings should have been as close to each other as possible in order to depict drift and draft of the same area of ice but not too close to avoid acoustic cross-talk between the instruments (Melling and Riedel, 1995). Practically, expedition logistics and weather conditions determined the distance between the respective mooring locations. For the comparison of draft time series from the two instruments the distance between the mooring sites led to sampling of different pieces of ice. For the purpose of this study we presume that, although we were not measuring the exact same ice at the respective ADCP and ULS moorings, the general ice conditions in those areas of the Laptev Sea were comparable on a daily scale for the observed distances (Tab. 3.1).

Fig. 3.5 shows two scatter plots of ULS-derived daily mean sea ice draft versus ADCP-derived daily mean sea ice draft at the 1893 and Taymyr stations and from the sampling periods 2013-2014 (13/14) and 2014-2015 (14/15). Pearson correlation coefficients between ULS and ADCP-derived daily mean ice draft are between 0.71 (Taymyr-14/15) and 0.90 (1893-13/14). Following the t-test, all four correlation coefficients are significant at the 99% confidence level. For the 14/15 period correlation coefficients are lower than for the 13/14 period, which coincides with larger distances between ULS and ADCP moor-

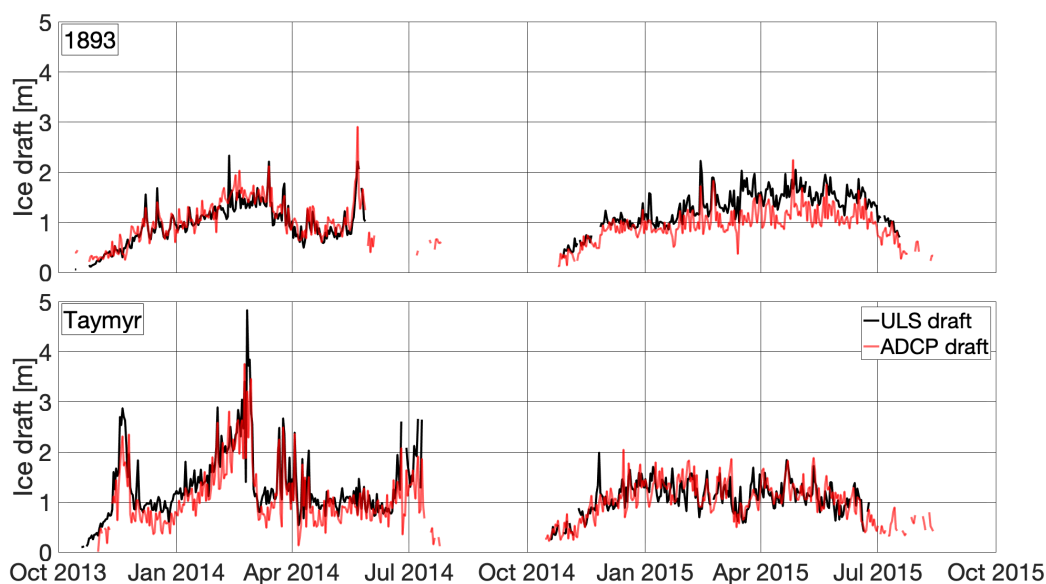


Figure 3.6: Daily mean sea ice draft time series derived from moored ULSs (black) and ADCPs (red) from the 1893 (top panel) and Taymyr (bottom panel) stations.

ings in 14/15 (Tab. 3.1). Figure 3.6 shows the agreement of the ULS and ADCP-derived time series with time. Dominant peaks in daily mean ULS ice draft that developed over longer time periods were also observed by the ADCP.

In the following we focus on a number of statistical values to compare ADCP and ULS-derived daily mean ice draft: minimum/maximum values, mean, median, modal values, percentage deviation as well as the range and offset between first and third quartiles. We also use these values to determine general offsets that occur for all data sets in order to define a general correction factor for ADCP-derived daily mean ice draft. Negative deviations indicate an overestimation of ADCP-derived ice draft compared to the ULS data while positive deviations represent an underestimation.

The percentage deviations of ADCP-derived daily mean sea ice drafts from the ULS-derived daily mean sea ice drafts are shown in Fig. 3.7. Other than the correlation coefficients, mean differences and percentage deviations between ULS and ADCP-derived ice draft indicate potential offsets between the compared time series in general. The daily percentage deviation values are variable and show large outliers but are consistent over time for three of the four data sets. The 1893-14/15 deviations between ULS and

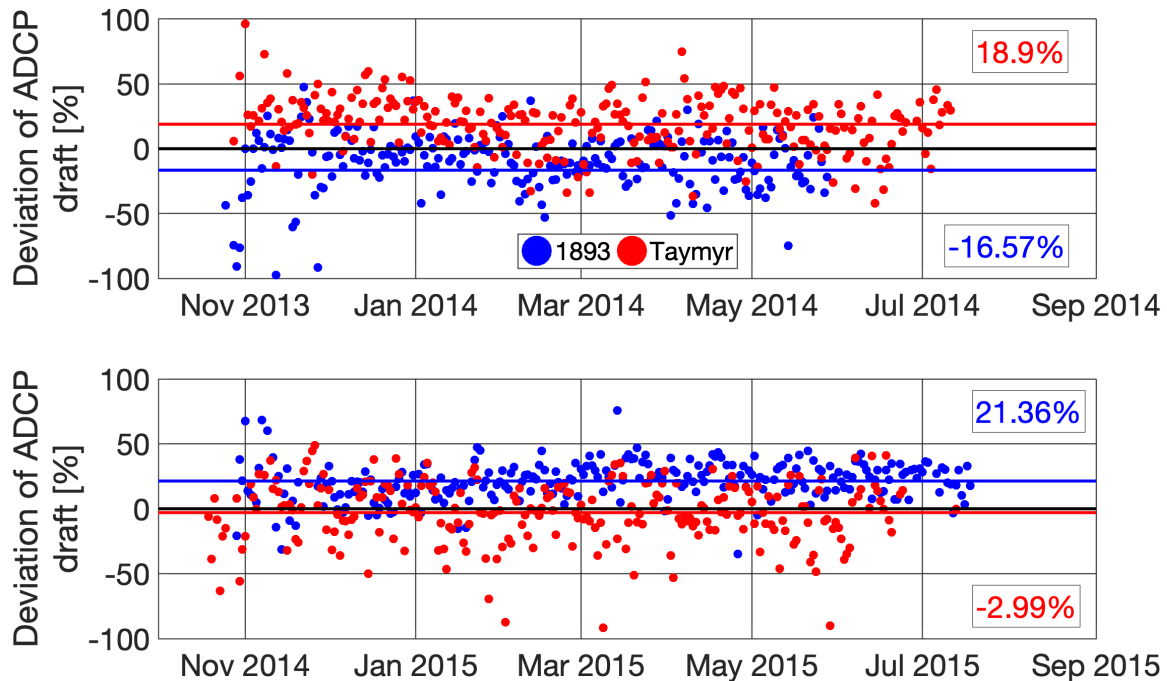


Figure 3.7: Percentage deviation of ULS-derived daily mean sea ice draft from ADCP-derived daily mean sea ice draft at 1893 (blue) and Taymyr (red) stations. Upper (lower) panel shows the 2013-2014 (2014-2015) sampling period. Solid lines indicate the mean percentage deviation of the ULS-derived to the ADCP-derived daily mean sea ice draft. The respective mean values of the percentage deviation are given on the right hand side (1893 in blue, Taymyr in red).

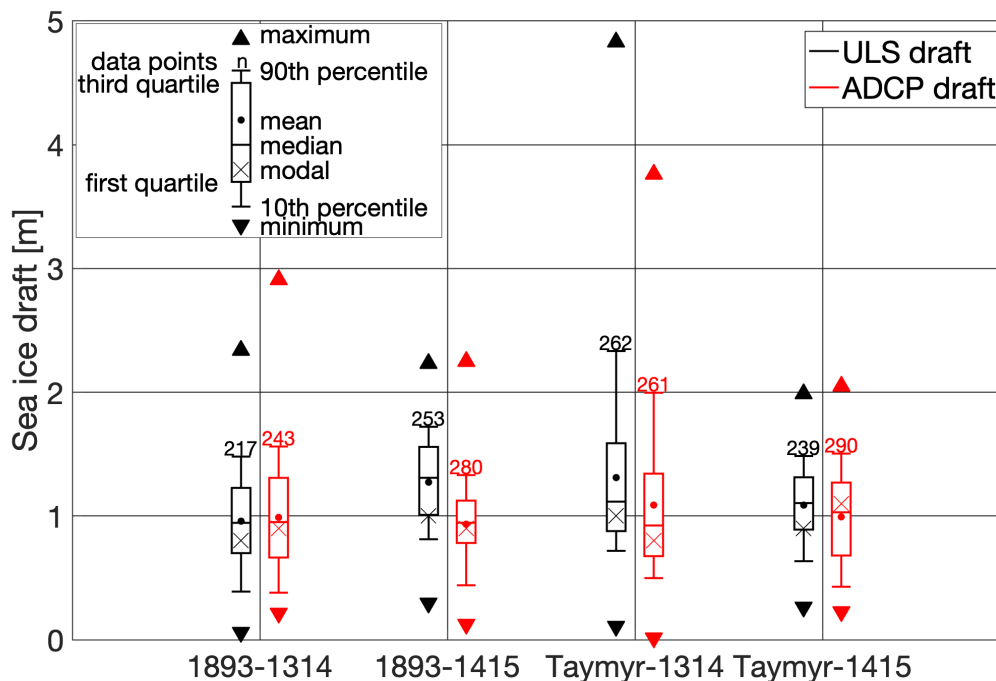


Figure 3.8: Boxplots for daily mean sea ice draft data derived from ULS (black) and ADCP (red). Boxes indicate first and third quartiles, while whiskers show 10th and 90th percentiles of the daily mean ice draft. Filled circles display means over the sampling period, while the horizontal dash gives median values. The cross marker provides modal draft values that were evaluated in 0.1 m bins and the number gives the number of data points that went into the statistics. Upward-pointing (downward-pointing) triangles indicate maximum (minimum) ice draft values. Data is shown for the stations 1893 and Taymyr and for the two sampling periods 2013-2014 (13/14) and 2014-2015 (14/15).

ADCP-derived draft seem to show a small increasing trend over the sampling period. On average ADCP-derived draft exceeds ULS draft by 16.60 and 2.99% for the 1893-13/14 and Taymyr-14/15, respectively. For the 1893-14/15 and Taymyr-13/14 data the ADCP underestimates ULS draft by 21.36 and 18.90%. Daily percentage deviation values indicate a general overestimation (underestimation) by the ADCP for 1893-13/14 (1893-14/15 and Taymyr-13/14), while Taymyr-14/15 shows no overall tendency for over-or underestimation.

The largest mean differences are 0.29 m at station 1893 in 14/15 and 0.25 m at Taymyr station in 13/14 (Fig. 3.8). Negative mean differences larger than -0.10 m occur for the 1893-13/14 and Taymyr-14/15 time series pairs. Largest single data point differences occur during spring seasons of both sampling periods (February-March), which also coincide with the largest daily mean ice draft values throughout the individual time series (not shown).

The differences between minimum daily mean ice draft range from approximately -0.15 m to 0.17 m, while three out of four difference values indicate an underestimation of the minimum ice draft by the ADCP. Maximum ice draft value differences range from approximately -0.70 m to 1.10 m. These largest differences occur for the two stations with the thickest ULS drafts of all the four time series.

Least differences between mean ULS and ADCP and median ULS and ADCP draft values occur for the 1893-13/14 time series. For the other three data set pairs ADCP-derived values underestimate ULS means and medians by approximately 0.10 to 0.37 m. Modal values differ between -0.20 and 0.20 m with no consistent indication for over or underestimation from the ADCP-derived data.

The spread between 10th and 90th percentiles is consistent for ULS and ADCP for the four time series pairs. However, except for the 1893-13/14 data, differences between the ULS and ADCP draft values indicate an underestimation of ice draft from ADCP data. This difference is especially pronounced for the 1893-14/15 and Taymyr-13/14 data sets.

After careful evaluation of the above-mentioned statistical values no consistent offset can be determined. Differences that occur for one or two statistical values at individual stations do not necessarily occur for others. However, in cases of notable differences between ULS and ADCP time series, more often than not, an underestimation of ADCP-derived ice draft compared to ULS-derived values is apparent.

3.4 Discussion

The ADCP's general instrument setup is designed to measure velocity fields within the water column rather than to derive sea ice draft. Therefore, the systematic errors introduced in the ADCP-derived ice draft time series are inherently larger than for ULS-based ice draft measurements. In order to reduce these errors previous studies (Shcherbina et al., 2005; Hyatt et al., 2008) developed and applied correction terms for beamwidth bias and sound speed variations. Both terms aim at correcting absolute range values that are required for the derivation of ice draft based on pressure-derived instrument depth. In contrast, to utilise the available Laptev Sea ADCP data we had to overcome the lack in auxiliary pressure data. Hence, contrary to the work of Shcherbina et al. (2005) and Hyatt et al. (2008) our approach is solely based on BT range values to determine instrument depth. This means that our retrieved open water range values are affected by the above-mentioned biases and errors as well as the range values during ice-covered periods. The largest error is introduced by the rather crude assumption of a constant quasi-depth per beam throughout the entire sampling period. ADCP moorings were deployed at water depths between 45 to 80 m with approximate instrument depths varying from 34 to 46 m. With mooring lengths between 29 and 59 m and inevitable mooring motion the assumption of one constant depth throughout the sampling period is unrealistic. However, for the presented data sets the agreement between ADCP and ULS-derived daily mean sea ice draft shows better results for the assumption of a constant instrument depth compared to calculations with time-varying depth.

In the following we discuss the mentioned correction terms and the extent to which we have considered them for the presented approach. In addition, we will discuss uncertainties of the final data product that can be expected when applying the presented approach of

determining instrument depth from open water BT range values. This is followed by an analysis of deviations and differences between ULS and ADCP-derived draft time series that we found in the results.

3.4.1 Open water detection

The presented open water detection is based on the assumption that all flag values in the error velocity output data result from large inhomogeneities in the velocity field at the surface during open water conditions. However, it has to be noted that these flag values can also occur from malfunctioning beams and outliers (Teledyne RDI, 2011). Even so, our selected open water data points are almost exclusively found during freeze up, melt and ice-free periods of the ADCP time series. This is expected, as open water areas are most frequent during these periods. For short beam malfunctions and outliers, the error velocity data is likely to indicate open water periods during winter, which is not the case for the presented data. We conclude that beam malfunctions and outliers, if at all, only occurred for a few isolated measurements and not over longer time periods. Furthermore, it is valid to assume that malfunctions of individual beams not only yield flag values in the error velocity output but also in the range output of the ADCP. Consequently, range values would not have been available for the retrieval of instrument depth, if the open water data point was selected erroneously.

Filtering of outliers and signal spikes that do not represent physical processes is a very important step in signal processing (Starkenburger et al., 2016). However, raw ADCP BT data is only filtered for spikes that were caused by physical processes like double bounces or returns from bubbles and biota in the water column. Further processing is not conducted because even single outliers of BT range values do not affect our instrument depth determination since the instrument depth is defined as the most frequent open water BT range value (Fig. 3.4). Individual data points can still be erroneous. However, the careful analysis of the open water data, the ADCP-internal ensemble averaging, the selection process of the instrument depth, the averaging over the four beams as well as the final averaging to daily mean values ensure that the impact of these outliers on the presented final data product is negligible.

For the presented case error velocities were flagged for values larger than 1 m/s. This value was pre-set for the given ADCPs and we consider it a definitive indicator for open water conditions. Smaller error velocity thresholds were applied as well, however, none of them increased the number of open water readings during winter. Therefore, no continuous instrument depth time series could be determined and a constant instrument depth is used for the calculation of ADCP draft. The crude assumption of constant instrument depth throughout the sampling period is the result of the continuous winter-time ice cover in the Laptev Sea region and the ADCP sampling frequency.

3.4.2 Tilt and beamwidth bias

The beamwidth bias arises from the general configuration of the ADCP (Fig. 3.2) and is dependent on instrument tilts, instrument depth and the roughness of the reflecting surface. Changes in instrument depth and tilts, e.g. through currents, result in a change

in beam footprint. Due to the beamwidth of 3.8° and the default mounting angle (20° to the normal incidence) of the ADCP beams the location of the echo maximum is shifted to indicate smaller range values (Shcherbina et al., 2005). Because of the skewed elliptical footprint and the coincidental shift of the echo intensity maximum, the effective beam angle is smaller than the nominal one. Consequently, BT range values are biased low. Considering a constant instrument depth, this bias is more pronounced during open water periods than during ice-covered periods as the reflecting ice surface is closer to the instrument than the open water surface.

The above-mentioned underestimation of range due to the beamwidth bias is based on the assumption of level surface conditions. Naturally, ice and water surfaces are rough which introduces additional errors (Shcherbina et al., 2005). As a consequence of comparably large instrument tilts these errors vary with ice deformation and increasing ice thickness as the insonified area changes (ASL, 2017). Due to the limited knowledge about the roughness of the reflecting surface it is almost impossible to define an accurate beamwidth bias correction term without external data.

In summary, for the first-year ice dominated Laptev Sea we assume level ice conditions and rely on internal range corrections for the default tilt angle of 20° to the normal incidence done by the ADCP. Furthermore, we correct the raw BT range data output for tilts measured by the ADCP (roll and pitch). This leads to an underestimation of all BT range values from the ADCP due to the difference between nominal and effective beam angle. The complex effects of changing beamwidth biases due to uneven ice surfaces are not considered due to the lack of data to quantify those variations. Accordingly, limitations and uncertainties arising from large tilts and footprint variations have to be accepted when applying the presented approach to derive ice draft time series from upward-looking ADCP BT data. However, since both, range and instrument depth are based on the biased BT range values the influences on the final draft values cancel each other out to some degree. Nevertheless, would it be beneficial to analyse additional ADCP/ULS data pairs to investigate how the agreement between ULS and ADCP-derived ice draft is affected by setups with larger tilts or deeper deployments of the ADCP. For the current setup on the shallow shelves in the Laptev Sea, the effects of the beamwidth bias are neglected.

3.4.3 Sound speed correction

Another important correction is required because of variations in water composition and the resulting change in two-way travel time of the emitted acoustic signal. There are multiple ways to correct for variations in sound speed.

The first correction approach is based on external measurements of water properties. Changes in temperature and salinity have an effect on how fast the acoustic signal travels through the water column. However, temperature and salinity, and therefore sound speed, not only vary in time but also within the vertical profile of the water column (Shcherbina et al., 2005; Hyatt et al., 2008). This means that in order to provide an accurate sound speed correction external measurements of temperature and salinity are required throughout the entire sampling period but also along the vertical profiles above the ADCPs.

Another way of correcting for changes in sound speed is based on the knowledge of open water periods, or 'zero drafts' (ASL, 2017; Shcherbina et al., 2005). Assuming a draft of zero (open water) in the uncorrected ice draft time series allows to compute a correction factor (using Eq. 3.1) from instrument depth, range and tilt. The correction factor, β , is considered to be the ratio of empirical to nominal sound speed. This approach is used to derive sea ice draft from the ULS (ASL, 2017). However, it requires accurate knowledge of instrument depth during times of open water which is not available from the presented Laptev Sea ADCP data. As mentioned before, open water periods derived from error velocity flag values almost exclusively occur during freeze up, melt and ice-free periods of the data sets, i.e. there is almost no open water data during winter. Additionally, the comparably long sampling interval of 1 h is not favourable to resolve open water, especially, as the hourly values consist of 60-value ensemble means. Therefore, the 'zero draft' approach is not applicable during the dominantly ice-covered winter months.

The presented approaches to correct for sound speed variations are based on accurate measurements of either temperature and salinity or pressure. For the Laptev Sea ADCPs we rely on available temperature and salinity data. BT range values are calculated using the speed of sound estimates based on the ADCPs internal temperature measurements and a pre-set constant salinity value that was measured at mooring deployment. This approach is valid since sound speed variations are more sensitive to changes in temperature than in salinity (Hyatt et al., 2008). However, it has to be noted that the impact of salinity changes over time are not negligible. This is especially true in the Laptev Sea which is characterized by seasonal variations in river runoff and surface salinity (Bauch et al., 2010). Due to a lack of additional measurements along the vertical profile the presented sound speed correction only takes temporal changes in sound speed into account.

As a consequence of the assumption of one constant quasi-depth per beam for the full sampling period, the long sampling intervals and the lack of auxiliary data, a more comprehensive sound speed correction, although preferable, is not possible in our case. We therefore rely on the ADCPs internal sound speed correction using temperature measurements and a constant salinity value.

3.4.4 Uncertainty estimates

Estimating the uncertainty of sea ice draft from upward-looking ADCPs is challenging and requires a number of assumptions about the influencing parameters. Uncertainties of the derived sea ice draft values arise from the ADCP range and tilt measurements as well as the determination of instrument depth, beamwidth bias and sound speed variations. Corrections for these parameters depend on information about roughness of the reflecting surface, vertical and temporal changes in water composition and accurate pressure measurements from the ADCP. Most of these additional details were not available for this study because they were not routinely measured from the moorings. To provide a rough uncertainty estimate we consider all available data to determine the uncertainties of the parameters involved in Eq. 3.3.

There are two sources of uncertainty: random uncertainties that arise from measurement fluctuations and systematic uncertainties that have a specific cause and occur for all measurements equally. Biases and systematic uncertainties are very much dependent on

the specific instruments and need to be considered for each data set separately. For the presented estimation of sea ice draft uncertainty we focus on the random uncertainties of the individual parameters of Eq. 3.3.

In order to determine the individual uncertainties that combine for the total uncertainty of the hourly mean sea ice draft from upward-looking ADCPs, σ_d , we divide Eq. 3.3 into two parts and estimate uncertainty for each one of them separately. Following the Joint Committee for Guides in Metrology (JCGM, 2008) the combined total uncertainty is given by:

$$\sigma_d = \frac{\sqrt{\sum_{i=1}^n \sigma_{z_i}^2 + \sigma_{r_{i\phi}}^2}}{\sqrt{n}}, \quad (3.4)$$

with σ_{z_i} being the uncertainty of the instrument depth and $\sigma_{r_{i\phi}}$ the uncertainty of the tilt-corrected range for each of the n beams.

Range uncertainty

Since the tilt-corrected raw ADCP range output is the basis for determining instrument depth we first estimate the uncertainty of the hourly ADCP range values. Following (Teledyne RDI, 2011), the range measurement uncertainty, σ_{r_i} , is about $\pm 1\%$ of the total measured range which means that it varies throughout our sampling periods. For the depths of the four presented ADCPs, uncertainties range from approximately ± 0.3 to ± 0.5 m. The ADCP hourly range data output is an ensemble mean of 60 values that were measured at a 1 min sampling interval. Although range values certainly differ on the scale of minutes the ADCP output data only provides one ensemble mean value. In order to estimate the uncertainty of the hourly range values we assume that the range variations within one hour are small enough so that each measurement can be considered one of a 60 sample measurement of an hourly range value. This assumption is necessary since the initially measured 60 hourly values are not available. Following this assumption the uncertainty of the ensemble mean range value decreases with $\sqrt{60}$. For longer sampling and averaging intervals this assumption needs to be reconsidered since variability of the individual values adds to the uncertainty of a mean value.

The ADCP corrects for the default 20° mounting angle to the vertical and for sound speed variations internally, which means that the estimated range uncertainty, σ_{r_i} already includes the uncertainties that arise from these corrections. We therefore consider σ_{r_i} to be the uncertainty of the raw hourly ADCP range values that were retrieved from the instrument after mooring recovery.

Before calculating instrument depth and sea ice draft, raw ADCP range data is corrected for additional instrument tilt. The uncertainty of the ADCPs tilt sensors, σ_ϕ , is approximately $\pm 1^\circ$ (Teledyne RDI, 2014). The uncertainty is calculated into the range equivalent for each measurement and beam individually. Like the range uncertainty it is specific to every data point and variable throughout the sampling period. Combining σ_{r_i} and σ_ϕ as the root sum of their squares (JCGM, 2008) provides the uncertainty of the tilt-corrected hourly range values, $\sigma_{r_{i\phi}}$.

Instrument depth uncertainty

The parameter introducing the biggest fraction to the combined uncertainty of hourly sea ice draft values is the instrument depth. Instrument depth is determined to be the most frequently occurring open water range value (modal open water range) and is calculated for each ADCP beam individually. We assume the distribution of open water range values from the ADCP to be approximately normal. This is valid since the high temporal resolution range measurements from the ULS show that open water range values are in fact distributed normally. Deviations from the normal distribution visible in the ADCP open water range data (Fig. 3.4) are likely a result of the averaging to hourly range values and the inherent low temporal resolution of the ADCP data. The assumption of normal distribution of open water range values allows us to roughly estimate the uncertainty of the modal open water range from the standard deviation of all open water range values. Since instrument depth is determined based on ADCP open water range values its combined uncertainty is the root sum of the squared tilt corrected range uncertainty, $\sigma_{r_{i\phi}}$, and the uncertainty of selecting the modal open water range, σ_{z_i} , squared.

Following the averaging over the four ADCP beams (Eq. 3.4) the mean combined uncertainty for the four presented hourly ADCP sea ice draft time series is approximately ± 0.96 m. Instrument depth uncertainty dominates this value and leads to almost constant uncertainty throughout the entire sampling period. Due to the limited amount of data available this can only be considered a rough uncertainty estimate. Furthermore, it has to be noted that this average uncertainty value is only valid for the presented ADCP hourly sea ice draft time series. Uncertainties of the four presented sea ice draft time series are very similar but need to be estimated for each new data set individually. The uncertainties of the daily mean values are even larger as the daily mean values are also dependent on the variance of the hourly values.

3.4.5 ULS versus ADCP-derived ice draft

Deviations between ULS and ADCP-derived daily mean drafts are expected simply due to the different processing of range data from the compared systems. Furthermore, upward-looking ADCPs and ULSs were never deployed at the exact same location, which certainly leads to deviations in the final results as different pieces of sea ice were sampled. Nevertheless, corresponding ULS and ADCP-derived ice draft time series show strong correlations (Fig. 3.5). Regardless of these correlations, offsets between ULS and ADCP-derived time series are apparent for individual data pairs (Figs. 3.7 and 3.8). These offsets are not consistent for the four presented data pairs and can therefore not be attributed to deficiencies in the presented method of deriving sea ice draft from upward-looking ADCPs. In fact, underestimations of ADCP results from stations Taymyr-13/14 and 1893-14/15 are likely to result from a sensor-specific bias. Data from these two stations originates from the same ADCP sensor (RDI ADCP 300 kHz, serial number: 12667) and the mean percentage deviations (18.90 and 21.36%) and mean underestimations (0.25 and 0.29 m) of the two data sets are of a similar magnitude. After the recovery in autumn 2014 the Taymyr mooring was redeployed at the 1893 mooring site for the 14/15 sampling period. The assumption that the offset is systematic, induced by the specific sensor, is confirmed by the fact that the correlation coefficients from the respective data pairs are not affected.

Correlation coefficients between ULS and ADCP-derived ice draft time series are 0.89 and 0.80, respectively. While the 1893-13/14 ULS followed the same deployment-redeployment pattern the ADCP sensor was substituted and a new sensor was deployed at the Taymyr station for the 14/15 sampling period. The corresponding mean differences between the two ULS and ADCP-derived time series indicate a comparably small overestimation by these ADCPs. On average the unbiased ADCP-derived daily mean drafts overestimate the ULS drafts by approximately 0.1 m.

The variations in correlation coefficients likely result from the inherent superiority of the ULS over the ADCP data, but more importantly the fact that ULS and ADCP measured at different locations. In fact, the highest correlation coefficients between ULS and ADCP-derived time series occur for the cases where ULS and ADCP moorings have been deployed closest to each other. The agreement of the daily mean draft time series is very dependent on whether the same ice is sampled by ULS and ADCP. With increasing distance between ADCP and ULS mooring the likelihood of measuring the same ice is decreasing due to the strong dependency on the direction and speed of the ice drift. Therefore, it might be valid to assume that a comparison of ice draft values from ADCP and ULS that are approximately 0.99 or 2.85 km apart from each other is not justified. However, it is impossible to compare the same pieces of sea ice for the given two-mooring setup. The fact that daily means are compared accounts for some of the influence by sea ice drift in regions that are very similar in ice type. Therefore, the displacement between ULS and ADCP moorings is considered small enough for a comparison of their sea ice draft time series.

In summary, deviations between ULS and ADCP-derived daily mean ice draft time series occur due to the distances between the corresponding moorings. Offsets arise from systematic errors induced by a specific sensor, but not from the general deficiencies of the presented method. However, it has to be acknowledged that the agreement between ULS and ADCP-derived time series is favoured by the shallow water conditions in the sampling region and the fact that we are comparing daily mean values rather than hourly data. Effects of sound speed variations and beamwidth bias become more important with larger tilts and for deployments in deeper waters. Similar studies and comparisons between ULS and ADCP-derived drafts are required to confirm the validity of the presented method.

3.5 Conclusions

Daily mean ice draft time series can be derived using upward-looking ADCPs, even if auxiliary pressure sensor data is not available. Previous efforts to derive ice draft from ADCPs relied on accurate pressure recordings to calculate ADCP instrument depth. However, we show that instrument depth can also be inferred from BT range values during open water periods. The distinction between ice-covered and open water periods is based on error velocity output data from the upward-looking ADCP.

Although this method is not sufficient to derive high-frequency ice draft time series, like ULS systems, it provides a low-cost opportunity to compute daily mean ice draft from upward-looking ADCP BT data that is, on average, within approximately 20% of the ULS-derived draft. More importantly, it allows to revisit existing ADCP records that have not been utilised to derive ice draft time series due to their lack in auxiliary pressure

data. For the four presented ADCP data sets the uncertainty of the hourly sea ice draft values is approximately ± 0.96 m on average. However, every ADCP data set and the corresponding uncertainties should be evaluated carefully, since higher sampling frequencies or ice regimes different from the one in the Laptev Sea allow for more sophisticated detections of instrument depth.

The ADCP data utilised in this study was recorded to provide complementary ice drift data to ULS draft time series. This fortunate setup with the two moorings being deployed next to each other enabled us to reference the ADCP-derived ice drafts to ULS-derived data that is considered to be the primary source of high-frequency, high-precision ice draft time series. The comparison to ULS data was one key factor missing for previous derivations of ice draft time series from upward-looking ADCPs and validates our presented approach. However, we have to point out that more comparisons are required to further validate the presented results.

The presented method is explicitly not a substitute for ice draft time series derived from ULS and will never reach the same level of accuracy or temporal resolution. Future ice draft measurements should still be conducted using ULSs or, if necessary, upward-looking ADCPs with higher sampling frequencies and additional pressure sensors. Furthermore, pre-ULS data from upward-looking ADCPs with reliable pressure information should be processed following the methods published by Shcherbina et al. (2005) and Hyatt et al. (2008). However, the presented method adapts to the data and instrument limitations in regions where ULS records are limited or simply not available and enables the extension of ice draft time series into the past with data that simply was not suitable for that purpose so far. Based on the ADCP data that is made available because of this study, the sea ice draft data archive of the Laptev Sea can be extended significantly. This data is vital, since the Laptev Sea is among the most difficult to access and hence understudied marginal seas in the Arctic. Furthermore, we gain access to unique validation data for sea ice thickness products from satellite missions such as CryoSat-2, SMOS or ENVISAT.

Acknowledgements

This study was carried out as part of the BMBF-funded Russian-German research cooperation QUARCCS (grant: 03F0777A). Moorings were deployed and recovered within the framework of the Russian-German project CATS/Transdrift (grant: 63A0028B). Special thanks to all the people involved on the various expeditions.

The 2013/2014 ULS data sets were processed by ASL Environmental Sciences Inc., Victoria, BC, Canada. ASL also provided valuable support and the toolboxes for the processing of the 2014/2015 ULS data sets. Additionally, the ECMWF provided ERA-Interim reanalysis surface pressure data (Dee et al., 2011) that was valuable for the ULS processing.

Data availability

ULS and raw ADCP bottom track data are accessible at the Data Publisher for Earth & Environmental Science PANGAEA (Belter et al., 2019a,b).

4 Satellite-based sea ice thickness changes in the Laptev Sea from 2002 to 2017: comparison to mooring observations

Published in *The Cryosphere*, 14, 2189-2203, <https://doi.org/10.5194/tc-14-2189-2020>

Belter, H. J.¹, T. Krumpfen¹, S. Hendricks¹, J. A. Hoelemann¹, M. A. Janout¹, R. Ricker¹, and C. Haas¹

¹*Alfred Wegener Institute, Helmholtz Centre for Polar and Marine Research, Bremerhaven, Germany*

Author contributions

HJB processed ULS and ADCP data, carried out the analysis and wrote the manuscript. All authors contributed to the discussion and provided input during the writing process. In addition to their input to the manuscript, TK conducted the backward-tracking of sea ice from the different mooring locations, SH provided CCI-2 data and conducted the analysis of CCI-2 sea ice thickness anomalies in the Laptev Sea and RR contributed CS2SMOS sea ice thickness data to the analysis. JAH and MAJ deployed and recovered ULS and ADCP moorings during multiple expeditions to the Laptev Sea.

Abstract

The gridded sea ice thickness (SIT) climate data record (CDR) produced by the European Space Agency (ESA) Sea Ice Climate Change Initiative Phase 2 (CCI-2) is the longest available, Arctic-wide SIT record covering the period from 2002 to 2017. SIT data is based on radar altimetry measurements of sea ice freeboard from the Environmental Satellite (ENVISAT) and CryoSat-2 (CS2). The CCI-2 SIT has previously been validated with in situ observations from drilling, airborne remote sensing and electromagnetic (EM) measurements and Upward-Looking Sonars (ULS) from multiple ice-covered regions of the Arctic. Here we present the Laptev Sea CCI-2 SIT record from 2002 to 2017 and use newly acquired ULS and upward-looking Acoustic Doppler Current Profiler (ADCP) sea ice draft (VAL) data for validation of the gridded CCI-2 and additional satellite SIT products. The ULS and ADCP time series provide the first long-term satellite SIT validation data set from this important source region of sea ice in the Transpolar Drift. The comparison of VAL sea ice draft data with gridded monthly mean and orbit trajectory CCI-2 data, as well as merged CryoSat-2/SMOS (CS2SMOS) sea ice draft shows that the agreement between the satellite and VAL draft data strongly depends on the thickness of the sampled ice. Rather than providing mean sea ice draft the considered satellite products provide modal sea ice draft in the Laptev Sea. Ice drafts thinner than 0.7 m are overestimated, while drafts thicker than approximately 1.3 m are increasingly underestimated by all satellite products investigated for this study. The tendency of the satellite SIT products to better agree with modal sea ice draft and underestimate thicker ice needs to be considered for all past and future investigations into SIT changes in this important region. The performance of the CCI-2 SIT CDR is considered stable over time, however, observed trends in gridded CCI-2 SIT are strongly influenced by the uncertainties of ENVISAT and CS2 and the comparably short investigation period.

4.1 Introduction

Sea ice is one of the most important indicators for climate change in the Earth's polar regions. Two of the primary parameters that are studied in this context are sea ice concentration (SIC) and sea ice thickness (SIT). While knowledge about SIC is widely available it provides limited insight into overall sea ice changes. A joint evaluation of SIC, SIT and sea ice drift is required for the analysis of sea ice mass balance, volume transports and the overall energy balance (Laxon et al., 2013), which comprehensively explain the complex sea ice state.

While in situ measurements of SIC and SIT are limited in time and space, satellite measurements of both parameters provide the means to assess Arctic-wide changes in the sea ice cover. Satellite remote sensing of SIC started in the 1970s with passive microwave sensors (Parkinson et al., 1999) and was further developed, updated and improved by multiple follow-on mission (Comiso and Nishio, 2008; Cavalieri and Parkinson, 2012; Lavergne et al., 2019) until today. While these measurements provide about 40 years of continuous SIC records, SIT satellite records of comparable length are not available. The longest existing SIT data record (from 2002 to 2017) was published by the European Space Agency's (ESA) Sea Ice Climate Change Initiative (CCI). The current SIT data record is

sufficiently long to achieve the objective of a long-term SIT climate data record (CDR) in the Arctic Ocean and is based on radar altimetry data from the Environmental Satellite (ENVISAT, 2002-2012) and from the CryoSat-2 (CS2) mission that was launched in 2010. SIT remote sensing with radar altimetry relies on retrievals of sea ice freeboard and is therefore an indirect method that is based on certain assumptions and parametrizations that introduce a number of uncertainty factors. These uncertainties can be separated into intrinsic uncertainties that arise from the radar measurements themselves and uncertainties that are induced during the ensuing processing. Processing uncertainties include: the impact of snow on radar backscatter and surface roughness on radar ranging and thus the retrieved elevation of the ice surface, the correct discrimination of sea ice and lead surface types with evolving altimeter footprints, the unknown variability of snow mass and snow and sea ice density that go into the conversion of freeboard to thickness (Wingham et al., 2006; Laxon et al., 2013; Ricker et al., 2014).

The CCI Phase 2 (CCI-2) SIT product was validated with observational data from multiple sources (Kern et al., 2018) including, in situ drill holes from a number of North Pole (NP) drift campaigns (Kern et al., 2018), observations from airborne and ground-based electromagnetic (EM) measurements (Haas, 2004; Haas et al., 2009, 2010), airborne remote sensing measurements from the Operation IceBridge (OIB) (Kurtz et al., 2013) and ice draft measurements from Upward-Looking Sonars (ULS) (Hansen et al., 2013; WHOI, 2014; NPI, 2018). However, these measurements are limited mainly to multi-year ice (MYI) dominated regions of the Arctic. While NP drill holes data is limited to the central Arctic, most airborne EM flights took place in the vicinity of Fram Strait, Lincoln Sea and in the Chukchi and Southern Beaufort Sea. ULS measurements were limited to Fram Strait (Hansen et al., 2013) and the Beaufort Sea (WHOI, 2014).

The Russian Shelf Seas are a region where observational data is very limited and which therefore has not been considered for the validation of the CCI-2 SIT CDR. At the same time the Russian Shelf Seas are also regarded to be the most important source regions of Arctic sea ice with the Laptev Sea being the origin of most of the sea ice passing Fram Strait (Rigor et al., 2002; Hansen et al., 2013; Itkin and Krumpfen, 2017). The Laptev Sea is located between the Siberian coast, the New Siberian Islands to the east and Severnaya Zemlya to the west (Fig. 4.1). It is ice-covered from October to June (Bareiss and Goergen, 2005) and very shallow with water depths between 15 and 200 m (Timokhov, 1994). The Laptev Sea is dominated by fast ice, flaw polynyas and pack ice (Reimnitz et al., 1994; Bareiss and Goergen, 2005; Krumpfen et al., 2013). Sea ice is formed in the polynyas and continuously transported northward by the persistent offshore-directed winds (Timokhov, 1994; Krumpfen et al., 2013). Due to the continuous formation and export of ice the Laptev Sea sea ice cover is dominated by first-year ice (FYI).

Recent studies indicate a thinning of Arctic sea ice within the Transpolar Drift (Haas et al., 2008) and in Fram Strait (Krumpfen et al., 2019). According to Krumpfen et al. (2019) this thinning is a consequence of faster ice transport across the Arctic and leads to more frequent interruptions of the FYI flow from the Russian Shelves towards the Transpolar Drift. Whether fundamental changes of the sea ice cover in the source regions cause the observed thinning of Fram Strait sea ice, needs to be further investigated.

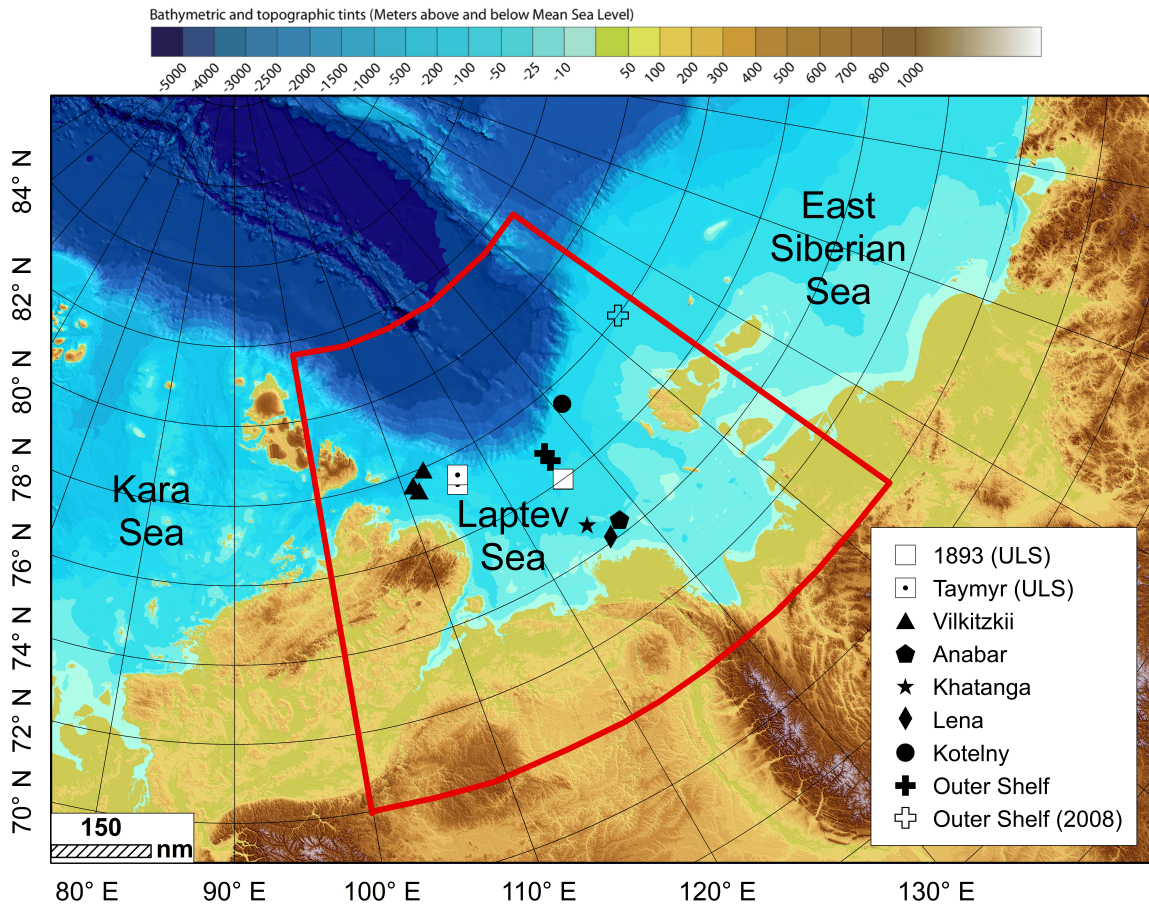


Figure 4.1: Map of the Laptev Sea showing the validation data (VAL) mooring sites. ESA CCI-2 SIT data from the enclosed area (red) was used for the calculation of satellite SIT anomaly (Fig. 4.2). IBCAO basemap provided by Jakobsson et al. (2008).

The available CCI-2 SIT CDR has not yet been fully exploited with respect to variability and trends on the Russian Shelves. This is partly due to the lack of validation data but also because the initial aim of the altimetry missions was to measure fluctuations in perennial SIT (Wingham et al., 2006) which is not prevalent in the FYI-dominated Russian Shelf Seas.

In order to close the observational data gap and validate the CCI-2 SIT CDR in this important source region of Arctic sea ice we present a new sonar-based sea ice draft data set from the Laptev Sea. This data set consists of ULS measurements from 2013 to 2015 and upward-looking Acoustic Doppler Current Profiler (ADCP) derived ice draft data that was acquired applying the approach of Belter et al. (2020c). Together with the ADCP-derived ice draft time series the full Laptev Sea validation (VAL) data set covers a period from 2003 to 2016. Since moored sonars are capable of detecting all ice types without a bias towards undeformed ice (Behrendt et al., 2015), this new data set provides comprehensive information about the full thickness range.

The objectives of this study are to examine the gridded monthly mean ESA CCI-2 SIT CDR and use the new in situ data set to evaluate its performance in the Laptev

Sea. We will analyse the time dependent stability of the CCI-2 SIT CDR in order to see whether potential trends in Laptev Sea SIT are caused by actual changes in SIT in the region or by a change in the ability of the satellites and the ensuing processing steps to characterize the Laptev Sea sea ice cover over time. In this context, stability is defined as the constancy of the mean difference of the CCI-2 SIT CDR to the Laptev Sea observational data. In addition, we will compare VAL data to satellite products with higher temporal resolution than the gridded monthly mean CCI-2 SIT CDR. Finally, the case study of the 2013/2014 ULS draft time series from the Taymyr mooring (Fig. 4.1) will highlight and further explain the findings of the presented comparison of satellite and sonar-derived sea ice draft time series.

The presented analysis will assist the interpretation and support future algorithm development of altimetry-based SIT CDR. It is an important addition to the existing validation data sets (Kern et al., 2018) and might provide the means to assess regional differences in the performance of the CCI-2 SIT products in the Arctic. For the Laptev Sea region the presented sonar-based data provides better interpretation and more confidence in the ESA CCI-2 SIT products. After all, this unique satellite-derived SIT record can be an important data set for future investigations into volume transports and will complement previous studies on the changes of the sea ice cover on the Russian Shelves.

4.2 Data and methods

4.2.1 Sonar-based ice draft measurements

The Laptev Sea sea ice draft time series were retrieved by two different instruments. The full ice draft time series from upward-looking ADCPs and ULSs (VAL) covers a period from 2003 to 2016 and was taken at water depths between 20 and 60 m. The data set consists of multiple one to two year long sea ice draft time series from a total of nine different locations all over the Laptev Sea (Fig. 4.1). This inconsistency in the location of the measurements is a considerable limitation for the analysis of sea ice draft variability in this region because we are not sampling a single location over the full period but multiple ones over short periods. Nevertheless, this data set provides important validation data to analyse the performance of satellite-derived sea ice draft over the Laptev Sea region. The proper validation of the satellite SIT products will then allow the targeted analysis of the long-term changes in SIT in this important region of sea ice formation.

Upward-Looking Sonar

ULSs measured from September 2013 to August 2015 at the Taymyr and 1893 stations (Belter et al., 2019b). The Laptev Sea ULSs were of the type Ice Profiling Sonar 5 (420 kHz, manufactured by ASL Environmental Sciences Inc.) and operated with a single vertical beam (1.8° beamwidth) at a sampling frequency of 1 Hz. Ice draft was inferred from measured values of range (distance between device and ice-water interface) and auxiliary measurements of instrument tilt, pressure and temperature at instrument depth (sampling frequency 1/60 Hz). Final sea ice draft time series with an approximate precision of ± 0.05 m were calculated as the difference between instrument depth and range

and corrected for instrument tilts and changes in sound speed (Ross et al., 2016; ASL, 2017).

Upward-looking ADCP

The second approach utilized upward-looking ADCPs to derive ice draft time series (Belter et al., 2020a). The available ADCPs were upward-looking Workhorse 300 kHz Sentinel ADCPs manufactured by Teledyne RDI. They measured with four different beams (beamwidth 3.8°) at a default angle of 20° from the vertical. Although ADCPs have been used to derive sea ice draft before (Shcherbina et al., 2005; Banks et al., 2006; Hyatt et al., 2008; Bjoerk et al., 2008), the Laptev Sea ADCPs were not equipped with reliable pressure sensors or lacked them altogether. These additional pressure measurements close to the ADCP proved essential for the determination of instrument depth. In order to determine instrument depth without additional pressure data Belter et al. (2020c) proposed an adaptive approach to derive instrument depth using ADCP bottom track mode measurements of surface and error velocity. Surface and error velocity provide measures for surface inconsistencies in vertical velocity between the four measuring beams. While vertical velocities are similar during ice-covered periods, large velocity differences indicate open water conditions (Belliveau et al., 1990). After determining open water and ice-covered periods the most frequently occurring open water range value was defined as instrument depth for the respective sampling period and mooring (Belter et al., 2020c,a). Ultimately, the approach by Belter et al. (2020c) yielded daily mean sea ice draft time series that are within ± 0.1 m of the reference draft time series from the coincidental ULS deployments in the Laptev Sea. Following their method we extended the existing Laptev Sea ULS sea ice draft time series with ADCP-derived sea ice draft in this vastly under-sampled source region of Arctic sea ice.

Sonar draft data processing

In order to compare daily VAL data to satellite SIT products, VAL data was averaged to weekly and monthly mean values. Open water values (draft values of zero) recorded by ULS and ADCP were excluded prior to weekly and monthly averaging of VAL sea ice draft. In cases where more than 50% of VAL data was missing or considered open water no weekly or monthly average VAL value was calculated.

4.2.2 Satellite data

ESA CCI-2 monthly mean gridded product

The ESAs CCI-2 SIT Level 3 collated (L3C) gridded product is based on pulse-limited radar altimeter measurements from ENVISAT (2002-2012) and along-track beam-sharpened Synthetic Aperture Interferometric Radar Altimeter measurements from the ongoing CS2 mission (Paul et al., 2018; Hendricks and Ricker, 2019b). The CCI-2 SIT data record is available on a 25×25 km EASE2 monthly grid in the Arctic winter season from October through April. The parameters available from the utilized monthly gridded L3C product include: freeboard, freeboard uncertainty, SIT and SIT uncertainty. For simplicity we distinguish between the CCI-2 ENVISAT gridded data (ENVISAT) for the period from 2003-2012 (Hendricks et al., 2018c) and CCI-2 CS2 gridded data (CS2) for

the period from 2010-2016 (Hendricks et al., 2018a). The separation of the two data sets that combine for the full CCI-2 SIT CDR is also required because of the different characteristics of the two satellite radar altimeters. Paul et al. (2018) identified differences in freeboard between ENVISAT and CS2 that are based on waveform parameter variations, footprint differences and the fact that ice surface properties are treated differently during the processing. These freeboard differences translate to the gridded monthly mean CCI-2 data presented here. Although Paul et al. (2018) minimized the inter-mission sea ice freeboard biases for the basin average, ENVISAT freeboards in MYI regions are still thinner than CS2 freeboards, while ENVISAT provides thicker freeboards than CS2 in regions that are dominated by FYI (Fig. 13 in Paul et al. (2018)). In the Laptev Sea typical ENVISAT (CS2) SIT uncertainties are 1.5 m (1.1 m).

ESA CCI-2 orbit data

The presented gridded monthly mean CCI-2 data is based on radar altimeter measurements along the orbit trajectories of ENVISAT and CS2 (Hendricks et al., 2018d,b). While the gridded mean data provides Arctic-wide monthly mean values of SIT, the orbital data sets (ENVISATorbit and CS2orbit) provide SIT and freeboard at sensor resolution (2 km in diameter for ENVISATorbit (Connor et al., 2009) and 0.3 km along and 1.5 km across-track for CS2orbit (Wingham et al., 2006)). Typical uncertainties of orbit SIT in the Laptev Sea are about 1.5 (ENVISATorbit) and 1.1 m (CS2orbit). The frequency of the overflights over a predefined 25 km area around the moorings varies between ENVISAT and CS2 due to their different orbit inclinations. However, with an average of about four overflights per month of both satellites orbit trajectory data delivers SIT at a higher frequency than the gridded CCI-2 data sets and allows for a comparison of observational data to a larger number of satellite values.

Merged CryoSat-2/SMOS data

The merged weekly CS2 and Soil Moisture and Ocean Salinity (SMOS) satellite record (CS2SMOS, Ricker et al. (2017)) provides an additional SIT data set with a higher temporal resolution than the gridded monthly mean CCI-2 SIT CDRs. SMOS utilizes 1.4 GHz (L-band) measurements of brightness temperature to retrieve SIT (Tian-Kunze et al., 2014). While the relative uncertainties of the altimetry-based method (CS2) are larger over thin ice regimes (below 1 m thickness), the radiometer-based method (SMOS) shows smaller relative uncertainties over these thin ice regimes (Ricker et al., 2017). Other than gridded CCI-2 and CCI-2 orbit data, CS2SMOS data is only available from 2010 onwards but provides weekly temporal resolution and shows typical uncertainties in the Laptev Sea of approximately 0.15 m. Furthermore, CS2SMOS combines the advantages of observing thick (> 1 m) and thin (< 1 m) ice with CS2 and SMOS, respectively, keeping the relative uncertainties for both ice regimes as small as possible (Ricker et al., 2017).

Satellite draft data processing

In order to be consistent with VAL sea ice draft data CCI-2 freeboard was subtracted from CCI-2 SIT to obtain CCI-2 gridded monthly mean and orbit sea ice draft. Since CS2SMOS SIT is derived by an optimal interpolation of two SIT products (Ricker et al.,

2017) and thus does not provide freeboard information, sea ice draft was calculated differently than for the CCI-2 products. CS2SMOS SIT was divided by a constant ratio of 1.136 to compute sea ice draft. This ratio between SIT and draft was derived through nearly 400 drillings of sea ice in Fram Strait (Vinje and Finnekasa, 1986) and is in good agreement with Arctic-wide SIT measurements from Russian drillings (Vinje et al., 1998). For the comparison to mooring-based VAL sea ice draft data, all satellite sea ice draft data points from within a predefined 25 km radius around the mooring site were selected and calculated into a weighted mean sea ice draft value. The weighted averaging accounts for the varying distances between the selected satellite data points and the mooring location and was done for each satellite product individually. Since all five data sets are based on radar altimetry data satellite sea ice draft data is only available from October through April.

4.2.3 **Data limitations**

VAL data

VAL data is based on sonar-derived ice drafts from two differing instruments. In general, the default setup, with a single narrow vertical beam and a sampling frequency of 1 Hz, makes the ULS the primary instrument for stationary long-term observation of sea ice draft. Although upward-looking ADCPs are based on the the same measurement principles they are build for measurements of currents and ice drift rather than sea ice draft. Consequently, the ADCP-derived sea ice draft time series are less accurate than ULS-derived time series (Belter et al., 2020c). As a result this study compares satellite data to VAL data sets of different quality. This compromise in data quality between ULS and ADCP was taken on because we consider the daily mean sea ice draft time series to be sufficiently accurate for the comparison to weekly and monthly mean sea ice draft from gridded satellite products. Since they are of sufficient quality, the ADCP-derived draft records allow us to significantly extend the available ULS-derived time series. Rather than analysing data from only two consecutive years we are able to investigate a time period of almost 13 years. The increased length of this unique Laptev Sea VAL data set is vital for the evaluation of the stability of the investigated CCI-2 records.

Despite the fact that we were able to extend our Laptev Sea VAL data set it has to be noted that in situ observations of sea ice draft are very limited in the Laptev Sea. The lack of mooring measurements over more than two years at any of the sampled locations prohibits us from comparing satellite data to VAL data from a single mooring location. Instead, the entire VAL data record is composed of one to two year time series from a total of nine different locations all over the Laptev Sea (Fig. 4.1). Although this inconsistency is unfavourable for the analysis of long-term variability of sonar-based SIT in this region the VAL data provides a new and unique validation record for the CCI-2 SIT CDR.

ESA CCI-2 gridded monthly mean draft data

Like the VAL data record, gridded and orbit CCI-2 data is based on measurements from two different systems. Inter-mission differences have been analysed previously and indicate that due to the different setups of the ENVISAT and CS2 radar altimeters the final SIT, and therefore draft, records contain residual intermission differences (Guerreiro

et al., 2017; Paul et al., 2018). These biases vary regionally and seasonally. The seasonal biases between ENVISAT and CS2 need to be considered for the temporal development of the Laptev Sea SAT-VAL differences between the two periods. For the Laptev Sea the ENVISAT SIT is, on average, approximately 0.22 m thicker than the CS2 SIT for the overlap period from November 2010 to March 2012.

In addition, the biggest limitation for the analysis of the performance of the gridded CCI-2 CDR is its temporal resolution of one month and its limitation to the period from October through April. This significantly limits the number of CCI-2 draft data points for the comparably short validation period from 2003 to 2016.

4.3 Results

4.3.1 ESA CCI-2 Laptev Sea SIT

The ESA CCI-2 SIT CDR shows no significant change of SIT in the Laptev Sea between 2002 and 2017 (Fig. 4.2). SIT anomaly was calculated for each month compared to the mean of the same month over the full period from 2002 to 2017. Anomalies were calculated for each grid point and averaged over the Laptev Sea (100-145 °E, 70-81.5 °N, enclosed area Fig. 4.1). Separating the CCI-2 CDR into the two satellite periods shows that the slightly negative, but highly uncertain, overall trend consists of opposing trends in SIT anomaly from the two CCI-2 data products. While the ENVISAT SIT anomaly (2002-

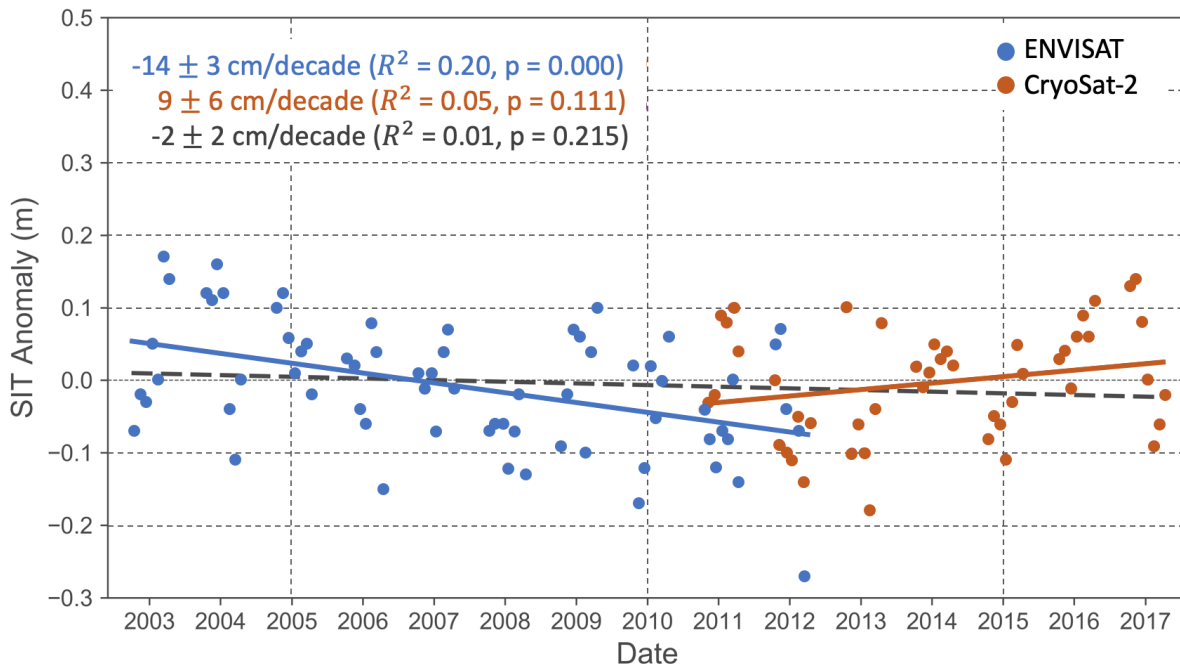


Figure 4.2: ESA CCI-2 gridded (25 km EASE grid) sea ice thickness (SIT) anomaly in the Laptev Sea. SIT anomaly was calculated for each month compared to the mean of the same month over the full period from 2002 to 2017. Anomalies were calculated for every grid point and averaged over a predefined area in the Laptev Sea (100-145 °E, 70-81.5 °N, enclosed area Fig. 4.1). R^2 provides the goodness of fit for each trend line.

2012) decreases by approximately 14 cm per decade, the trend in CS2 SIT anomaly shows an increase in SIT from 2010 to 2017. In order to investigate the validity of these satellite-derived trends in SIT anomaly the following section provides the results of the statistical analysis of the differences between VAL and satellite-derived sea ice draft data from the Laptev Sea. To determine the agreement between satellite and VAL sea ice draft data, values of root mean square difference (RMSD), mean difference and correlation coefficient (r) were calculated for each of the individual data sets from the stations shown in Fig. 4.1. For comparison between the ENVISAT and CS2 missions, averages of these three statistical parameters were calculated for all stations during the overlap period from November 2010 to March 2012.

4.3.2 Validation of CCI-2 products

Gridded monthly CCI-2 sea ice draft

Figure 4.3a shows the differences between gridded monthly mean CCI-2 and VAL sea ice draft (SAT-VAL difference) for the period from 2003 to 2016. Individual SAT-VAL differences show substantial scatter around zero but the overall trend (black line) indicates an almost constant mean difference of approximately -0.3 m over the full investigation period. The SAT-VAL differences are normally distributed around the mean SAT-VAL difference of approximately -0.3 m (Fig. 4.3b). Table 4.1 and 4.2 provide RMSD, mean difference and correlation coefficients between the gridded ENVISAT and CS2 and VAL draft data from each station, respectively.

For the ENVISAT period RMSD values average 0.70 m, with minimum RMSD of 0.37 m for the Anabar 2007/2008 and maximum RMSD of 1.0 m for the Khatanga 2008/2009 data. The average mean difference is -0.22 m indicating an average under-estimation of monthly mean sea ice draft by the ENVISAT data. The ENVISAT under-estimation of sea ice draft occurs for all but two data sets. Lena 2003/2004 and Outer

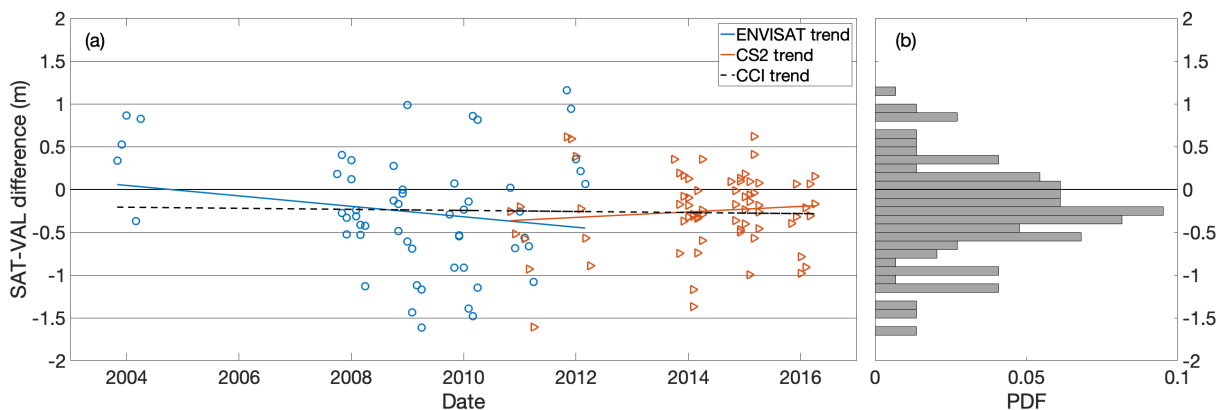


Figure 4.3: (a) Difference (SAT-VAL difference) between gridded monthly mean ENVISAT/CS2 and VAL ice drafts. VAL data consists of ice draft data derived from upward-looking ADCPs for the ENVISAT period (blue) and a combination of ADCP and ULS data for the CS2 period (orange). (b) Probability density function (PDF) of SAT-VAL differences over the full period from 2003 to 2016.

Table 4.1: Statistics of the comparison of gridded monthly mean ENVISAT and ENVISATorbit draft data with VAL mean sea ice draft for the period from 2003 to 2012. RMSD and mean difference were calculated for the differences of ENVISAT minus VAL mean sea ice draft. The Pearson correlation coefficient, r , was calculated for each station. Bold correlation coefficient values indicate significant correlation at the 95% confidence level. Bottom line values show the averages of RMSD, mean difference and correlation coefficient over all stations.

Period	Station	ENVISAT			ENVISATorbits		
		RMSD [m]	Mean difference [m]	r	RMSD [m]	Mean difference [m]	r
2003-2004	Lena	0.63	0.44	0.25	0.95	0.02	-0.05
2007-2008	Anabar	0.37	-0.17	0.53	0.75	-0.30	-0.01
	Khatanga	0.54	-0.30	0.43	1.20	-0.60	-0.01
2008-2009	Khatanga	1.00	-0.45	-0.14	1.06	-0.61	-0.02
	Outer Shelf	0.73	-0.60	0.90	0.92	-0.65	0.54
2009-2010	Anabar	0.75	-0.14	0.05	0.84	-0.09	0.20
	Khatanga	0.92	-0.72	0.81	1.11	-0.73	0.11
2010-2011	Outer Shelf	0.64	-0.54	0.86	0.84	-0.61	0.60
2011-2012	Outer Shelf	0.69	0.55	0.29	0.65	0.27	0.12
2003-2012	Mean	0.70	-0.22	0.44	0.93	-0.37	0.16

Shelf 2011/2012 mean differences are 0.44 and 0.55 m, respectively, indicating a mean overestimation of sea ice draft by the ENVISAT product at these stations. The average correlation coefficient between gridded monthly mean ENVISAT and VAL sea ice draft data is 0.44 for the period from 2003 to 2012. Results from multiple stations show little or almost no correlation, while correlations are significant at the 95% confidence level for data from only three stations.

Compared to ENVISAT, differences between gridded monthly mean CS2 and VAL sea ice draft show a smaller average RMSD (0.48 m) and a higher mean correlation coefficient (0.50). The average mean difference of -0.27 m is slightly more negative than for ENVISAT. This indicates a stronger mean underestimation of VAL sea ice draft by CS2 compared to ENVISAT. Mean differences are negative for all stations, showing consistent underestimation by CS2 data. Although the mean correlation coefficient is larger compared to the ENVISAT period none of the individual coefficients is significant at the 95% confidence level during the CS2 period.

By grouping VAL sea ice draft values in 0.2 m bins and comparing them to their corresponding monthly mean ENVISAT (2003 to 2012) and CS2 (2010 to 2016) sea ice draft values we are able to examine the agreement between gridded CCI-2 and VAL drafts along the full range of sea ice drafts that were measured by the moorings (Fig. 4.4). Both scatter plots indicate an overestimation by the gridded CCI-2 products for draft values below ap-

Table 4.2: Statistics of the comparison of gridded monthly mean CS2 and CS2orbit draft data with VAL mean sea ice draft for the period from 2010 to 2016. RMSD and mean difference were calculated for the differences of CS2 minus VAL mean sea ice draft. The Pearson correlation coefficient, r , was calculated for each station. Bold correlation coefficient values indicate significant correlation at the 95% confidence level. Bottom line values show the averages of RMSD, mean difference and correlation coefficient over all stations.

Period	Station	CS2			CS2orbits		
		RMSD [m]	Mean difference [m]	r	RMSD [m]	Mean difference [m]	r
2010-2011	Outer Shelf	0.83	-0.68	0.61	0.94	-0.65	0.39
2011-2012	Outer Shelf	0.58	-0.02	0.29	0.71	-0.06	0.38
2013-2014	1893	0.23	-0.06	0.71	0.22	-0.02	0.82
	Taymyr	0.68	-0.53	0.53	0.71	-0.47	0.43
	Kotelnyy	0.61	-0.41	0.74	0.61	-0.46	0.68
	Vilkitzkii	0.24	-0.02	0.46	0.44	-0.35	0.73
2014-2015	1893	0.55	-0.46	0.46	0.51	-0.39	0.55
	Taymyr	0.32	-0.27	0.70	0.41	-0.28	0.54
2014-2016	Vilkitzkii1	0.40	-0.02	0.10	0.57	0.02	-0.06
	Vilkitzkii3	0.40	-0.19	0.37	0.58	-0.14	0.21
2010-2016	Mean	0.48	-0.27	0.50	0.57	-0.28	0.47

proximately 0.7 m. The magnitude of the overestimation decreases with increasing draft. The best agreement occurs for draft values between 0.7 and about 1.2 m, while monthly mean VAL sea ice draft is underestimated for draft values above approximately 1.3 m. The underestimation increases with increasing ice draft values. Additionally, Fig. 4.4 shows that the variability of the ENVISAT draft values is substantially larger within the selected 0.2 m bins compared to CS2 draft values in the same bins. The difference in the performance of ENVISAT and CS2 data is also revealed for the overlap period between the two satellite missions (2010-2012). While mean differences show the same tendency with -0.54 m (ENVISAT, Table 4.1) and -0.68 m (CS2, Table 4.2) for the 2010-2011 Outer Shelf data sets, they disagree considerably for the 2011-2012 period (ENVISAT: 0.55 m, CS2: -0.02 m).

In order to complement the results shown for the comparison between gridded CCI-2 and mean VAL data, we conducted an additional analysis with satellite data products that are based on the measurements from the ENVISAT and CS2 missions and the gridded CS2 data but provide higher temporal resolution of sea ice draft than the gridded CCI-2 record. RMSD, mean difference and correlation coefficients were calculated for the comparison of sea ice draft from ENVISATorbit (Table 4.1) and CS2orbit (Table 4.2) trajectory data and merged CS2SMOS (Table 4.3) data with VAL sea ice draft data.

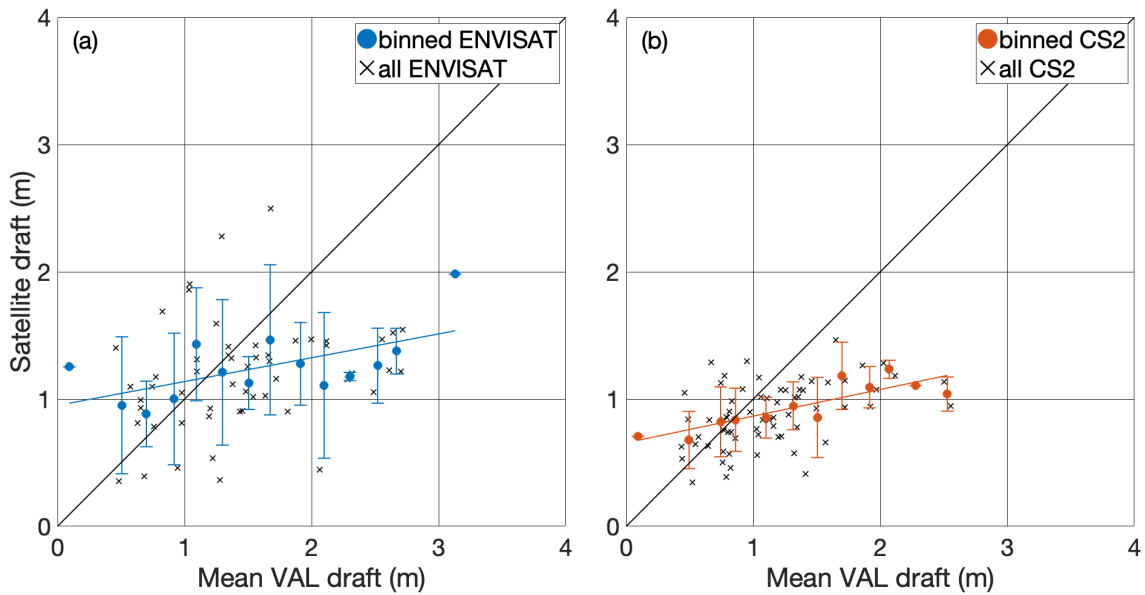


Figure 4.4: Scatterplot comparing gridded monthly mean CCI-2 sea ice draft to VAL sea ice draft (black crosses). Panel (a) shows the comparison for the ENVISAT period superimposed by the mean ENVISAT draft per 0.2 m VAL data bin, while panel (b) shows the same for CS2 data and period. Error bars indicate \pm one standard deviation of the CCI-2 data within the specific 0.2 m bin.

Orbit CCI-2 sea ice draft

While the average RMSD, mean difference and correlation coefficients are very similar for the VAL data comparison to gridded CS2 and CS2orbit, almost all stations show significant (at the 95% confidence level) correlations between CS2orbit and VAL sea ice draft (Table 4.2). ENVISATorbit data shows a higher average RMSD, stronger average underestimation of VAL sea ice draft and much lower average correlation with VAL sea ice drafts compared to the gridded ENVISAT data (Table 4.1). This suggests that the CS2 component of the CCI-2 CDR is superior to the ENVISAT sea ice draft data. It also confirms the inter-mission biases between ENVISAT and CS2 that were published by Paul et al. (2018).

Intercomparison of CCI-2 and merged CS2SMOS sea ice draft

The comparison of weekly CS2SMOS and VAL sea ice draft data reveals the largest average correlation coefficient. On the other hand, the CS2SMOS and VAL draft comparison also shows the largest average underestimation of any of the presented satellite data products. Figure 4.5 shows the comparison of the agreement between the gridded and orbit CCI-2 and the CS2SMOS data products with the corresponding VAL sea ice draft data. While the overall tendency of the gridded CCI-2 products to overestimate ice draft for thin ice and increasingly underestimate thickening ice is confirmed by CCI-2 orbit and CS2SMOS data a general offset between the individual satellite products is visible for most of the selected 0.2 m VAL data bins. While both ENVISAT draft data sets indicate thickest drafts over the full thickness range, gridded CS2 and CS2orbit agree

Table 4.3: Statistics of the comparison of gridded weekly mean CS2SMOS draft data with VAL mean sea ice draft for the period from 2010 to 2016. RMSD and mean difference were calculated for the differences of CS2SMOS minus VAL mean sea ice draft. The Pearson correlation coefficient, r , was calculated for each station. Bold correlation coefficient values indicate significant correlation at the 95% confidence level. Bottom line values show the averages of RMSD, mean difference and correlation coefficient over all stations.

Period	Station	CS2SMOS		
		RMSD [m]	Mean difference [m]	r
2010-2011	Outer Shelf	0.88	-0.70	0.41
2011-2012	Outer Shelf	0.48	-0.07	0.72
2013-2014	1893	0.32	-0.17	0.70
	Taymyr	0.92	-0.76	0.51
	Kotelnyy	0.73	-0.64	0.92
	Vilkitzkii	0.29	-0.18	0.78
2014-2015	1893	0.46	-0.42	0.80
	Taymyr	0.40	-0.36	0.77
2014-2016	Vilkitzkii1	0.50	-0.24	0.10
	Vilkitzkii3	0.59	-0.41	0.42
2010-2016	Mean	0.56	-0.39	0.61

rather well. CS2SMOS data shows smallest draft values throughout the entire thickness range compared to the CCI-2 products. The overestimation of sea ice draft values below 0.7 m that is apparent in the gridded and orbit CCI-2 data is minimized by the impact of SMOS on the merged CS2SMOS product. The Laptev Sea is dominated by newly formed and thinner FYI, accordingly the gridded merged product is dominated by SMOS data. Consequently the underestimation of sea ice draft with increasing thickness is largest for CS2SMOS because of the larger influence of SMOS data on the final SIT values in this region.

In summary, the gridded CCI-2 products underestimate monthly mean sea ice draft in the Laptev Sea by an average of -0.22 m (-0.27 m) during the ENVISAT (CS2) period. This underestimation by the monthly mean gridded CCI-2 products is not a constant bias. The agreement between gridded CCI-2 and VAL sea ice drafts is in fact dependent on the thickness of the observed ice. Thin ice (drafts < 0.7 m) is overestimated by the gridded CCI-2 products and thicker ice (drafts > 1.3 m) is increasingly underestimated with increasing ice draft. The overall spread in SAT-VAL difference values is smaller for the CS2 period. ENVISATorbit and CS2orbit and merged CS2SMOS sea ice draft data, which provide higher temporal resolution than the gridded monthly mean products confirm these results. It has to be noted that sea ice draft values from the four presented satellite products deviate considerably from one another.

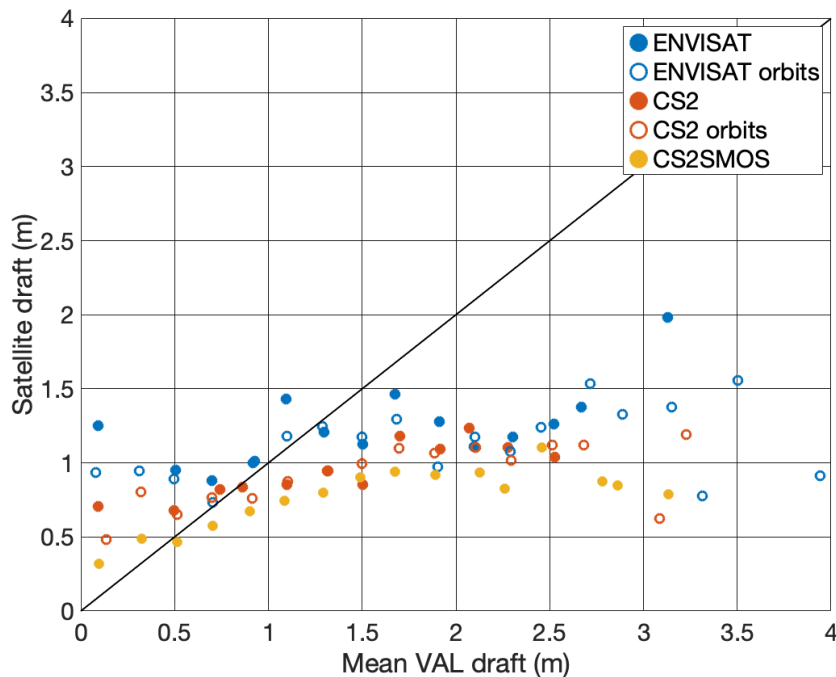


Figure 4.5: Mean sea ice drafts per 0.2 m VAL data bin from ENVISAT (filled blue circles), ENVISATorbit (blue circles), CS2 (filled orange circles), CS2orbit (orange circles) and CS2SMOS (filled yellow circles) data products.

4.4 Discussion

4.4.1 Comparability of satellite and sonar measurements

ENVISAT and CS2 average mean differences to VAL sea ice draft are of similar magnitude, which indicates a consistent average underestimation of Laptev Sea sea ice draft from the gridded monthly mean CCI-2 CDR between 2003 and 2016. In order to discuss these results and most importantly their meaning for the apparent trends in CCI-2 SIT in the Laptev Sea (Fig. 4.2) the deficiencies of the VAL and CCI-2 data products have to be examined.

The comparison between gridded satellite products and point measurements from moorings is by default challenging. A significant difference between sonar and altimetry-based measurements are the parameters that are measured. While moored sonars provide sea ice draft data, radar altimeters infer SIT from measurements of freeboard. Altimeter freeboard is converted into SIT based on parametrizations of snow depth and constant densities of snow and sea ice. Snow depth, snow and sea ice density are parameters that are not routinely measured and therefore are based on climatologies: modified Warren snow climatology and Warren snow water equivalent climatology (Warren et al., 1999; Ricker et al., 2014). These assumptions contribute to the uncertainties of the final SIT data records and consequently to the CCI-2 sea ice draft values that are calculated for the presented comparison to VAL sea ice draft. Additionally, both measurements take place on completely different spatial scales. Moored sonars sample a single point throughout the

respective sampling period. In contrast, the location of radar altimetry measurements is defined by footprints of the instruments and the trajectories of the satellites. Additionally, the final CCI-2 data product is gridded to achieve Arctic-wide coverage which means that variability within an 25×25 km grid cell is not resolved. These fundamental differences between the compared measurement principles have to be considered when comparing the presented satellite and sonar-based sea ice draft data sets. Additionally, VAL and CCI-2 time series are derived from multiple different instruments during the investigated period from 2003 to 2016. Accordingly, each of these individual records consists of data from different measurement configurations themselves.

4.4.2 Stability of the CCI-2 SIT CDR

In general, the stability of the satellite records is defined as the constancy of the SAT-VAL differences over time. However, the fact that the full VAL data record consists of multiple one to two year sea ice draft time series from various stations all over the Laptev Sea rather than a single time series from one location inhibits us from assessing an overall trend in sea ice draft over the full VAL period. Therefore, the observed near-consistent average mean differences over the ENVISAT and CS2 periods (Fig. 4.3) do not provide enough proof of a stable performance of the gridded CCI-2 data. SAT-VAL differences are dependent on the thickness of the ice that is sampled, which means in order to investigate the stability of the gridded CCI-2 records, SAT-VAL differences need to be analysed for different thickness ranges. We therefore consider the presented gridded CCI-2 draft record stable only if the SAT-VAL differences within the selected thickness ranges stay constant over time.

The limiting factor for the analysis of temporal changes in the SAT-VAL difference from different thickness ranges is, again, the small number of data points and the comparably short observational period. The following thickness ranges were selected in or-

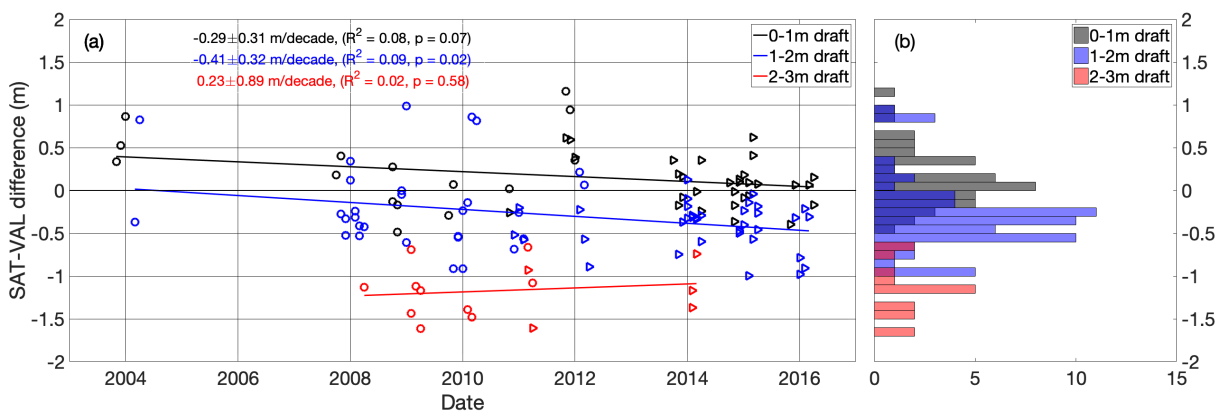


Figure 4.6: (a) Difference (SAT-VAL difference) between gridded monthly mean ENVISAT (CS2) and VAL ice drafts in circles (triangles) for thickness ranges from 0 to 1 m (black), 1 to 2 m (blue) and 2 to 3 m (red). Linear trends were computed for each of the thickness ranges. (b) Distributions of 0 to 1 m (black), 1 to 2 m (blue) and 2 to 3 m (red) thickness range SAT-VAL differences.

der to provide a reasonable number of data points for the analysis of trends: 0 to 1 m, 1 to 2 m and 2 to 3 m. For the thickness ranges between 0 and 1 m and 1 and 2 m negative trends are visible while a positive trend is apparent for the thickness range from 2 to 3 m (Fig. 4.6). However, the coefficients of determination, R^2 , for all three trends are very small indicating that linear trends poorly represent the Laptev Sea SAT-VAL difference and are in fact not suitable to explain the temporal development of SAT-VAL differences over time. Nevertheless they allow us to investigate the stability of the mean difference for different thickness ranges. The trends indicate a decrease (increase) in mean difference for the thickness ranges 0 to 1 m and 1 to 2 m (2 to 3 m). All three trends have large uncertainties and only one is significant at the 95% confidence level (1 to 2 m thickness range, p -values below 0.05). These trends are dependent on the length of the observed time series, the selected thickness ranges and in the presented case on the inter-mission biases between the two CCI-2 products that combine for the full gridded CCI-2 sea ice draft CDR. The above-mentioned ENVISAT overestimation of freeboard in FYI-dominated regions like the Laptev Sea leads to an overestimation of ice draft compared to CS2. SAT-VAL differences during the overlap period (2010 to 2012) show larger differences between satellite and VAL draft for ENVISAT than for CS2 (Fig. 4.3). This tendency of the ENVISAT data to generally provide thicker ice in FYI regions than CS2 can also be seen in Fig. 4.4 and might explain the negative trends observed in the 0 to 1 and 1 to 2 m thickness ranges (Fig. 4.6). The trend for the 2 to 3 m thickness range is less conclusive which is attributed to the small number of data points compared to the other two thickness ranges and the thickness dependency of the SAT-VAL differences that strongly increases for thickness values between 2 and 3 m.

Based on this analysis we consider the trends within the three thickness ranges to be caused by the limited number of data points, the selected thickness ranges and the inter-mission bias between ENVISAT and CS2 and the overall gridded CCI-2 CDR to be stable for the investigated period from 2003 to 2016.

4.4.3 Taymyr 2013/2014 case

In order to support the interpretation and underline the current deficiencies of satellite-derived sea ice draft data in the Laptev Sea we present a case study based on the 2013/2014 ULS deployment at Taymyr station (Fig. 4.7).

The Taymyr station is located in the western Laptev Sea (Fig. 4.1). The region is dominated by offshore winds that open coastal polynyas. The ice formed in these polynyas is transported northwards (Itkin and Krumpfen, 2017) and passes by the mooring site. Changes in wind direction can lead to temporary closing of the polynyas and convergence towards the coast or fast ice. Sea ice piling up against the south-western coast is deformed and increases in thickness.

We utilized a Lagrangian tracking tool, ICETrack (Krumpfen, 2017), to determine the trajectories of the ice that was passing by the mooring. ICETrack has been used in multiple studies to determine sea ice source regions, pathways and thickness changes (Damm et al., 2018; Peeken et al., 2018; Krumpfen et al., 2019, 2020) and utilizes sea ice motion information from a combination of three different products: motion estimates from scatterometer and radiometer data from the Center for Satellite Exploitation and

Research (Girard-Ardhuin and Ezraty, 2012), the OSI-405-c motion product provided by the Ocean and Sea Ice Satellite Application Facility (Lavergne, 2016) and Polar Pathfinder Daily Motion Vectors from the National Snow and Ice Data Center (NSIDC) (Tschudi et al., 2019). The tracking provides us with information about the source regions of the ice measured by the ULS and the atmospheric and oceanic conditions the ice experienced on its trajectory to the mooring location. The NSIDC's Polar Pathfinder sea ice motion product (Tschudi et al., 2019) was used to estimate convergence along the trajectories of the Taymyr sea ice. Analysing daily convergence along the trajectories allowed us to calculate accumulated convergences over each track. Accumulated convergence is a measure for the total amount of deformation the ice that passed by the Taymyr mooring has experienced before it reached the mooring site.

The daily mean ULS draft time series from the Taymyr station indicates a consistent increase in sea ice draft between January and March 2014. Since the Laptev Sea is dominated by newly formed FYI the observed daily mean draft values cannot be explained by thermodynamic growth only. An additional dynamic influence on the ice is confirmed by the increase in accumulated convergence along the trajectories over the same period from January to March 2014. When comparing the daily mean ULS time series to the gridded monthly mean CS2 draft time series it is apparent that the CCI-2 product is not able to reproduce the dynamic increase in sea ice draft. Rather than showing the mean sea ice draft CS2 data shows better agreement with the modal sea ice draft derived from the ULS (Fig. 4.7). A similar result is visible for the weekly draft values from CS2SMOS.

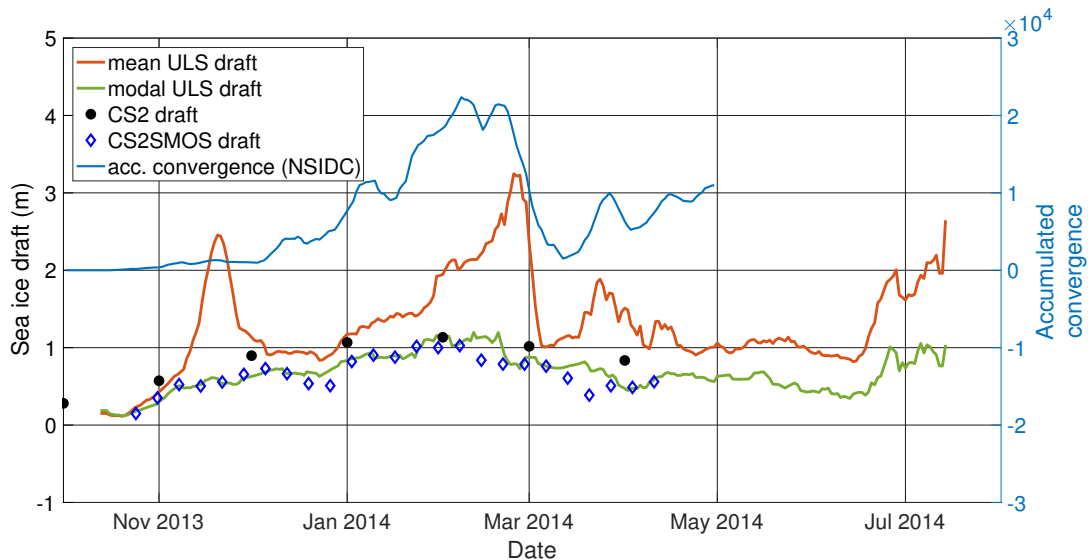


Figure 4.7: Time series of CS2 (black circles) and CS2SMOS (blue diamonds) sea ice draft compared to ULS-derived mean (orange) and modal (green) sea ice draft from Taymyr station (2013-2014). Sea ice passing the mooring site was tracked using the Lagrangian ice tracking tool ICETrack (Krumpfen, 2017). Based on the NSIDC Polar Pathfinder sea ice motion product (Tschudi et al., 2019) accumulated convergence (blue) along the daily sea ice trajectories was calculated.

Table 4.4: Statistics for the comparison between gridded CS2, CS2orbit and gridded CS2SMOS mean sea ice draft with modal Taymyr and 1893 ULS sea ice draft from the 2013/2014 and 2014/2015 periods. Due to the low temporal resolution of the ADCP-derived VAL data, modal sea ice draft was only calculated for ULS data. RMSD and mean difference were calculated for the difference between mean satellite minus modal VAL data. The Pearson correlation coefficient, r , was calculated for each of the four VAL data sets. The values show the mean of RMSD, mean difference and r over the four VAL data sets. Bold mean correlation coefficients indicate significance of all four correlation coefficients at the 95% confidence level. None of the correlations was significant for the CS2 data.

	CS2	CS2orbit	CS2SMOS
RMSD [m]	0.25	0.30	0.21
Mean difference [m]	0.05	0.06	-0.05
r	0.61	0.63	0.77

Table 4.4 shows RMSD, mean difference and correlation coefficients for the comparison between gridded CS2, CS2orbit and CS2SMOS with modal sea ice draft data from the ULS moorings (Taymyr and 1893) for the 2013/2014 and 2014/2015 periods. Gridded CS2, CS2orbit and CS2SMOS show small mean differences to modal sea ice drafts in the Laptev Sea. Mean correlation coefficients between modal ULS and mean satellite data are between 0.61 and 0.77 and significant at the 95% confidence level for the higher temporal resolution satellite products (CS2orbit and CS2SMOS). Due to the low temporal resolution of the ADCP measurements reliable modal draft values could not be calculated. Therefore the comparison between mean satellite and modal VAL draft values is limited to the 2013-2015 period when ULS data is available.

Another observation from this case study and the comparison of satellite and VAL sea ice draft in general concerns the differences in length of the time series. While satellite data is only available from October and through April, ULS and ADCP are able to measure sea ice draft even after melt onset. It is known that warm snow and ice as well as the formation of melt ponds prevent CS2 retrieval of Arctic SIT between May and September (Ricker et al., 2017). That means that for investigations into the sea ice cover in the Laptev Sea it is important to be aware that sea ice can persist during the summer melt season when the presented satellites do not provide SIT data.

4.5 Conclusion

The ESAs CCI-2 gridded SIT CDR covers a period from 2002 to 2017 and has been validated mainly for MYI-dominated regions around the Arctic Ocean. These validation efforts over MYI indicated that CS2 is representing thicker ice rather well, while ENVISAT shows a general tendency towards overestimating thin and underestimating thicker sea ice (Kern et al., 2018). The presented in situ observations of sea ice draft from Laptev

Sea ULS and ADCP moorings provide an additional important validation data set from one of the most under-sampled and FYI-dominated regions of Arctic sea ice.

The comparisons between sea ice draft data from ULS and upward-looking ADCPs with gridded monthly mean CCI-2 sea ice draft, higher resolution CCI-2 orbit trajectory and the merged CS2SMOS data in the Laptev Sea indicate:

- The agreement between in situ sonar and satellite data is very sensitive to the thickness of the sampled sea ice.
- Sea ice drafts below 0.7 m are overestimated, while sea ice drafts above approximately 1.3 m are increasingly underestimated by all considered satellite data products.
- The presented satellite products represent the same VAL sea ice drafts differently.

The Taymyr 2013/2014 case study highlights the current deficiencies of the satellite-derived SIT records in the FYI-dominated Laptev Sea region:

- Rather than representing mean sea ice draft, the considered satellite products show better agreement with modal sea ice draft.
- Significant, lasting deformation events that lead to large mean sea ice drafts are not represented in any of the shown satellite data products.

These results indicate distinct differences and deficiencies in the performance of the ESA CCI-2 SIT products over FYI- and MYI-dominated regions that require further investigations. The presented stability analysis of SAT-VAL draft differences in the Laptev Sea reveals that the agreement between gridded monthly mean CCI-2 and VAL sea ice draft data is dependent on the thickness of the ice that is sampled but mean differences are consistent over time for similar thicknesses. Linear changes in mean differences for individual thickness ranges are attributed to inter-mission bias in SIT representation between the two missions (ENVISAT and CS2) composing the gridded CCI-2 record and the comparably small number of data points that were available for the individual thickness ranges.

Applying these results to the presented Laptev Sea CCI-2 SIT anomaly trends (Fig. 4.2) we conclude that the trends of the ENVISAT and CS2 component are not caused by a change in the performance of the CCI-2 products over time but rather actual changes in SIT in this region. However, due to the high uncertainties of the data products and the comparably short sampling periods these trends need to be investigated further. Although, the stability analysis provides confidence in the CCI-2 SIT CDRs it has to be noted that satellite-derived SIT data is not sufficient to explain overall changes in SIT in the Laptev Sea. In agreement with Haas (2004) we conclude that current satellite SIT data allows examination of changes in modal SIT and therefore the thermodynamic component of the changes in the Laptev Sea, however, dynamic changes in SIT are not reproduced by the satellite CDRs. Therefore, improvements in the processing of radar altimetry data are required for the estimation of surface roughness but also for the parametrizations of snow depth and densities of snow and ice. Unknown snow properties and depth distribution are

a major source for uncertainty in the freeboard retrieval process. Uncertainties in freeboard as well as slight changes in the utilized average ice column densities translate into the final SIT product. As suggested by Wingham et al. (2006) ice type densities should be replaced by thickness dependent ice densities to account for the currently unknown density variations due to deformation processes. Furthermore, continuous long-term SIT measurements in the Laptev Sea are required to provide much needed information on deformation processes. However, with limited access to the vastly under-sampled Russian Shelf regions the satellite-derived SIT CDRs remain a crucial source of long-term SIT data for this region. Their improvement as well as large-scale observations of dynamic changes of SIT redistribution and model simulations are required to investigate the effects governing SIT changes in the Laptev Sea.

Acknowledgements

This study was carried out as part of the BMBF-funded Russian-German research cooperation QUARCCS (grant: 03F0777A). Moorings were deployed and recovered within the framework of the Russian-German project CATS/Transdrift (grant: 63A0028B). Special thanks to all the people involved on the various expeditions.

The 2013/2014 ULS data sets were processed by ASL Environmental Sciences Inc., Victoria, BC, Canada. ASL also provided valuable support and the toolboxes for the processing of the 2014/2015 ULS data sets. Additionally, the ECMWF provided ERA-Interim reanalysis surface pressure data (Dee et al., 2011) that was valuable for the ULS processing.

The production of the merged CryoSat-SMOS sea ice thickness data was funded by the ESA project SMOS & CryoSat-2 Sea Ice Data Product Processing and Dissemination Service, and data from 2010 to 2016 were obtained from AWI.

We would like to use the opportunity to thank the three anonymous reviewers for their valuable suggestions and constructive comments during the review process. We would also like to thank our editor Dr. John Yackel and his team at The Cryosphere for their support and quick processing of our manuscript.

Data availability

ULS (Belter et al., 2019b) and ADCP-derived daily mean sea ice draft time series (Belter et al., 2020a) are available at the Data Publisher for Earth & Environmental Science PANGAEA.

ESA Sea Ice Climate Change Initiative (Sea_Ice_cci): Northern hemisphere sea ice thickness from ENVISAT satellite (Hendricks et al., 2018c) and from CryoSat-2 satellite (Hendricks et al., 2018a) on a monthly grid (L3C), v2.0 are available from the Centre for Environmental Data Analysis data base.

ESA Sea Ice Climate Change Initiative (Sea_Ice_cci): Northern hemisphere sea ice thickness from ENVISAT (Hendricks et al., 2018d) and CryoSat-2 (Hendricks et al., 2018b) on satellite swath (L2P), v2.0 are available from the Centre for Environmental Data Analysis data base.

Merged CryoSat-2/SMOS sea ice thickness: A weekly Arctic sea-ice thickness data record from merged CryoSat-2 and SMOS satellite data (2017). The Cryosphere, 11, 1607-1623, <https://doi.org/10.5194/tc-11-1607-2017>

5 From the Laptev Sea to the Fram Strait – Life cycle of Arctic sea ice

Chapter 3 presented an adaptive approach for the derivation of daily mean sea ice draft from upward-looking ADCPs moored in the Laptev Sea. This new approach allowed the generation of a sea ice draft data archive for the period from 2003 to 2016, which was used to validate the ESA CCI-2 and the CS2SMOS satellite sea ice thickness products in the Laptev Sea (Chapter 4). In addition to making multiple ADCP data sets accessible for the derivation of sea ice draft time series in the Laptev Sea, the presented method provides new means to exploit similar ADCP data sets from the ice-covered polar seas of potentially both hemispheres. These data sets, initially analysed for ocean current and sea ice motion information, can potentially serve as additional time series to close temporal gaps in existing records or provide sea ice draft and ultimately thickness records in regions that lack them altogether. Even for future studies lacking the financial resources for costly IPSs this newly developed approach could provide a low cost alternative for sonar-based observations of sea ice thickness.

Due to the spatial distribution of the ADCP and ULS moorings all over the Laptev Sea and the temporal limitations of the individual time series a reliable investigation of interannual variability in sea ice thickness was not possible on the basis of these data. However, these newly acquired time series still provided crucial validation data for satellite sea ice thickness records in that area. In turn, the improved understanding of these satellite sea ice thickness records facilitated the desired investigation of interannual sea ice thickness variability in the Laptev Sea.

Average sea ice thickness anomalies in the Laptev Sea showed an overall negative trend in thickness composed of opposing trends over the ENVISAT (negative trend) and CS2 (positive trend) data periods. More importantly, the study revealed that the best agreement between sonar-based and satellite-based sea ice draft was achieved between 0.7 and 1.3 m. For the current ice situation in the Laptev Sea this means that the ESA CCI-2 and CS2SMOS satellite sea ice thickness products provide modal rather than mean sea ice thickness. It follows that the current versions of these satellite products only allow for the investigation of thermodynamically grown sea ice thickness and do not provide sufficient information about the influence of deformed sea ice on the Laptev Sea mean sea ice thickness. This limitation of the investigated satellite-derived sea ice thickness products has to be considered especially for the investigation of sea ice volume fluxes in this region.

The first two studies presented in this dissertation added valuable new data records from the vastly under-sampled Laptev Sea and in combination provide the means to monitor monthly mean (2002 to 2020) and even weekly mean (2010 to 2020) thickness of thermodynamically grown sea ice in one of the most important regions of Arctic sea ice formation. Applying this knowledge and combining it with additional data sets, the following analysis deals with the governing processes of Laptev Sea sea ice thickness

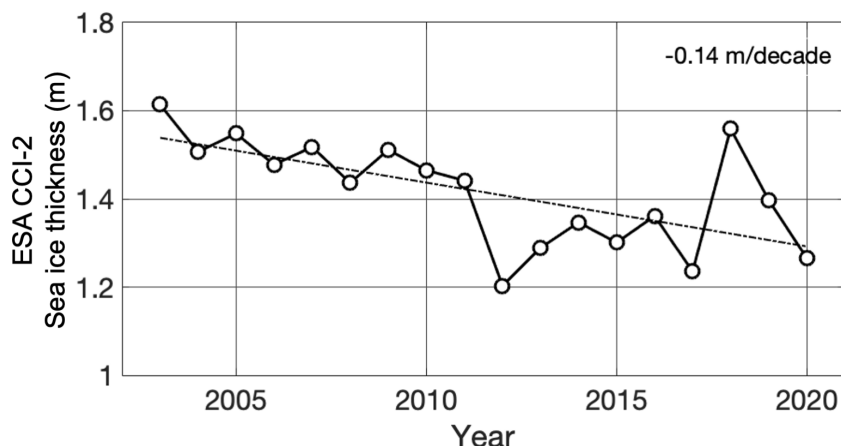


Figure 5.1: European Space Agency’s Climate Change Initiative Phase 2 winter average (January to April) sea ice thickness in the Laptev Sea (76 to 81.5°N, 100 to 145°E, Hendricks and Ricker, 2019a).

variability and their potential to precondition sea ice ahead of its passage through the Arctic Ocean.

Today most of the Laptev Sea already belongs to the seasonal ice zone with trends towards complete ice loss in summer. One important contributor to the observed reduction in summer sea ice extent and thickness in the Laptev Sea is the trend towards the extension of the summer melt season, which leads to earlier ice breakup and melt in spring and later freeze up in autumn (Markus et al., 2009; Onarheim et al., 2018; Krumpfen et al., 2020). However, the observed thinning of sea ice in the Laptev Sea also occurs during the winter season (Fig. 5.1) and is likely a result of multiple factors including increased offshore transport of thin sea ice and the subsequent formation of even thinner new ice (Krumpfen et al., 2013). Observations by Polyakov et al. (2017, 2020) showed that the influence of upward-directed ocean heat fluxes has been increasing as well. The observed change in upper ocean stratification on the shelf edges in the eastern Arctic has led to the enhanced release of heat from intermediate-depth (150 to 900 m) Atlantic Water to the surface mixed-layer in winter (Polyakov et al., 2020). This process, termed Atlantification, has previously been observed in the Barents Sea (Smedsrud et al., 2013) and north of Svalbard (Ivanov et al., 2012; Onarheim et al., 2014) but is progressing eastward, affecting sea ice growth in almost the entire Russian Arctic (Polyakov et al., 2017). Atlantification potentially decelerates the winter growth of sea ice originating from the shallow Russian shelves (Polyakov et al., 2017) and contributes to premature melt of sea ice before it even reaches the Transpolar Drift (Krumpfen et al., 2019, see also Chapter 7).

Single position mooring measurements or even larger-area observations, such as the ones from the validated satellite products, are not suitable for the purpose of investigating the impact of the above-mentioned mechanisms on sea ice and its thickness. Especially the potential preconditioning effects of these mechanisms on ice in the Laptev Sea need to be investigated by following the ice along its pathways through the Arctic or at least by sampling it at different stages along those pathways. For example, sea ice exiting the Arctic through its main exit gate, the Fram Strait, carries the integrated signal of the

thickness changes that occurred along the pathways of this ice through the Arctic Ocean (Hansen et al., 2013). This makes the Fram Strait and its immediate vicinity an area of major interest for such investigations. Combining observational data sets especially from a region like Fram Strait with additional analysis tools allows the investigation of whether anomalies in sea ice thickness induced in the regions of ice formation persist and can be observed even at the end of the Arctic sea ice life cycle.

The final study presented in this dissertation (Chapter 6) focuses on this approach. It utilises the advantages of observing sea ice thickness on large spatial scales using EM sounding to obtain sea ice thickness observations at the end of the Transpolar Drift (just north of Fram Strait). This data set is used to describe sea ice thickness variability and change over the past almost 20 years and due to its length provides the unique opportunity to put sea ice thickness measurements conducted during the MOSAiC drift experiment into a historical context. Lagrangian ice tracking is used to determine the pathways of the observed sea ice and a basic thermodynamic sea ice growth model is applied along the obtained sea ice trajectories. The modelling approach is used to simulate sea ice thickness changes along the pathways and to bridge regions that are not accessible and times when sea ice thickness observations of sufficient accuracy are not possible.

6 Interannual variability in Transpolar Drift ice thickness and potential impact of Atlantification

Published as a pre-print and currently under review in *The Cryosphere Discuss.*,
<https://doi.org/10.5194/tc-2020-305>

Belter, H. J.¹, T. Krumpfen¹, L. von Albedyll¹, T. A. Alekseeva², S. V. Frolov², S. Hendricks¹, A. Herber¹, I. Polyakov^{3,4,5}, I. Raphael⁶, R. Ricker¹, S. S. Serovetnikov², M. Webster⁷, and C. Haas¹

¹*Alfred Wegener Institute, Helmholtz Centre for Polar and Marine Research, Bremerhaven, Germany*

²*Arctic and Antarctic Research Institute, St. Petersburg, Russian Federation*

³*International Arctic Research Center, University of Alaska Fairbanks, Fairbanks, USA*

⁴*College of Natural Science and Mathematics, University of Alaska Fairbanks, Fairbanks, USA*

⁵*Finnish Meteorological Institute, Helsinki, Finland*

⁶*Thayer School of Engineering at Dartmouth College, Hanover, USA*

⁷*Geophysical Institute, University of Alaska Fairbanks, Fairbanks, USA*

Author contributions

HJB and TK analysed the sea ice thickness data and conducted the backward-tracking and model simulations for the sea ice sampled north of Fram Strait. HJB prepared the manuscript with contributions from all co-authors. HJB, TK, and CH participated in the different expeditions during which the EM sea ice thickness data were gathered. AH was vital for the organisation of multiple flight campaigns including the one in 2020. IP provided ocean heat flux estimates and calculations for the model analysis. LvA, IR, MW, and SH planned and conducted the ice thickness measurements during leg 4 of the MOSAiC campaign and processed the preliminary data used for this study. RR added preliminary data from the airborne thickness measurements conducted during leg 3 of MOSAiC. TA, SF, and SS gathered and analysed the observational data from the Russian cruises to the North Pole.

Abstract

Changes in Arctic sea ice thickness are the result of complex interactions of the dynamic and variable ice cover with atmosphere and ocean. Most of the sea ice exits the Arctic Ocean through Fram Strait, which is why long-term measurements of ice thickness at the end of the Transpolar Drift provide insight into the integrated signals of thermodynamic and dynamic influences along the pathways of Arctic sea ice. We present an updated time series of extensive ice thickness surveys carried out at the end of the Transpolar Drift between 2001 and 2020. Overall, we see a more than 20% thinning of modal ice thickness since 2001. A comparison with first preliminary results from the international Multidisciplinary drifting Observatory for the Study of Arctic Climate (MOSAiC) shows that the modal summer thickness of the MOSAiC floe and its wider vicinity are consistent with measurements from previous years. By combining this unique time series with the Lagrangian sea ice tracking tool, ICETrack, and a simple thermodynamic sea ice growth model, we link the observed interannual ice thickness variability north of Fram Strait to increased drift speeds along the Transpolar Drift and the consequential variations in sea ice age and number of freezing degree days. We also show that the increased influence of upward-directed ocean heat flux in the eastern marginal ice zones, termed Atlantification, is not only responsible for sea ice thinning in and around the Laptev Sea, but also that the induced thickness anomalies persist beyond the Russian shelves and are potentially still measurable at the end of the Transpolar Drift after more than a year. With a tendency towards an even faster Transpolar Drift, winter sea ice growth will have less time to compensate the impact of Atlantification on sea ice growth in the eastern marginal ice zone, which will increasingly be felt in other parts of the sea ice covered Arctic.

6.1 Introduction

The Arctic sea ice cover is undergoing rapid changes. Besides the continuous decline in annual mean sea ice extent by almost 14% per decade from 1979 to 2010 (Cavalieri and Parkinson, 2012; Stroeve et al., 2012), sea ice volume has decreased as well. Based on a combination of submarine sea ice draft and satellite sea ice thickness (SIT) measurements from ICESat and CryoSat-2 from 1958 to 2018, Kwok (2018) found that central Arctic summer mean SIT decreased by about 60% over six decades. This thinning was accompanied by a reduction in second-year and multi-year ice (SYI and MYI) fraction of more than 50%, which resulted in substantial sea ice volume loss (Kwok, 2018).

The importance of continuous measurements of Arctic SIT change is demonstrated by the implications these changes have on the Arctic summer sea ice energy and mass balance. Changing optical properties and thinning of sea ice allow increased penetration of solar energy into the ocean (Nicolaus et al., 2012; Katlein et al., 2019), with implications for ocean heat deposition (Perovich et al., 2007; Pinker et al., 2014) and primary productivity (Assmy et al., 2017). Intensified melt and thinning of Arctic sea ice also impact the pathways of sea ice from the major source regions on the Russian shelves. Due to the thinner ice cover sea ice drift is increased and sea ice is transported faster along the Transpolar Drift system (Spren et al., 2011; Krumpfen et al., 2019). However, the intensified summer melt and the initially thinner ice cover in the Siberian Arctic also lead

to more frequent interruptions of the long-range transports of ice and ice-rafted matter from the shallow Russian shelves to the central Arctic Ocean (Krumpfen et al., 2019). In order to predict the future development of these mechanisms reliable measurements of sea ice parameters, like SIT, are vital.

Satellite-based radar altimeters provide the means to investigate Arctic-wide SIT changes, but due to the influence of warm snow and ice and the formation of melt ponds during the melt season, these data sets are only available from October through April (Ricker et al., 2017; Hendricks and Ricker, 2019a). However, in light of recent model predictions of a nearly ice-free Arctic in summer (Johannessen et al., 2004; Holland et al., 2006; Wang and Overland, 2009; Overland and Wang, 2013; Overland et al., 2019), long-term and large-scale melt season SIT observations are more important than ever. Melt season SIT measurements from upward-looking sonars (Hansen et al., 2013; WHOI, 2014; NPI, 2018; Belter et al., 2020b), ground-based and airborne electromagnetic induction (EM) measurements (Haas, 2004; Haas et al., 2008, 2010), airborne remote sensing (Kurtz et al., 2013) and in situ drill holes (Kern et al., 2018) are spatially and temporally limited and therefore not sufficient for the investigation of long-term variability.

Here we present an extended long-term summer SIT time series from 2001 to 2020 obtained within the framework of the IceBird summer campaign. The IceBird campaign, led by the Alfred Wegener Institute, Helmholtz Centre for Polar and Marine Research, was designed to provide a long-term time series of large-scale SIT measurements in, but not limited to, the vicinity of the main exit gate of Arctic sea ice - Fram Strait. The extensive IceBird survey activity provides a unique basis for the investigation of large-scale SIT distributions. In IceBird, SIT is measured using an airborne EM (AEM), which makes use of the contrasting electromagnetic conductivities between sea ice and sea water (Haas et al., 2008). Since the area covered during IceBird (Fig. 6.1 a)) includes a wide range of different ice types from various sources, a careful analysis is required for the investigation of interannual SIT variability.

For the current study we focus on the SIT measurements from a selected area of interest (AOI, enclosed area in Fig. 6.1 a)) just north of Fram Strait. Sea ice reaching Fram Strait originates from multiple regions of the Arctic, which means long-term observations of SIT in its vicinity provide insight into integrated Arctic-wide thermodynamic and dynamic changes in the sea ice cover (Hansen et al., 2013). While previous studies recorded substantial thinning and across Fram Strait (79°N) SIT gradients during the first decade of the 21st century (Hansen et al., 2013; Renner et al., 2014), we focus on the evolution of summer (July/August) SIT further upstream of the Transpolar Drift. With the AEM being towed by a fixed-wing aircraft longer transects and ultimately a greater areal distribution of the measurements are achieved as compared to other in situ observations.

The objectives of this study are to extend the summer SIT time series (from 2012 to 2020), first published by Krumpfen et al. (2016), at the end of the Transpolar Drift and investigate the interannual variability in SIT in the selected AOI close to the export gate of Arctic sea ice. We will use the Lagrangian sea ice tracking tool, ICETrack (Krumpfen, 2018) to determine the source regions and drift trajectories of the sea ice sampled in the AOI. In order to provide insight into the driving mechanisms of the observed SIT variability a thermodynamic model is applied along the determined sea ice trajectories

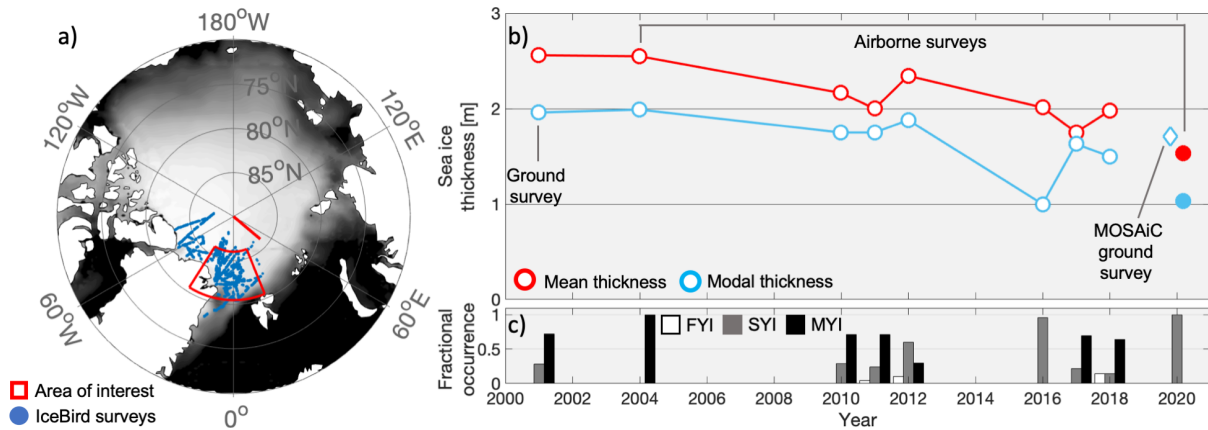


Figure 6.1: a) Map showing all EM-based summer (July/August/September) SIT measurements obtained between 2001 and 2020, as well as July/August mean sea ice concentration (OSI-450 and OSI-430-b) for the period from 2000 to 2019 (Lavergne et al., 2019). Enclosed area (red, 80.5-86°N and 30°W-20°E) indicates the selected area of interest (AOI, see Table 6.1 for an overview of the corresponding expeditions and basic SIT statistics for the selected AOI). The red line (86 - 90°N, 50°E) shows the transect of Russian sea ice observations. b) Summer (July/August) mean (red) and modal (blue) SIT based on EM measurements conducted in the AOI (circles). Diamond shows modal EM SIT measured on the MOSAiC floe in July 2020 and filled circles indicate mean and modal EM SIT values obtained during the IceBird MOSAiC campaign in September 2020. c) shows the fractional occurrence of first-year (white), second-year (grey) and multi-year ice (black, ice older than two years) for the individual years. The age classification is based on ICETrack calculations of the number of days the ice particles travelled along their trajectories.

to reconstruct the AOI-sampled SIT. In addition we will compare the SIT changes in the AOI to long-term observations gathered during regular Russian cruises from Franz Josef Land to the North Pole. This additional comparison is conducted to discuss whether the observed changes are limited to the AOI or induced during ice formation and transit through the Arctic Ocean. Finally, we will use the unique opportunity to compare the long-term SIT time series to IceBird and ground-based EM (GEM) measurements conducted within the framework of the Multidisciplinary drifting Observatory for the Study of Arctic Climate (MOSAiC). At 85°N and 136°E the German icebreaker RV Polarstern (Alfred Wegener Institute, 2017) moored to a 2.8×3.8 km sized ice floe in October 2019 (Krumpfen et al., 2020). After about 9 months of drifting through the Arctic Ocean, RV Polarstern and the MOSAiC floe reached the selected AOI in summer 2020. This allows us to consider the MOSAiC floe in the context of the long-term time series, and determine whether the SIT of the MOSAiC floe in 2020 was exceptional or in agreement with historical observations.

6.2 Data and methods

6.2.1 EM sea ice thickness measurements

Electromagnetic induction (EM) SIT measurement systems take advantage of contrasting electrical conductivities between sea ice and sea water to determine the distance between the ice-water interface and the EM device (Kovacs and Morey, 1991; Haas et al., 1997). In 2001, measurements were conducted using a Geonics EM31 ground-based EM instrument (GEM). The GEM was pulled over the ice on a sledge and obtained the distance to the ice-water interface (Haas, 2004). GEM measurements included SIT values over melt ponds and pressure ridges, however, open water and thin ice were not adequately represented in the data sets due to the practical limitations of sampling those areas on foot (Haas, 2004). The 2020 GEM measurements on the MOSAiC floe were taken with the Geophex GEM-2, a broadband EM sensor used for advanced thickness observations (Hunkeler et al., 2016). After 2001, SIT was obtained using the airborne EM system (AEM), EM Bird, that was towed by a helicopter (in 2004) and the research aircrafts *Polar 5* and *6* (from 2010 onwards). The EM Bird was operated between 12 and 20 m above the ice surface (Krumpfen et al., 2016). Following Pfaffling et al. (2007), SIT was calculated as the difference between EM-derived distance to the ice-water interface and laser altimeter-recorded distance between EM device and the air-snow interface. EM measurement accuracy is within 0.1 m to drill-hole measurements over level sea ice, while water inclusions within pressure ridges lead to a general underestimation of ridges by as much as 40 to 50% (Pfaffling et al., 2007; Haas et al., 2009).

Thickness measurements using the ground-based and airborne EM methods always represent the total combined sea ice and snow thickness (Haas et al., 1997). Given the study period from mid-July to mid-August and following climatological values of snow depth (Warren et al., 1999; Renner et al., 2014; Krumpfen et al., 2016), we assume a 0.1 m snow or weathered layer thickness, which is negligible for the EM measurements. More snow may still have been present during episodic precipitation events, but likely melted within a few days.

In order to ensure comparability of the available EM-based measurements from 2001 to 2020 only data taken between 80.5 to 86°N and 30°W to 20°E (AOI, Fig. 6.1 a) were selected for the analysis. Following Krumpfen et al. (2016), the AOI was also selected to be north of Fram Strait to concentrate the analysis on sea ice that was shaped along its pathways through the Arctic rather than by local melt phenomena in Fram Strait. Finally the selected AOI allows for a more reliable analysis of the trajectories of the sampled sea ice since low resolution sea ice motion products used for Lagrangian tracking are highly uncertain in Fram Strait (Krumpfen et al., 2019). Expedition logistics and the prevailing weather conditions prevented us from acquiring continuous and overlapping measurements over the full AOI each year. However, following Rabenstein et al. (2010) the lengths of the conducted EM profiles were adequate to consider the data to be sufficiently homogeneous in time and space and representative for the sampled region and time of year. Table 6.1 provides an overview of all relevant field campaigns, duration, profile lengths, basic statistics and references for the measurements from within the selected AOI.

The analysis of trends and interannual variability of summer SIT in the AOI is based on temporal and spatial averages and the most frequently occurring EM SIT - the mode of the distribution. Modal SIT is a representation for the thickness of thermodynamically grown level ice, while mean SIT includes thermodynamically and dynamically grown sea ice and therefore is an indication for the general variability of SIT (Haas, 2017). Prior to the calculation of summer mean and modal SIT values from all available data points within the predefined AOI (Fig. 6.1), SIT values < 0.1 m, including open water values, were excluded to avoid biases due to different fractions of open water areas in the data sets.

6.2.2 Sea ice pathways and source regions

In order to determine the pathways and source regions of the ice that was sampled in the selected AOI we utilized the Lagrangian ice tracking tool, ICETrack (Krumpen, 2018). The starting points for the backward tracking of AOI-sampled sea ice were derived based on the positions of the EM measurements. EM SIT data were gridded to a 25×25 km Equal-Area Scalable Earth Grid. For a minimum of 2000 AEM SIT values within a single grid cell the respective grid point was selected to be a starting point for the backward tracking with ICETrack. Due to the limited number of measurements available from the short GEM surveys ICETrack starting points for the year 2001 were calculated even for less than 2000 SIT values per grid cell. The MOSAiC floe trajectory is based on position records from RV Polarstern and backward tracking of the floe from the MOSAiC starting point at 85°N and 136°E in October 2019.

Ice parcels were tracked backward in time on a daily basis. Termination criteria for the tracking were either met when the ice reached a coastline or when SIC dropped to 25% or less. When SIC reaches 25% or less ICETrack assumes that ice is formed. The applied SIC product is provided by the Center for Satellite Exploitation and Research (CERSAT) and is based on 85 GHz SSM/I brightness temperatures, using the ARTIST Sea Ice algorithm (Ezraty et al., 2007). The number of days from the first day of tracking until ice formation provided the age of the sea ice sampled in the AOI. The tracking was based on a weighted approach to determine the most appropriate of the three available low resolution sea ice motion products (Krumpen et al., 2019): (i) motion estimates from scatterometer and radiometer data from CERSAT (Girard-Ardhuin and Ezraty, 2012), (ii) the OSI-405-c motion product produced by the Ocean and Sea Ice Satellite Application Facility (OSISAF) (Lavergne, 2016) and (iii) Polar Pathfinder Daily Motion Vectors from the National Snow and Ice Data Center (NSIDC) (Tschudi et al., 2019). CERSAT was prioritized as it provides the most consistent time series of motion vectors (from 1991 onwards). However, when CERSAT data were missing (especially during summer months), OSISAF data were used. Prior to 2012 or when OSISAF data were not available NSIDC data were utilized (Krumpen et al., 2019). A detailed description of the three motion products is given by Sumata et al. (2014). Beside sea ice trajectories, ICETrack provided information about satellite-derived SIT and sea ice concentration (SIC) as well as atmospheric parameters, like surface air temperature, 10 m wind speed and surface pressure in daily increments along the trajectories. Due to this comprehensive approach to analyse sea ice along its trajectories through the Arctic ICETrack has been widely used

in previous studies, e.g. Damm et al. (2018); Peeken et al. (2018); Krumpfen et al. (2019, 2020).

6.2.3 Thermodynamic sea ice model

In order to investigate the driving mechanisms of interannual variability in modal SIT in the AOI, ICETrack was combined with a simple one-dimensional thermodynamic sea ice model developed by Thorndike (1992). Parallel to retrieving SIC, SIT, atmospheric parameters, and sea ice motion from ICETrack, the model calculated daily sea ice growth and melt along the determined sea ice trajectories. Latent heat of melting/freezing, ocean heat flux, and conductive heat loss are balanced to model ice growth at the bottom, $\frac{\Delta H}{\Delta t}$ (Thorndike, 1992; Pfirman et al., 2004):

$$\frac{\Delta H}{\Delta t} = \frac{-1}{L} \cdot \left(F + (T_{surf} - T_0) \cdot \frac{(k_{ice} \cdot k_{snow})}{(k_{ice} \cdot H_{snow} + k_{snow} \cdot H_{ice})} \right) \quad (6.1)$$

The model used along-track snow depth, H_{snow} , computed from the Warren climatology (Warren et al., 1999) as well as the NCEP re-analysis sea surface temperature (T_{surf}) data (Kanamitsu et al., 2002) that were extracted along the trajectories by ICETrack (Krumpfen et al., 2019). T_0 is the temperature at the ice-water interface (-1.9°C) and k is the thermal conductivity ($k_{ice} = 2 \text{ Wm}^{-1}\text{K}^{-1}$, $k_{snow} = 0.33 \text{ Wm}^{-1}\text{K}^{-1}$). Latent heat of fusion, L , was constant at $3 \cdot 10^8 \text{ Jm}^{-3}$. Δt equals 86400s for daily increments of ice growth. Ocean heat flux, F , was assumed to be constant at 2 Wm^{-2} . Based on these input parameters the model computed daily changes in SIT along the trajectories. Summer melt at the surface was set to 0.005 md^{-1} (Thorndike, 1992). Modelled SIT values at the end of each track were used to calculate AOI summer mean thermodynamic SIT for each year. This modelled value provides SIT excluding the snow layer that is inherently included in the EM SIT values. We therefore added a 0.1 m snow layer to the final model SIT averages for the comparison to EM SIT. Like modal EM SIT, the modelled SIT is a representation of thermodynamically grown level sea ice.

Snow depth is an important parameter in modelling sea ice growth, and due to the limitations of the Warren snow depth climatology (Warren et al., 1999), a major source for uncertainty in the modelled SIT values calculated for each trajectory ending in the AOI. Following Laxon et al. (2013) and Ricker et al. (2014) we also reduced Warren snow depth by 50% over FYI. This step accounts for the fact that Warren et al. (1999) snow depth is based on observations during a period where Arctic sea ice was dominated by MYI with thicker snow.

Another major source of uncertainty of the modelled SIT is the selected ocean heat flux value. However, due to the simplicity of the selected sea ice model (Thorndike, 1992) for this current study the input of a constant ocean heat flux value was required. We followed previous studies (Maykut and Untersteiner, 1971; Pfirman et al., 2004; Peeken et al., 2018; Krumpfen et al., 2019) and selected a constant ocean heat flux value of 2 Wm^{-2} . This value was applied to the sea ice growth model along each trajectory from ice formation to the AOI.

6.2.4 Shipborne sea ice thickness observations

In general, ship-based observations of SIT benefit from the increasing number of regular ship transits through the Arctic Ocean. SIT data used here were either observed visually by a group of Arctic and Antarctic Research Institute (AARI) sea ice scientists using the traditional unified methodological principles in accordance with the requirements of the regulatory guidance (AARI, 2011; Alekseeva et al., 2019), or by the so-called shipborne television complex (STK). The STK consists of a high resolution telecamera, a computer for camera control and processing, and a GPS recorder. The system records images of overturning sea ice floes in the vicinity of the moving ship as well as GPS time and coordinates. After manual selection of appropriate images the software is able to measure the detailed geometry of single ice blocks from the ice camera feed and retrieve ice and snow thickness data. The purpose of this system is to provide navigation data for following ships and reliable SIT data for the validation of satellite- and model-derived SIT. Over the last decades the AARI conducted visual and STK observations regularly during summer (June-August) tourist cruises from Franz Josef Land to the North Pole. The SIT data used here are based on STK (2006 to 2011) and visual observations (1977 to 1996 and 2012 to 2019) in July on a transect from 86 to 90°N along the 50°E meridian. Sea ice was categorized as FYI or MYI (including SYI) and mean SIT was calculated for both. Depending on the fractional occurrence of FYI and MYI along the transect a mean summer SIT value was calculated.

6.3 Results and Discussion

6.3.1 Processes driving interannual SIT variability between 2001 and 2018

IceBird surveys: sea ice thickness, origin and age

Figure 6.1 b) provides an overview of the interannual variability and changes of SIT in the AOI from 2001 to the MOSAiC year 2020. Modal SIT, which is a measure for the fraction of sea ice that grew thermodynamically, decreased by approximately 24% from 2001 (approximately 2 m) to 2018 (approximately 1.5 m). The decrease of modal SIT was not gradual but showed an 11% drop after 2004 and an absolute minimum of approximately 1 m in 2016. The change in modal SIT was accompanied by a change in the fractional occurrences of FYI, SYI, and MYI. This categorization of different ice ages is based on the ICETrack-derived lengths of the sea ice trajectories. While the sampled sea ice almost exclusively consisted of MYI in 2001 and 2004, the fractions of SYI and even FYI increased notably between 2010 and 2018 (Fig. 6.1 c). In 2012 and especially 2016 sea ice in the AOI was dominated by SYI.

Mean SIT decreased by a similar percentage (23%) from 2001 (approximately 2.6 m) to 2018 (approximately 2 m). The difference between mean and modal SIT was in the order of 0.5 m in 2001, 2004, 2012, and 2018 and showed a decrease to values of 0.2 to 0.3 m in 2010/2011. During the modal minimum in 2016 the mean-mode-difference peaked at about 1 m and showed its minimum of 0.1 m in the following year 2017. The differences between the time series of modal and mean SIT are likely caused by the interannual variability in ridged sea ice (mean of the upper 10% of the EM SIT distribution, Table 6.1).

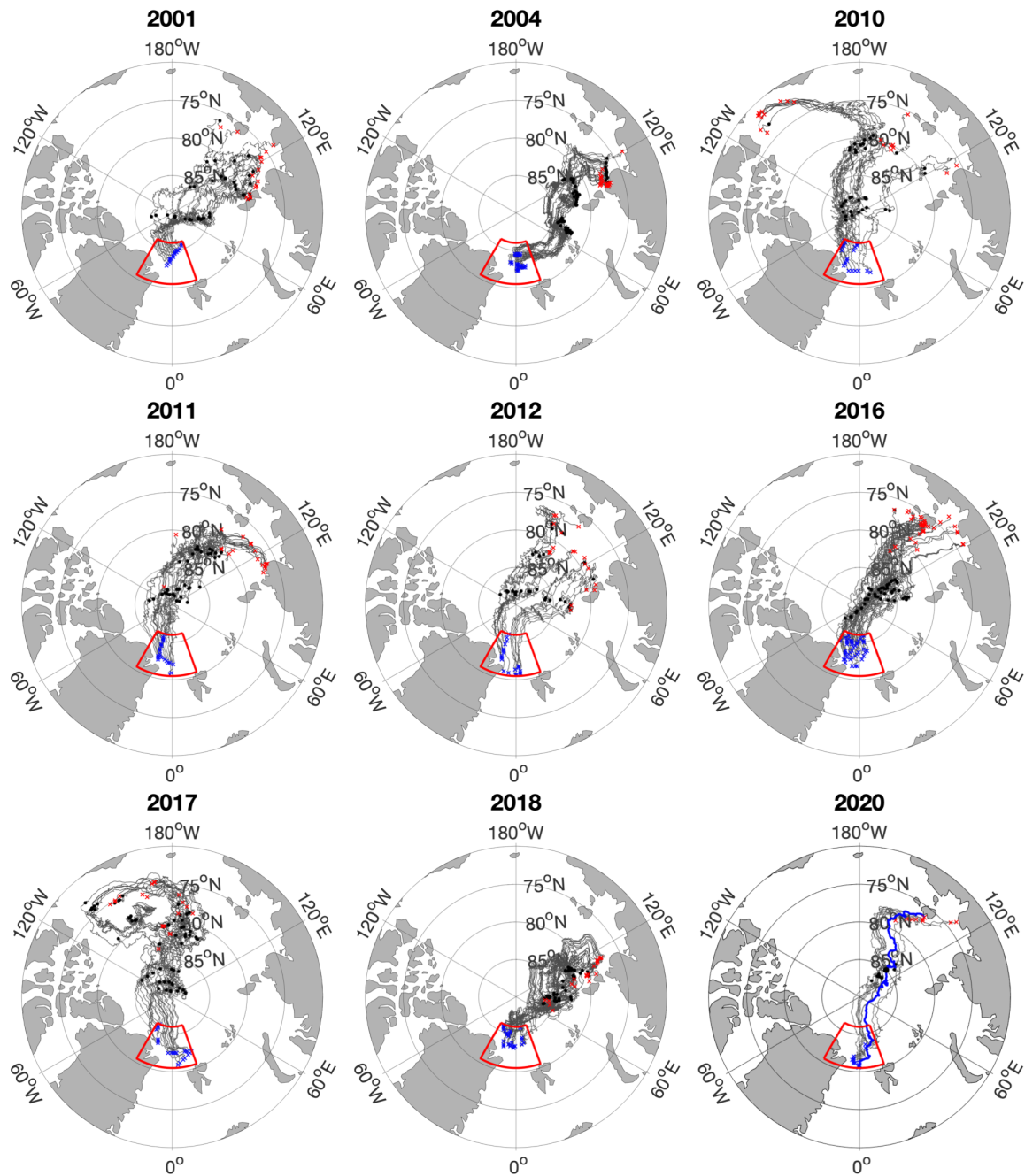


Figure 6.2: Drift trajectories of sea ice sampled in the AOI (enclosed area). Starting points of the backtracking (blue crosses) correspond to the positions where EM SIT measurements were conducted during summer (July/August/September) from 2001 to 2020. Backward tracking ended when sea ice concentration dropped to 25% or less, which is defined as the time and location of ice formation (red crosses). Black dots present sea ice position on September 21 of each year, when ice particles are considered to have survived the summer, becoming second-year or multi-year ice, respectively. The blue trajectory in 2020 represents the MOSAiC floe trajectory.

To some degree the interannual modal thickness variability can be explained by the variability in source regions of the ice (Fig. 6.2), its age and the number of freezing degree days (FDDs) the ice experienced during the transit through the Arctic Ocean (Fig. 6.3 a)). FDDs are defined as days with surface air temperatures below 0°C . Figure 6.2 indicates that about 65% of all analysed tracks of the ice surveyed in the AOI originated in the Laptev Sea (70 to 81.5°N , 100 to 145°E). Even though most of the surveyed ice can be linked to the Laptev Sea the actual places of ice formation differed within this shallow shelf sea. While ice surveyed in 2001, 2004, 2011, and 2018 was formed close to the Taymyr Peninsula and Severnaya Zemlya, the ice sampled in 2012 and 2016 was formed in the northern and eastern Laptev Sea, respectively. The sea ice surveyed in the AOI in 2001 and 2004 took, on average, approximately 3 years from its origin in the Laptev Sea to the AOI. In the following years, ice that originated in similar regions of the Laptev Sea took less time to reach the AOI (2011 and 2018). The decrease in sea ice age is linked to the observed increase in sea ice drift speed after 2004 (Sprenn et al., 2011). With an average age of about 1.7 years, the ice sampled in the AOI in 2016, which showed the minimum modal SIT, was by far the youngest during the period from 2001 to 2018. The on average oldest ice was sampled in the AOI in 2017 and originated mostly from the Beaufort Sea. It has to be noted that ice of strongly varying ages was sampled in the AOI in 2017. These variations in age and FDDs in 2017 are likely the reason why maximum modal and mean SIT values do not coincide with the on average oldest ice in 2017. Apart from the year 2017 variations in modal SIT of the ice sampled in the AOI can be largely explained by the variations in age and number of FDDs. Older ice showed larger modal SIT values in the AOI, while younger ice was thinner. However, the unknown magnitude of melt during days with surface air temperatures above 0°C (difference between ice age and FDDs) also contributes to the observed variability.

It has to be noted that the varying number of EM surveys each year and the variation in areal coverage within the AOI of the different surveys makes the analysis of SIT trends challenging. However, large-scale and year-to-year overlapping surveys as well as sampling during the same season each year strengthen the assessment that sea ice sampled in the AOI is changing in thickness and age.

Reconstruction of observed SIT using a thermodynamic model

To further investigate the processes driving interannual variability of modal SIT we compare observed AOI values with modelled SIT values of thermodynamically grown sea ice. Sea ice growth along the ICETrack sea ice trajectories was calculated using the thermodynamic sea ice model by Thorndike (1992). The modelled SIT values at the end of the trajectories provide the AOI-mean modelled SIT for each year. Figure 6.3 b) indicates that the modelled SIT time series shows similar values compared to the modal EM SIT time series. Except in 2016, all modal EM SIT values are within the uncertainty of the modelled SIT, that is based on the snow depth error provided by Warren et al. (1999). The value in 2016 is significantly smaller than the modelled value compared to the other years of the time series. While the modelled SIT is almost equal to modal EM SIT values in 2001 and 2004, it underestimates the observed values by approximately 0.2 to 0.3 m

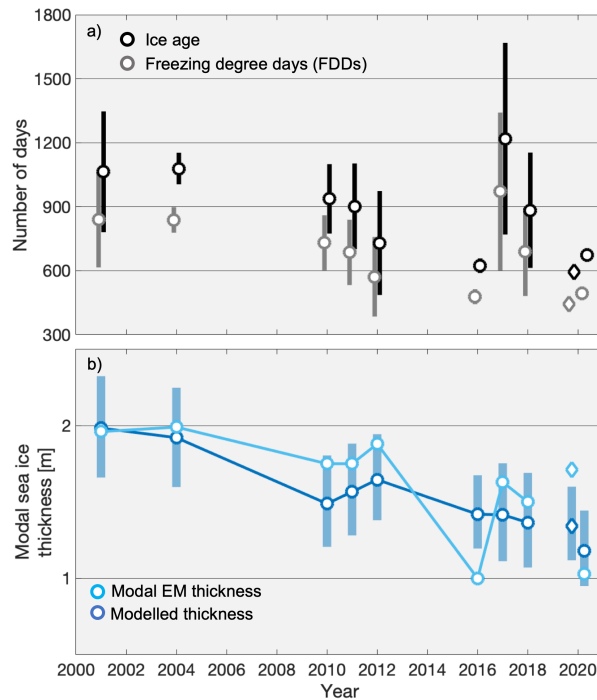


Figure 6.3: a) Mean sea ice age (black) and mean number of freezing degree days (grey, FDD) of AOI-sampled sea ice. Error bars indicate one standard deviation of age and FDDs for each year. b) Modal EM SIT (light blue, see Fig. 6.1) and reconstructed modal SIT from the Thorndike (1992) thermodynamic sea ice model. Error bars show maximum modelled SIT error due to Warren et al. (1999) snow climatology. Circles indicate larger area measurements, while diamonds show values referring to the MOSAiC floe.

from 2010 to 2012 and from 2017 to 2018. The year 2016 is the only one where modal EM SIT is overestimated by the model (by almost 0.5 m).

The general agreement between modal EM and modelled SIT supports the hypothesis that sea ice age and FDDs govern the modal SIT in the AOI. However, it is evident that the exceptional modal SIT observed in 2016 can not be explained by the model i.e. atmospheric processes alone, indicating that additional factors contributed to this minimum in modal SIT in the AOI.

6.3.2 Possible impact of Atlantification on SIT in 2016

The two major sources for uncertainty of the reconstructed SIT time series are snow depth uncertainty and the assumption of constant ocean heat flux from below. While modal SIT values are within the range of the reconstructed SIT values \pm snow depth uncertainty in most years, the model significantly overestimates the modal SIT in 2016. The sea ice sampled in the AOI in 2016 was about 0.5 m thinner than the modelled SIT, which suggests an additional heat source, unaccounted for by the model, that reduced ice growth along the trajectories. Following Eq. 6.1 bottom sea ice growth/melt are the result of the heat fluxes from either the atmosphere or the ocean. Considering that the variability of the atmospheric component of the model was accounted for along the trajectories, the other

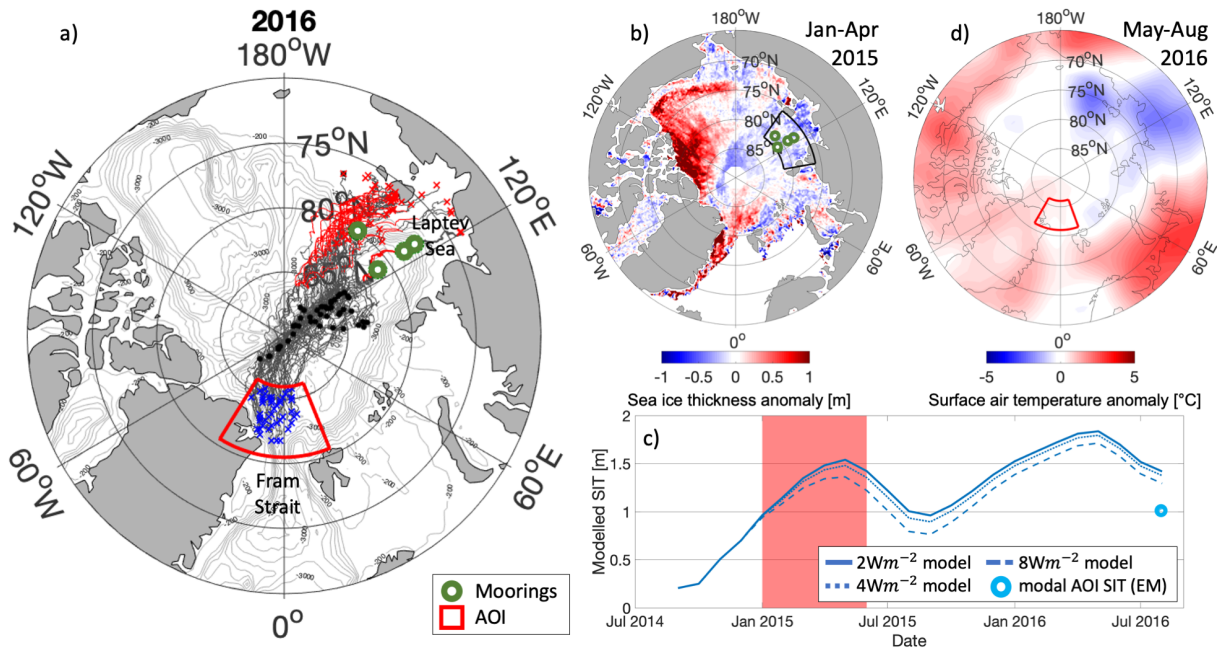


Figure 6.4: a) Drift trajectories of AOI-sampled (enclosed area) sea ice in 2016. Starting points for the backtracking (blue crosses) correspond to the positions where EM SIT measurements were conducted during July and August 2016. Tracking ended when sea ice concentration dropped to 25% or less, which is defined as time and position of ice formation (red crosses). Black dots present sea ice position on September 21, when ice particles are considered to have survived the summer, becoming second-year and multi-year ice, respectively. The sections of the trajectories coloured in red indicate sea ice position between January to through May 2015. Green markers indicate the positions of oceanographic moorings operated between summer 2013 and summer 2015 (Polyakov et al., 2017). b) January to April 2015 SIT anomaly (compared to the January to April mean from 2003 to 2020) from the ESA CCI-2 SIT climate data record (Hendricks et al., 2018a,c). c) Mean SIT modelled along the drift trajectories of the sea ice sampled in the AOI in 2016. Solid blue line indicates the mean modelled thickness over all trajectories using a constant ocean heat flux value of 2 Wm^{-2} . Dotted (dashed) blue line shows average modelled SIT using 2 Wm^{-2} ocean heat flux along the black parts of the trajectories (Fig.6.3 a) and 4 Wm^{-2} (8 Wm^{-2}) along the red parts of the trajectories (shaded red area). Light blue marker indicates the observed modal EM SIT in the AOI in 2016. d) 2016 May to August surface air temperature anomaly in comparison to the 2000 to 2019 long-term mean (data source (last accessed: July 08, 2020): www.esrl.noaa.gov/psd/products).

parameter potentially responsible for the overestimation of modal SIT is the insufficient assumption of constant ocean heat flux along the trajectories of the AOI-sampled ice in 2016.

Ocean heat flux is a widely debated and still investigated parameter that is the main source of sea ice bottom melting (Lin and Zhao, 2019). It is the sum of heat that enters the surface mixed layer from the deep ocean and heat that enters the surface mixed layer through leads and openings in the ice cover (Zhang et al., 2000). Multiple existing studies

have shown that Arctic ocean heat flux is highly variable in time and space (Maykut, 1982; Maykut and McPhee, 1995; Krishfield and Perovich, 2005; Lin and Zhao, 2019). Nevertheless, the assumption of a constant average ocean heat flux value seemed sufficient for thermodynamic sea ice modelling in the past (Peeken et al., 2018; Krumpfen et al., 2020) and is confirmed in this study by the agreement between modelled and modal SIT in all years except 2016.

The studies by Polyakov et al. (2017, 2020) showed that the observed decline in sea ice extent and increased open water area enables increased ocean ventilation and weakening of the upper ocean stratification in the eastern marginal ice zones. The resulting change in stratification, warming of the upper pycnocline and shoaling of the Atlantic Water (AW) layer result in enhanced upward AW heat flux in winter, which leads to further thinning of the overlaying ice cover. This process of so-called Atlantification is considered to be a positive feedback mechanism (Polyakov et al., 2020) and was mainly observed at the inflow gates of AW into the Arctic Ocean in the Barents Sea (Smedsrud et al., 2013) and north of Svalbard (Ivanov et al., 2012; Onarheim et al., 2014). However, based on mooring and buoy data, Polyakov et al. (2017, 2020) showed that Atlantification is progressing eastward, impacting ocean stratification and sea ice growth even in the main regions of Arctic sea ice formation in and around the Laptev Sea.

Figure 6.4 summarizes the relevant parameters and conditions for the observed modal SIT minimum in the AOI in 2016 and the potential linkage to intensified AW heat flux events along the Russian shelf. Polyakov et al. (2017) observed a significant Atlantification event with increased upward transport of AW heat at multiple mooring sites in the northern and eastern Laptev Sea (Fig. 6.4 a) between January and May 2015 (Fig. 3 A in Polyakov et al. (2017)). These moorings were part of a larger network and measured ocean properties between autumn 2013 and autumn 2015. The red coloured sections of the sea ice drift trajectories in Fig. 6.4 a) indicate that the ice sampled in the AOI in 2016 passed the region around the Laptev Sea moorings during the exact period of the observed Atlantification event, exposing the ice to increased ocean heat from below. As a result of the observed upward ocean heat flux, Polyakov et al. (2017) suggested reduced sea ice growth of approximately 0.4 m for the 2015 winter period. Satellite-derived mean SIT from the ESA Climate Change Initiative Phase 2 (CCI-2) climate data record confirms that a negative SIT anomaly existed in the Laptev Sea during this Atlantification event in 2015 (Fig. 6.4 b)). This anomaly is likely a result of multiple factors, including increased upward ocean heat fluxes due to Atlantification, but also the observed increase in ice export from the Russian shelves (Krumpfen et al., 2013; Itkin and Krumpfen, 2017).

In order to quantify the impact of increased upward ocean heat flux on sea ice in the Laptev Sea and in the AOI we adjusted the thermodynamic model to provide a constantly higher ocean heat flux value along the 2016 sea ice trajectories during the Atlantification event observed by Polyakov et al. (2017) in winter 2015 (Fig. 6.3 c)). Conservative estimates of ocean heat flux during the Atlantification event between January and May 2015 (shaded red area) vary between averages of 4 Wm^{-2} from moorings closer to the Laptev Sea shelf (Polyakov et al., 2020) and averages of 8 Wm^{-2} estimated for the moorings further north (Polyakov et al., 2017). Based on these estimates we adjusted the model to provide both values along the red parts of the sea ice trajectories (Fig. 6.4 a)), which

resulted in a mean reduction of SIT of 0.03 (4 Wm^{-2} run) and 0.15 m (8 Wm^{-2} run) at the end of the winter (May 2015, Fig. 6.4 c)). These values are significantly lower than the 0.4 m reduced sea ice growth suggested by Polyakov et al. (2017), which indicates that our adjusted heat fluxes might still be too low. However, the model confirms that increased ocean heat flux reduces sea ice growth in the Laptev Sea. In the AOI, modelled SIT reduced by 0.04 (4 Wm^{-2} run) and 0.13 m (8 Wm^{-2} run) in July 2016 (Fig. 6.4 c)). Although the adjusted model runs show that SIT anomalies induced by increased ocean heat fluxes at the beginning of the drift trajectories persist, they are not able to fully overcome the overestimation of observed SIT in the AOI. The adjusted model assumptions about ocean heat fluxes are still too crude and it is clear that a more realistic representation of ocean heat fluxes along sea ice trajectories are required. Additionally, more data are needed to determine the spatial extent on which Atlantification effects sea ice growth. Nevertheless, the presented downstream EM measurements of SIT and our model analyses suggest that the winter 2015 SIT anomaly in the Laptev Sea persisted into the central Arctic Ocean and was ultimately recorded in the AOI as late as summer 2016. In general, atmospheric influences are able to induce SIT anomalies similar to the one measured in the AOI in 2016. However, there is no indication that increased air temperatures at the sea surface between May to August 2016 resulted in the measured AOI modal SIT minimum (Fig. 6.4 d)). We therefore consider the ice conditions measured in the AOI in 2016 to be the result of extreme events of intensified upward ocean heat fluxes that occurred between ice formation in autumn 2014 and sampling in July/August 2016. Our adjusted ocean heat fluxes were not able to explain the entire offset between modelled and measured modal SIT in the AOI, which is likely the result of conservative estimates and insufficient temporal and spatial representation of ocean heat fluxes as well as other influences that effected ice growth along the trajectories that remain unknown.

We argue that the analysis of the 2016 IceBird SIT data allow for a first estimation of the impact of Atlantification on sea ice, its thickness and the time-scale on which these signals can persist. However, it has to be noted that the upward AW heat fluxes vary in strength from year to year, but Atlantification is a process that continuously increases in the eastern marginal ice zone. In fact, Polyakov et al. (2020) showed that the influence of AW heat flux on the ice in the Laptev Sea showed a dramatic increase during the last decade. The upward directed AW heat fluxes in the Laptev Sea showed an increase during winter periods between 2007/2008 to 2018, that resulted in a more than two-fold reduction of winter ice growth in the last decade (Polyakov et al., 2020).

The example of the 2016 minimum in modal SIT in the AOI is a first indication that the increasing influence of Atlantification potentially persists far beyond the eastern Arctic shelf regions due to its preconditioning effect on SIT. However, to further confirm this discovery it is vital to build continuous long-term SIT time series in the Laptev Sea as well as in the vicinity of the Fram Strait. The current IceBird SIT time series in the AOI is not sufficiently continuous to fully confirm that the AW heat flux preconditioning of sea ice in the Laptev Sea is still measurable in Fram Strait. The measurement gap between 2012 and 2016 prevented us from potentially discovering the influence of Atlantification on SIT in the AOI earlier. The ice sampled in the AOI in 2017 originated largely from the Beaufort Sea and accordingly did not show the signature of Atlantification. The

2018 ice was formed in the Laptev Sea in autumn 2015. However, it passed the shelf region where Atlantification was prominent in previous years in winter 2016 when the stratification was strong, and upward AW heat flux was anomalously weak for the new regime discovered by Polyakov et al. (2020). According to Polyakov et al. (2020) the strongest recorded upward AW heat flux, so far, occurred in winter 2018. The averages of AOI sea ice age indicate that the ice influenced by this event likely reached the AOI in 2019. Unfortunately, no IceBird campaign was conducted in the AOI in summer 2019. These missing measurements only confirm the importance of yearly IceBird campaigns in the AOI to further investigate the strength of the preconditioning of sea ice, as well as the persistence of SIT anomalies due to oceanic influences.

6.3.3 Interpretation of sea ice surveys from the MOSAiC year

The continuation of the IceBird SIT time series in the MOSAiC year 2020 was aggravated by the corona pandemic which only allowed for survey flights over the AOI from Longyearbyen (Svalbard) and after the usual sampling period from mid-July to mid-August (Table 6.1). Mean and modal SIT were obtained over the AOI in September 2020 and are shown in Fig. 6.1 b). The pathway analysis (Fig. 6.2) confirms the trend, that ice reaching the AOI in summer is increasingly dominated by SYI (Fig. 6.1 c)). Although the modal SIT is similar to the 2016 value, it has to be noted that measurements were conducted considerably later in the melt season, which makes a direct comparison difficult and shows that summer melt has a considerable impact on SIT in the AOI.

Due to the late IceBird MOSAiC campaign in 2020 and the ensuing limitations for the comparability to the existing IceBird time series we turn to the only other available SIT data set that was obtained in the AOI during the relevant period between mid-July and mid-August of 2020 - GEM SIT measurements from the MOSAiC floe. Compared to the areal coverage achievable with the AEM, GEM SIT values provide point measurements that are only partly representative for a larger area. Nevertheless, these floe-scale measurements provide the means for an important first estimation of whether the MOSAiC floe is thicker or thinner compared the sea ice that was sampled in the AOI in the years prior to 2020.

The MOSAiC Central Observatory (CO) and the ice in its immediate vicinity (radius of approximately 40 km), which accommodated the Distributed Network (DN) of various autonomous measurement stations (Krumpfen and Sokolov, 2020), was formed during a polynya event north of the New Siberian Islands (Fig. 6.2) in early December 2018 (Krumpfen et al., 2020). The ice originated in shelf waters less than 10 m deep, drifted eastward along the shallow shelf and ultimately reached deeper waters in February 2019. By the time the German icebreaker RV Polarstern (Alfred Wegener Institute, 2017) moored to the floe in October 2019 (begin of the drift at 85°N and 136°E) the CO and DN regions (DNR) were surrounded by thicker residual ice that was formed in early November 2018 (Krumpfen et al., 2020). Due to the comparably fast drift along the Transpolar Drift (the floe was only about 1.65 years old when it was sampled in the AOI, Fig. 6.3 a)) the DNR reached the southernmost border of our selected AOI already in the second half of July 2020 (Fig. 6.2). Along its trajectory through the Arctic Ocean DNR SIT was continuously measured using ground-based and airborne EM devices. Unfortu-

nately, technical problems and unfavourable weather conditions limited the availability of SIT measurements covering larger areas in the vicinity of the floe in the second half of July 2020. However, regular GEM measurements were conducted on the remainders of the CO. The GEM thickness results shown here are based on the rapid-release quickview thickness data, have undergone initial quality control, and have been calibrated against manual observations. In order to ensure the best possible comparability to the IceBird SIT time series, we only consider GEM measurements that were conducted while the floe was in the AOI and during the sampling period of the previous measurements. The resulting preliminary AOI SIT values are based on a total of 4 surveys obtained between July 16 and July 21. Although GEM measurements were only conducted on the central, more stable part of the MOSAiC floe, large-scale, AEM measurements conducted over the DNR in April 2020 indicate that modal and mean SIT values measured on the extended MOSAiC floe were representative for the DNR (Fig. 6.S1). Additional AEM measurements conducted in the beginning of July 2020 confirm that the modal SIT derived from the GEM surveys is in fact reliable and representative for the wider area (Fig. 6.S2).

On the basis of AEM surveys conducted over the DNR in April and early July 2020 and the already existing IceBird time series we argue that the modal SIT of 1.71 m measured on the MOSAiC floe is not just representative for the wider area around the floe but also in line with measurements from previous years (Fig. 6.1 b)). The modal thickness of the MOSAiC floe is within one standard deviation of the long-term average over all modal SIT values derived for the AOI. This agreement indicates that the MOSAiC floe and its wider vicinity are not exceptional in terms of modal thickness compared to the long-term time series. The comparison of the MOSAiC floe modal SIT with SIT values reconstructed by the thermodynamic model from Thorndike (1992) confirms that the MOSAiC floe was not exceptionally thin. In fact, Fig. 6.3 b) shows a stronger underestimation of modal SIT by the model as observed in previous years (with the exception of the year 2016). Despite the fact that when the MOSAiC floe reached the AOI it was of a similar age as the ice in 2016, modal SIT was considerably thicker. This indicates that the MOSAiC floe might have been less impacted by oceanic heat than the ice that reached the AOI in 2016.

Nevertheless, it is important to note that these results are preliminary. Detailed studies of the ice thickness development of the MOSAiC floe along its drift path through the Arctic and its surroundings are the basis for future studies.

6.3.4 Comparison to Russian shipborne SIT observations

Due to the position of the selected AOI just north of the Fram Strait the presented SIT time series provides the possibility to investigate interannual variability of the time-integrated signal of Arctic-wide SIT changes. Nevertheless, the selected AOI is a highly variable, and small excerpt of the Arctic Ocean. Additionally, the presented time series is interrupted and still too short to provide insight into SIT changes on climatological scales. For example, the transition from a MYI-dominated towards a FYI/SYI-dominated Transpolar Drift (Kwok, 2018) that was accompanied by a drastic reduction in Arctic SIT and sea ice volume (Kwok, 2018) and accelerated drift speeds along the Transpolar Drift (Spreen et al., 2011; Krumpfen et al., 2019) between 2005 and 2007 is hardly recognisable in the presented IceBird time series. In order to determine whether the reduction in SIT

in the AOI is also observed upstream in the central Arctic we turn to the only continuous long-term SIT observational data set available close to the North Pole. Visual and STK July SIT observations obtained during Russian tourist cruises from Franz Josef Land to the North Pole (86 to 90°N along the 50°E meridian, see red line in Fig. 6.1 a)) confirm a step-wise decrease in SIT between 2005 and 2007 (Fig. 6.5), which is hardly visible in the AOI time series. The Russian observations in fact indicate that a similar regime shift already occurred between 1992 and 1993. Although SIT shows interannual variability, no trends are observed during each of the three regimes (prior to 1993, between 1993 and 2006 and from 2006 onwards). In years where both time series provide mean SIT values (2010 to 2012 and 2018) Russian observations tend to show thinner sea ice compared to IceBird measurements. Considering that the Russian observations were conducted during the same season as the IceBird measurements and upstream of the AOI one would expect those values to be thinner than the downstream measurements. However, we also attribute the lower estimates of SIT from the Russian observations to the inherent differences between the observation techniques. While visual and STK SIT observations are largely dependent on the ships route and the avoidance of thicker ice patches for faster navigation through the ice, AEM measurements provide SIT distributions on larger spatial scales. We would therefore assume a bias towards, on average, thinner sea ice for the Russian observations compared to AEM measurements. Nevertheless, the Russian observations provide a much longer time series than the IceBird measurements, which allows us to confirm general changes in the overall SIT regime in the central Arctic (Kwok, 2018). While the AOI time series indicates further thinning of sea ice between 2010 and 2020, Russian observations show no trend at all.

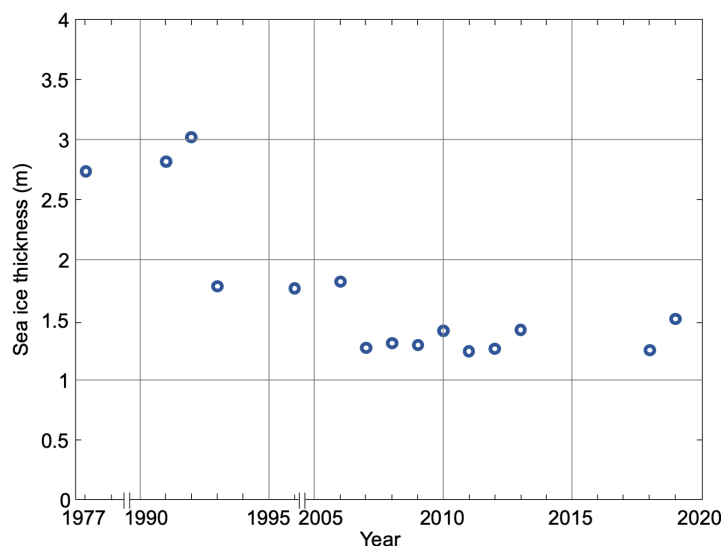


Figure 6.5: Sea ice thickness (SIT) observations conducted on regular tourist cruises from Franz Josef Land to the North Pole in July. SIT was determined using visual observations from AARI ice specialists or TV-complex calculations and averaged over a transect from 86 to 90°N, along the 50°E meridian.

The length of the Russian observational time series and its ability to show the previously observed regime shift in SIT indicates how valuable consistent long-term time series are. However, the deviations from the IceBird measurements also show its limitations and the importance of joint observations for a better understanding of differences and ultimately a better basis for the interpretation of past, present and future ship-based observations from Russian sea ice experts.

6.4 Conclusion

This study provides an important extension of the first long-term EM-derived summer SIT time series at the end of the Transpolar Drift. We combine these large-scale summer SIT measurements conducted within the framework of the IceBird campaign with Lagrangian ice tracking and a reconstructed SIT time series from a thermodynamic sea ice growth model. With this comprehensive approach we explain the observed interannual SIT variability within our selected area of interest (AOI, 80.5-86°N and 30°W-20°E) and investigate the driving mechanisms and source regions of this variability. Based on preliminary results from SIT measurements gathered during the MOSAiC drift experiment, we also put the MOSAiC floe into a historical context in terms of its thickness.

The analysis of pathways and sea ice origin with the Lagrangian ice tracking tool ICETrack reveals that approximately 65% of the ice sampled in the AOI originated in the Laptev Sea. Sea ice reaching the end of the Transpolar Drift is thinning. AOI mean and modal SIT values decreased by about 20% from 2001 to 2020. Most of the observed interannual variability in modal SIT is explained by the increase in drift speeds along the Transpolar Drift and the ensuing decrease in sea ice age and FDDs. The fact that ice has less time to grow is also represented in the increasing fractions of FYI and especially SYI observed in the AOI. SIT measurements conducted on the MOSAiC floe, when it reached the southern border of the AOI in July 2020, show that the MOSAiC modal SIT is consistent with IceBird measurements from previous years.

The absolute modal SIT minimum that was measured in the AOI in 2016 is partly attributed to the influence of intensified upward Atlantic Water (AW) heat flux during a strong Atlantification event in the Laptev Sea in winter 2015. Using ICETrack we were able to detect that the ice sampled in the AOI in 2016 formed in autumn 2014 and passed the region where Polyakov et al. (2017, 2020) observed strong Atlantification between January and May 2015. Increased ocean heat flux reduced ice growth in the Laptev Sea during this period. Based on the analysis with the thermodynamic sea ice growth model and the IceBird SIT time series we are able to show how persistent in time and space the impact of Atlantification on Arctic sea ice potentially is. It seems that, due to the fast drift across the Arctic Ocean, winter ice growth was not able to compensate the low initial ice thickness after the Atlantification event. With a tendency towards even faster ice drift along the Transpolar Drift in the future, the impact of Atlantification on sea ice in the eastern marginal ice zone will increasingly be felt in other parts of the sea ice covered Arctic. The presented model analyses also revealed that the assumption of a constant and also our adjusted ocean heat fluxes along the sea ice trajectories are insufficient to fully explain the observed modal SIT minimum in 2016. However, it is evident that the influence of oceanic heat on sea ice is drastically increasing (Polyakov et al., 2020) and sea

ice growth models require improved representations of spatial and temporal variability of ocean heat fluxes.

Further investigations and measurements are required to monitor the development of Atlantification in the eastern marginal ice zones. But in order to strengthen our conclusion that Atlantification is able to precondition sea ice and that this preconditioning persists far beyond the eastern Arctic, additional uninterrupted SIT time series are vital along the pathways and at the exit gates of Arctic sea ice. The presented IceBird SIT time series at the end of the Transpolar Drift is an important effort to establish long-term measurements of SIT, especially during the melt season. Airborne EM measurements of SIT during IceBird campaigns provide the necessary accuracy and areal coverage that is unmatched by any other non-satellite SIT measurement approach. Russian shipborne SIT measurements show significant differences to EM-based measurements, but their regularity and spatial consistency enable the depiction of regime shifts in SIT that are hardly resolved by the presented IceBird SIT time series. Obtaining SIT distributions over large areas and developing and continuing long-term SIT time series will provide unique input data for modelling efforts, and ultimately will improve predictions of Arctic sea ice and its thickness in the future. Continuing regular IceBird measurement campaigns in the vicinity of Fram Strait and combining the results with reliable models and ice tracking tools will prove indispensable for monitoring the complex and radical change of sea ice on an Arctic-wide scale.

Table 6.1: Summary of used research platforms, sampling periods, profile lengths, and basic sea ice thickness statistics for the selected area of interest (see Fig.6.1 a)) and individual research campaigns.

Year	Campaign	Platform	Measurement periods	Total profile length (km)	SIT (m)		Mean SIT of upper 10% (m)	Fraction of open water	Reference
					Mean/Mode				
2001	ARK-XVII/2	RV Polarstern	Aug 6 - Aug 23	50	2.56/1.96		5.12	-	Haas (2004)
2004	ARK-XX/2	RV Polarstern	Jul 28 - Aug 14	2270	2.55/1.99		5.25	1 %	Haas et al. (2008)
2010	IceBird/TIFAX	Polar 5	Aug 19 - Aug 22	400	2.17/1.75		4.51	1 %	Haas et al. (2010)
2011	IceBird/TIFAX	Polar 5	Aug 2 - Aug 3	450	2.04/1.75		4.15	4 %	Kruppen et al. (2011)
2012	IceBird/TIFAX	Polar 5	Jul 20 - Jul 21	300	2.49/1.88		5.28	1 %	Kruppen (2012)
2016	IceBird/TIFAX	Polar 6	Jul 25 - Aug 1	1070	2.01/1.00		5.84	0 %	Kruppen and Sellmann (2016)
2017	IceBird/TIFAX	Polar 6	Aug 13 - Aug 20	500	1.77/1.63		3.71	7 %	Kruppen et al. (2017)
2018	IceBird Summer	Polar 6	Aug 7 - Aug 13	600	1.98/1.50		4.19	1 %	Kruppen et al. (2018)
2020	MOSAIC	RV Polarstern	Jul 16 - Jul 21	14	2.33/1.71		4.53	-	
	IceBird MOSAIC	Polar 6	Sep 7 - Sep 8	300	1.53/1.03		3.94	1 %	

Supplements

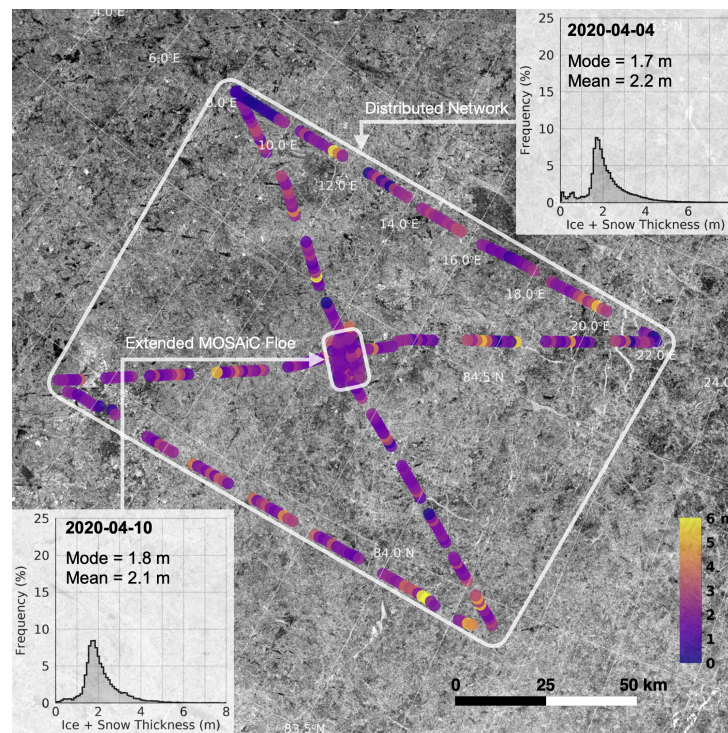


Figure 6.S1: Sentinel-1 SAR image from April 10, 2020 (source: ESA) superimposed by airborne EM survey lines and sea ice thickness (SIT) values gathered during Leg 3 of the Multidisciplinary drifting Observatory for the Study of Arctic Climate (MOSAiC). Modal and mean EM SIT values are given for the extended MOSAiC floe (bottom left) and the larger Distributed Network area (top right). At the time of the survey flights the floe was located at approximately 84.5°N and 14°E .

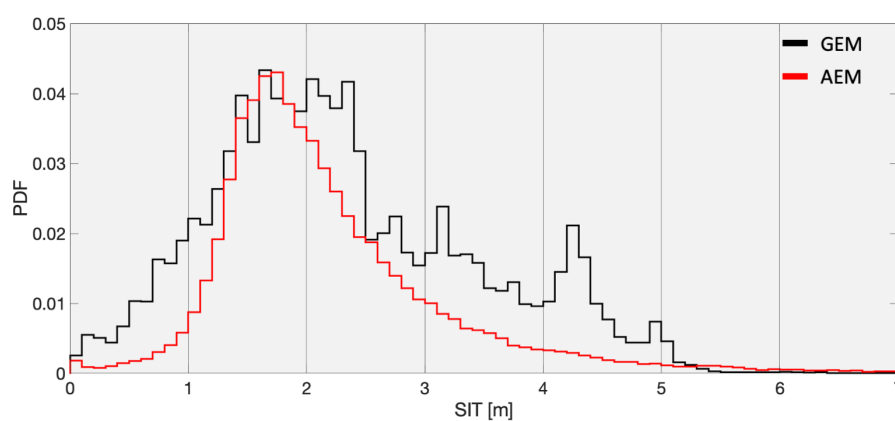


Figure 6.S2: Comparison of MOSAiC floe sea ice thickness distribution gathered with the ground-based EM (GEM) between July 16 to July 21, 2020 (black) and airborne EM (AEM) derived sea ice thickness distribution (red) of the floe and wider area (radius about 5 km around the floe) from July 1 and July 7, 2020.

Acknowledgements

This project was carried out in the framework of the BMBF-funded Russian-German cooperation QUARCCS (grant: 03F0777A).

2020 AEM and GEM data used in this manuscript were produced as part of the international Multidisciplinary drifting Observatory for the Study of the Arctic Climate (MOSAiC20192020) during IceBird MOSAiC summer (P6-222_IceBird_MOSAiC_2020) and the RV Polarstern Legs 3 (AWI_PS122_03) and 4 (AWI_PS122_04).

The processing of visual and STK data by T. A. Alekseeva, S. V. Frolov and S.S. Serovetnikov was funded by the Russian Foundation for Basic Research (RFBR) according to the research project number 18-05-60048.

We want to thank the AWI logistics department, the crews of the research aircrafts *Polar 5* and *6*, the crews of Station North in Greenland, the pilots and crews on RV Polarstern (Alfred Wegener Institute, 2017) and the observers on the Russian icebreakers for their tireless efforts during the various expeditions. This unique collection of data from different expeditions would not exist without you!

Data availability

IceBird EM data are available on request from Thomas Krumpen and Jakob Belter (tkrumpen@awi.de, jbelter@awi.de).

All MOSAiC-related data are archived in the MOSAiC Central Storage (MCS) and will be available on PANGAEA after finalisation of the respective datasets according to the MOSAiC data policy.

ESA Sea Ice Climate Change Initiative (Sea_Ice_cci): Northern hemisphere sea ice thickness from ENVISAT satellite (Hendricks et al., 2018c) and from CryoSat-2 satellite (Hendricks et al., 2018a) on a monthly grid (L3C), v2.0 are available from the Centre for Environmental Data Analysis data base.

Surface air temperature reanalysis data is available from www.esrl.noaa.gov/psd/product.

7 Conclusion and outlook

The overarching goal of the studies presented in this dissertation was to observe and analyse sea ice thickness variability and change in the regions of ice formation to determine their impact on the overall Arctic sea ice budget. The first objective was to develop a method to derive sea ice thickness data in the FYI-dominated Laptev Sea and extend the existing data set derived from high resolution ULSs. ULSs of the type IPS are specifically deployed with moorings for the purpose of measuring sea ice draft, which is converted into sea ice thickness. However, IPSs have been deployed in the Laptev Sea for comparably short time periods. Other moored, sonar-based instruments, such as upward-looking ADCPs, which can be used for the derivation of sea ice draft as well, have been deployed in this region since the beginning of the 21st century. The prospect of exploiting these ADCP records promised a significant extension of sea ice thickness data sets in the Laptev Sea and a basis for the investigation of sea ice thickness variability in a region where this was not possible so far.

While previous studies (Shcherbina et al., 2005; Banks et al., 2006; Bjoerk et al., 2008; Hyatt et al., 2008) already used upward-looking ADCPs for the derivation of sea ice draft, they relied on accurate pressure sensors to determine instrument depth. This integral parameter is required for the derivation of sea ice draft using moorings equipped with sonars and internal pressure sensors were previously considered indispensable for determining the instrument depth. However, ADCPs previously deployed in the Laptev Sea were not equipped with complementary pressure sensors. The method described in Chapter 3 contributes to eliminate this limitation and shows that upward-looking ADCPs can be used to derive instrument depth, even without using a pressure sensor. It is shown that the instrument depth of upward-looking ADCPs operated in bottom track mode can be inferred from routine measurements of error velocity. The fact that the investigated ADCPs measured alongside the specifically-designed IPSs in the Laptev Sea from 2013 to 2015 was used to validate this adaptive approach. It is shown that it is possible to derive daily mean sea ice draft time series from bottom track mode operated ADCPs lacking complementary pressure sensors.

The application of the newly developed approach to the data from previously deployed ADCPs, yielded a valuable sea ice draft data archive covering the period from 2003 to 2016, which marks a significant extension of the data record in the Laptev Sea. One of the purposes of obtaining new sea ice thickness data in the Laptev Sea was to investigate interannual sea ice thickness variability. However, the spatial distribution of the exploited ADCP moorings all over the Laptev Sea prevented this investigation due to the fact that no single-location, long-term time series was generated. Nevertheless, these newly available time series can answer other research questions. For example, sea ice thickness observations from different regions and from different time periods can be used to gain insight into regional differences in ice formation processes. Additionally, regional differences in sea ice thickness distribution can be investigated during different atmospheric and oceanic forcing patterns that are typical for the Laptev Sea. Finally, these time series can also be used to support other approaches to observe sea ice thickness. Their tempo-

ral coverage proved to be sufficient to achieve the second main objective, which was the validation of satellite sea ice thickness data.

While previous validation studies were limited to MYI-dominated regions, the newly acquired sonar-based data allowed for the first time validation of satellite-derived sea ice thickness in a FYI-dominated region. The dominance of FYI in the Laptev Sea is a result of continuous northward transport of newly formed thin ice. Given the location of the Laptev Sea, this flow of FYI feeds directly into the Transpolar Drift and strongly influences the Arctic sea ice budget. This makes the new interpretation of satellite sea ice thickness records in this region extremely valuable for estimating sea ice volume fluxes with an improved accuracy.

For the validation study presented in Chapter 4, ESA CCI-2 and CS2SMOS sea ice thickness data were converted into sea ice draft and compared to the new sonar-based draft data set. This comparison revealed that the agreement between satellite and sonar-based draft is sensitive to the thickness of the sampled ice. While ice thinner than approximately 0.7 m is overestimated by almost all of the investigated satellite products, ice thicker than approximately 1.3 m is increasingly underestimated. In the Laptev Sea, the ESA CCI-2 and CS2SMOS products provide modal rather than mean sea ice draft, which effectively means that they can only be used to analyse the thickness of thermodynamically grown sea ice in that region. The effects of dynamic deformation events on sea ice thickness are not resolved in the investigated satellite records. These discoveries are vitally important for the interpretation of current satellite sea ice thickness products and have to be considered in further improvements of their retrieval algorithms. Satellite-derived ice volume flux estimates from the Laptev Sea likely underestimate actual volume fluxes and are not comparable to estimates from MYI-dominated regions. Even more uncertainty arises for regions that are covered by similar fractions of FYI and MYI.

Although the newly acquired sonar-based sea ice draft data archive did not allow for the investigation of interannual sea ice thickness variability itself, it facilitated this investigation through the validation of satellite-derived sea ice thickness. The ESA CCI-2 and CS2SMOS data products can not be used to estimate sea ice volume fluxes reliably, but show monthly respectively weekly sea ice thickness variations of thermodynamically grown ice in the Laptev Sea during the winter periods from 2002 to present day. The general thinning of sea ice observed from satellites in the winter months from October through April showed that this region of Arctic sea ice formation was undergoing continuous change over the past almost 20 years. This change was investigated in more detail to put the initial ice conditions observed at the start of the MOSAiC drift experiment into the historical context (see Appendix for my contribution to the study by Krumpen et al., 2020). Sea ice has been thinning as a result of atmospheric and oceanic influences and regional feedback mechanisms, that affect ice growth, melt, and distribution in both summer and winter (Krumpen et al., 2020). Increased offshore-directed transport of sea ice in winter results in dynamic thinning all over the Laptev Sea, which in turn preconditions the ice for the subsequent summer season (Itkin and Krumpen, 2017). Additionally, studies by Polyakov et al. (2017, 2020) showed that winter sea ice growth is decelerated through events of strong upward-directed AW heat fluxes, termed Atlantification. Vast ice areas remain thin and melt faster during the following summer season. The already thin-

7 Conclusion and outlook

ning ice cover is also exposed to increasingly long melt periods. Increasing temperatures at the end of the winter lead to earlier melt onset and ice break-up in spring (Onarheim et al., 2018), while increased warming of the upper ocean (Janout et al., 2016) results in delayed freeze-up in autumn (Krumpfen et al., 2020).

In order to answer the overarching question whether these regional changes of sea ice thickness have a lasting effect on sea ice as it is transported through the Arctic Ocean, a comprehensive study combining AEM sounding measurements, Lagrangian ice tracking, and sea ice growth modelling was conducted (Chapter 6). It is shown that approximately 65% of the sea ice reaching Fram Strait in summer originates from the Laptev Sea, which allowed the investigation of whether the sea ice thickness anomalies observed in this region of ice formation propagated to the end of the Transpolar Drift. Due to the decrease in sea ice age, faster drift speeds across the central Arctic Ocean, and the decrease in FDDs, sea ice reaching the end of the Transpolar Drift decreased in thickness by about 20% between 2001 and 2020. Thermodynamic sea ice growth was modelled along the trajectories across the Arctic Ocean and in general the modelled values at the end of the trajectories agreed well with the observed modal sea ice thicknesses. However, observed modal sea ice thickness at the end of the Transpolar Drift were largely overestimated by the model in 2016. The conducted sea ice pathway analysis revealed that the 2016 ice was potentially affected by a strong Atlantification event in the Laptev Sea in the winter of 2015. The model representation of ocean heat flux was adjusted to investigate whether the influence of such a strong Atlantification event at the beginning of the Arctic sea ice life cycle is in fact able to persist until the ice reaches the end of the Transpolar Drift. Conservative estimates for the ocean heat flux influence resulted in a decrease in the difference between modelled and observed modal sea ice thickness. However, these estimates were not able to overcome the overestimation completely. It is concluded that improved estimates of ocean heat fluxes and the areal extent on which they impact sea ice growth are required for future analyses of the effect of Atlantification on Arctic sea ice thickness. Thermodynamic models also require better representation of snow distribution and melt processes, as they strongly impact thermodynamic sea ice growth as well and likely contributed to the observed variability. Nevertheless, the adjusted model runs showed that sea ice thickness anomalies can potentially persist for more than a year and over thousands of kilometres.

The conclusion drawn from these results is that mechanisms such as, but not limited to, Atlantification that decelerate sea ice growth in the source regions of Arctic sea ice can alter the initial sea ice thickness in a way that may not be compensated by sea ice growth along the drift trajectories of sea ice through the Arctic Ocean. The tendency towards faster transport of sea ice across the Arctic Ocean supports this preconditioning, as sea ice drifting from the Russian shelf seas towards Fram Strait will likely have even less time to grow. For the 2016 case, the observed modal sea ice thickness anomaly at the end of the Transpolar Drift was attributed partially to the preconditioning effect of Atlantification on sea ice growth in the Laptev Sea. However, considering that the transport of sea ice from the shallow Russian shelves was interrupted more frequently in recent years (Krumpfen et al., 2019), it is more likely that future preconditioning of sea ice on the shallow Russian shelves, independent of the mechanism causing it, is not

measurable downstream at the end of the Transpolar Drift anymore. Ice forming on the Russian shelves will potentially be too thin to withstand the first summer season and melt before even reaching the Transpolar Drift. In the future, ice reaching the end of the Transpolar Drift will likely have formed in deeper waters north of the shallow Russian shelves.

The evolution of Arctic sea ice thickness remains an active field of research and there is a fundamental need for further improvement of the ways sea ice and its thickness are monitored and analysed. The studies presented in this dissertation contribute to achieve that. The developed method (Chapter 3) made the acquisition of a long-term sea ice thickness data archive in the FYI-dominated Laptev Sea possible. It also provides the means to revisit previous data sets to close gaps in sea ice thickness records and even a low-cost alternative for future derivations of sea ice thickness from sonar-equipped moorings in other ice-covered regions. The generated data archive provided valuable new data for the validation of available satellite sea ice thickness products, which contributes to a better interpretation of these products in a region that is considered the starting point of the Arctic sea ice life cycle (Chapter 4). The third study applied different methods to investigate sea ice growth along the Transpolar Drift, connect influences on sea ice growth in the source regions to anomalies measured at the end of the life cycle of Arctic sea ice, and promotes the approach of combining different data sets and tools to describe observed sea ice thickness changes in the Arctic comprehensively (Chapter 6).

Outlook

In light of the continuous reduction of the Arctic sea ice cover and the growing public and economic interest in the Arctic, sea ice research should put even more focus on three main objectives: reliably monitoring and analysing the current state of the most important sea ice parameters, in particular in regions of major interest for the Arctic sea ice life cycle; investigating the influences these parameters have on other components of the Arctic and global climate system and vice versa; and the prediction of Arctic sea ice and its role in the future. Applying these objectives specifically to the parameter sea ice thickness leads to a number of key milestones that need to be accomplished:

- The monitoring of the current state requires reliable continuous data sets that cover the Arctic as a whole but also resolve relevant processes on short temporal and small spatial scales. The lack of a single-source, comprehensive sea ice thickness data set shows the need for the combination of the advantages of the existing and new techniques and approaches to monitor and describe the thickness of the complex and variable sea ice cover. The most commonly used measurement techniques obtain parameters related to sea ice thickness, which requires additional knowledge for the conversion of these parameters to sea ice thickness. While this is true for measurements from ULSs and, to some degree, EM sounding instruments, it is perhaps most critical for the improvement of the satellite sea ice thickness retrieval process. Some of the most important, because least understood, parameters required for the derivation of sea ice thickness are related to snow. Snow properties such as depth, distribution, density, salinity, and surface roughness are considered to be the

7 Conclusion and outlook

main sources of uncertainty, especially for the satellite retrieval of freeboard (Ricker et al., 2014; Sallila et al., 2019). These parameters affect the penetration of the radar altimeter signal and the reflection of the laser altimeter signal and lead to biases and uncertainties in the determination of the snow-ice and air-snow interface, respectively (Kwok et al., 2007; Kwok, 2014; Ricker et al., 2014; Nandan et al., 2017). However, they are as important to the retrieval of freeboard as they are to the conversion of freeboard, or draft in the case of ULSs, to sea ice thickness. The assumption of hydrostatic equilibrium used for this conversion relies on knowledge about snow and ice densities as well as snow depth (Ricker et al., 2014; Tilling et al., 2018; Hendricks and Ricker, 2019a). Advances in observing snow depth are being made by conducting snow radar measurements over sea ice during airborne campaigns, such as Operation IceBridge and IceBird, and improving the processing algorithms to retrieve snow data (Kwok et al., 2017; Jutila et al., 2020). Another important puzzle piece for more reliable representations of snow and ice properties are the comprehensive in situ data sets gathered during the MOSAiC drift experiment.

In general, the acquisition of new and the continuation and improvement of existing long-term sea ice thickness records, but also the validation of current and future satellite products (e.g. from ICESat-2 (Petty et al., 2020) and CRISTAL (Kern et al., 2020)), remain important for understanding the processes affecting Arctic sea ice and its thickness. The three studies conducted in the framework of this dissertation are a testament to that and show that data sets from all possible sources need to be combined to complement each other and monitor the current state of Arctic sea ice and its thickness. Where the strategic application of different measurement techniques and tools falls short, improved ice tracking tools, such as ICETrack, and models have to fill in the gaps in regions that are inaccessible and during times when data collection is simply not possible.

- While models can fill observational gaps for the monitoring of sea ice, they also provide the means to connect sea ice observations to other relevant components of the Arctic and global climate system. Data sets, like the ones generated in the framework of this dissertation (Chapters 3 and 6), are an important part of improving sea ice thickness growth models. These models have different levels of sophistication for the relevant mechanisms responsible for the growth and melt of sea ice and facilitate the holistic approach of analysing the Arctic climate not only through single parameters but as a complex system. This approach is advantageous particularly in the currently changing system, where ocean heat seems to play a more dominant role. The application of the simple thermodynamic growth model described in Chapter 6 gives a prospect of the capabilities of models for the investigation of sea ice interactions with other parts of the Arctic climate. However, assumptions of constant ocean heat flux proved to be insufficient to model observed sea ice thickness changes and comprehensive representations of these fluxes are required to improve sea ice growth models in the future. These model improvements heavily rely on observational data. Again, the unique data sets gathered during the MOSAiC drift experiment will contribute, as they provide valuable reference data for modelling

of a system that is virtually inaccessible during most of the year. However, the financial and logistical burdens of expeditions like MOSAiC prevent the research community from conducting these comprehensive experiments regularly, which is why models have to incorporate the knowledge that was and will be gained in the field and apply it in the future.

- The strong interplay of different atmospheric and oceanic mechanisms with the reducing ice cover needs to be thoroughly understood and modelled in order to predict the development of the Arctic sea ice cover reliably in the future. The Laptev Sea sonar-based sea ice thickness data sets derived using the method presented in Chapter 3 as well as the EM-based data sets presented in Chapter 6 are already being used to further improve and tune sea ice models, such as ICEPACK (Urrego-Blanco et al., 2016; CICE Consortium, 2020) and NAOSIM (Sumata et al., 2019). Simulating sea ice thickness observations from the past (hindcasting) will potentially improve the forecasting capabilities of these models. In that regard, the sonar-based data archives in the Laptev Sea and the EM-based observations at the end of the Transpolar Drift can be considered extremely valuable as they provide data from strategically important areas of interest along the Arctic sea ice life cycle. In addition to predicting changes in sea ice thickness, these models have the potential to simulate the effects a changing sea ice cover may have on the Arctic and global climate and vice versa.
- Another major milestone mentioned here is relevant for all three of the objectives sea ice research should address in particular. It concerns the better representation of dynamic and especially deformation processes in the monitoring and modelling of Arctic sea ice thickness. The overall sea ice thickness distribution is shaped by the superimposition of thermodynamic and dynamic processes. Thermodynamic sea ice growth is slow and eventually limited when the equilibrium thickness is reached. Dynamic deformation processes on the other hand can lead to rapid changes in thickness and therefore are most responsible for shaping the overall thickness distribution (Haas, 2017; von Albedyll et al., 2020). However, deformation and its immediate impact is difficult to observe and currently poorly understood. The validation of satellite sea ice thickness products presented in Chapter 4 showed that deformation is not at all represented in the average satellite sea ice thickness products in regions like the Laptev Sea. This absence of information about deformation processes results in significant deficiencies of these products and prevents a reliable investigation of sea ice volume fluxes in the Arctic. It also prevents the research community from predicting the full extent of imminent changes in sea ice thickness. It has been hypothesised that the observed thinning and increased mobility of the Arctic sea ice cover may favour deformation processes (Itkin et al., 2018; von Albedyll et al., 2020). This could have significant implications for the overall sea ice thickness distribution and reliable observations are required to confirm these relationships. Apart from this being a research interest, it may also be relevant for shipping activities in the Arctic, which are projected to increase with the continuous decline in the Arctic sea ice cover (German Arctic Office, 2019).

7 Conclusion and outlook

Reaching the above-mentioned milestones and objectives will allow the comprehensive monitoring and prediction of sea ice thickness as a parameter of the Arctic sea ice cover. In combination with sea ice extent and motion information, it will provide the means to link the comparably thin, but complex, layer between ocean and atmosphere to the global climate system and help us understand and adjust to the changes we are potentially facing.

Appendix

Co-authorships of related publications

This section presents publications related to this dissertation that I co-authored. These publications utilised the Lagrangian ice tracking tool, ICETrack. Over the course of my doctorate I contributed to the improvement of the algorithm, especially for the combination of the thermodynamic sea ice growth model with ICETrack. These improvements lay the groundwork for the model analysis presented in my first-author publication presented in Chapter 6.

Arctic warming interrupts the Transpolar Drift and affects long-range transport of sea and ice-rafted matter, (2019) by T. Krumpfen, H. J. Belter, A. Boetius, E. Damm, C. Haas, S. Hendricks, M. Nicolaus, E.-M. Noethig, S. Paul, I. Peeken, R. Ricker, and R. Stein published in *Scientific Reports*, 9, 5459, doi:10.1038/s41598-019-41456-y

This study investigates the increasing summer melt along the Russian shelves, which prevents sediment-laden sea ice to be incorporated into the Transpolar Drift and ultimately the release of the ice-rafted substances during melt in the Fram Strait. The interruption of this long-range transport leads to the premature release of climate relevant gases, sediments, and pollutants and increases the accumulation of these matters in the central Arctic Ocean. I contributed to the design of the experiments for the analysis of sea ice pathways. I also helped include the thermodynamic sea ice growth model (Thorndike, 1992) into ICETrack and contributed to the writing and editing of the manuscript.

The MOSAiC ice floe: sediment-laden survivor from the Siberian Shelf, (2020) by T. Krumpfen, F. Birrien, F. Kauker, T. Rackow, L. von Albedyll, M. Angelopoulos, H. J. Belter, *et al.* published in *The Cryosphere*, 14, 2173-2187, doi:10.5194/tc-14-2173-2020

This study focusses on the start region of the MOSAiC drift experiment, the origin of the MOSAiC floe, and its growth from the East Siberian Islands to the starting point of the drift experiment in September 2019. In addition to my contributions to the search of the MOSAiC floe, I contributed to the improvement of the thermodynamic model algorithm and the writing and editing of the manuscript. The EM-based sea ice thickness measurements I conducted on multiple potential floes in the vicinity of the MOSAiC floe provided data for the analysis and helped me gain a deeper understanding of EM-based sea ice thickness measurements. I was able to apply that knowledge during the IceBird MOSAiC summer campaign 2020, which provided valuable data for the extension of the sea ice thickness time series presented in my first-author publication (Chapter 6).

List of Figures

1.1	Sea ice concentration in March and September 2020	2
2.1	Schematic of sea ice thermodynamics	8
2.2	Example of sea ice thickness distribution	9
2.3	Schematic of dynamic sea ice growth	11
2.4	Mean Arctic sea ice thickness (January to April 2020)	12
2.5	Schematic of an Upward-Looking Sonar	15
2.6	Schematic of an airborne electromagnetic induction sounding (AEM) instrument	17
3.1	Map of the Laptev Sea showing ULS and ADCP moorings (2013-2015) . .	25
3.2	Schematic of an upward-looking ADCP	28
3.3	Tilt magnitude calculated from ADCP data	29
3.4	ADCP beam 2 open water range values (Taymyr-13/14)	31
3.5	ULS versus ADCP-derived daily mean sea ice draft	32
3.6	Daily mean sea ice draft timeseries from ADCP and ULS	33
3.7	Percentage deviation of ULS from ADCP-derived sea ice draft	34
3.8	Boxplots of sea ice draft data derived from ULS and ADCP	35
4.1	Map of the Laptev Sea showing sonar mooring sites	48
4.2	ESA CCI-2 sea ice thickness anomaly in the Laptev Sea	53
4.3	Difference between ENVISAT/CS2 and sonar sea ice draft	54
4.4	Binned scatter plot: ESA CCI-2 versus sonar sea ice draft	57
4.5	Binned scatter plot: all satellite products versus sonar sea ice draft	59
4.6	Difference between ENVISAT/CS2 and sonar sea ice draft for different thickness ranges	60
4.7	Taymyr station time series (2013-2014): CS2 and CS2SMOS compared to sonar sea ice draft	62
5.1	ESA CCI-2 winter sea ice thickness in the Laptev Sea	68
6.1	Map and time series of EM ice thickness measurements (2001-2020)	74
6.2	Sea ice drift trajectories from the AOI-sampled ice (2001-2020)	79
6.3	AOI sea ice age, number of FDDs and modelled thickness	81
6.4	Analysis of the potential impact of Atlantification	82
6.5	Russian shipborne ice thickness observations (1977-2019)	87
6.S1	Airborne EM surveys conducted during MOSAiC leg 3 (April 2020)	91
6.S2	Ice thickness distributions from ground-based and airborne EM surveys conducted during MOSAiC leg 4 (July 2020)	91

List of Tables

3.1	Distances between ADCP and ULS moorings (2013-2015)	26
4.1	Statistical comparison between ENVISAT/ENVISATorbit and sonar sea ice draft data	55
4.2	Statistical comparison between CS2/CS2orbit and sonar sea ice draft data	56
4.3	Statistical comparison between CS2SMOS and sonar sea ice draft data . .	58
4.4	Statistical comparison between CS2-based mean and sonar-based modal sea ice draft data	63
6.1	Summary of relevant EM measurement (2001-2020)	90

References

- AARI: Guidance to Special Shipborne Ice Observations, Arctic and Antarctic Research Institute, St. Petersburg, 2011.
- Alekseeva, T., Tikhonov, V., Frolov, S., Repina, I., Raev, M., Sokolova, J., Sharkov, E., Afanasieva, E., and Serovetnikov, S.: Comparison of Arctic Sea Ice Concentrations from the NASA Team, ASI, and VASIA2 Algorithms with Summer and Winter Ship Data, *Remote Sensing*, 11, 2481, <https://doi.org/10.3390/rs11212481>, 2019.
- Alfred Wegener Institute: Polar Research and Supply Vessel POLARSTERN Operated by the Alfred Wegener Institute Helmholtz Centre for Polar and Marine Research, *Journal of large-scale research facilities*, 3, <https://doi.org/10.17815/jlsrf-3-163>, 2017.
- ASL: IPS Processing Toolbox User's Guide, ASL Environmental Sciences Inc., Victoria, B. C., 2017.
- Assmy, P., Fernández-Méndez, M., Duarte, P., Meyer, A., Randelhoff, A., Mundy, C. J., Olsen, L. M., Kauko, H. M., Bailey, A., Chierici, M., Cohen, L., Doulgeris, A. P., Ehn, J. K., Fransson, A., Gerland, S., Hop, H., Hudson, S. R., Hughes, N., Itkin, P., Johnsen, G., King, J. A., Koch, B. P., Koenig, Z., Kwasniewski, S., Laney, S. R., Nicolaus, M., Pavlov, A. K., Polashenski, C. M., Provost, C., Rösel, A., Sandbu, M., Spreen, G., Smedsrud, L. H., Sundfjord, A., Taskjelle, T., Tatarek, A., Wiktor, J., Wagner, P. M., Wold, A., Steen, H., and Granskog, M.: Leads in Arctic pack ice enable early phytoplankton blooms below snow-covered sea ice, *Scientific Reports*, 7, <https://doi.org/10.1038/srep40850>, 2017.
- Banks, C. J., Brandon, M. A., and Garthwaite, P. H.: Measurement of sea-ice draft using upward-looking ADCP on an autonomous under water vehicle, *Annals of Glaciology*, 44, 211–216, <https://doi.org/10.3189/172756406781811871>, 2006.
- Bareiss, J. and Goergen, K.: Spatial and temporal variability of sea ice in the Laptev Sea: Analyses and review of satellite passive-microwave data and model results, 1979 to 2002, *Global Planetary Change*, 48, 28–54, <https://doi.org/10.1016/j.gloplacha.2004.12.004>, 2005.
- Bauch, D., Hoелеmann, J., Willmes, S., Gröger, M., Novikhin, A., Nikulina, A., Kassens, H., and Timokhov, L.: Changes in distribution of brine waters on the Laptev Sea shelf in 2007, *Journal of Geophysical Research: Oceans*, 115, <https://doi.org/10.1029/2010JC006249>, 2010.
- Behrendt, A., Dierking, W., and Witte, H.: Thermodynamic sea ice growth in the central Weddell Sea, observed in upward-looking sonar data, *Journal of Geophysical Research: Oceans*, 120, 2270–2286, <https://doi.org/10.1002/2014JC010408>, 2015.
- Belliveau, D., Budgen, G. L., Eid, B. M., and Calnan, C. J.: Sea Ice Velocity Measurements by Upward-Looking Doppler Current Profilers, *Journal of Atmospheric and*

- Oceanic Technology, 7, 596–602, [https://doi.org/10.1175/1520-0426\(1990\)007<0596:SIVMBU>2.0.CO;2](https://doi.org/10.1175/1520-0426(1990)007<0596:SIVMBU>2.0.CO;2), 1990.
- Belter, H. J., Janout, M. A., Krumpfen, T., Hoelemann, J. A., Timokhov, L., Novikhin, A., and Kassens, H.: Raw bottom track error velocity and range data from moored upward-looking Acoustic Doppler Current Profilers in the Laptev Sea between 2013 and 2015, PANGAEA data set, <https://doi.org/10.1594/PANGAEA.899269>, 2019a.
- Belter, H. J., Janout, M. A., Krumpfen, T., Ross, E., Hoelemann, J. A., Timokhov, L., Novikhin, A., Kassens, H., Wyatt, G., Rousseau, S., and Sadowy, D.: Daily mean sea ice draft from moored Upward-Looking Sonars in the Laptev Sea between 2013 and 2015, PANGAEA data set, <https://doi.org/10.1594/PANGAEA.899275>, 2019b.
- Belter, H. J., Janout, M. A., Hoelemann, J. A., and Krumpfen, T.: Daily mean sea ice draft from moored upward-looking Acoustic Doppler Current Profilers (ADCPs) in the Laptev Sea from 2003 to 2016, PANGAEA data set, <https://doi.pangaea.de/10.1594/PANGAEA.912927>, 2020a.
- Belter, H. J., Krumpfen, T., Hendricks, S., Hoelemann, J., Janout, M. A., Ricker, R., and Haas, C.: Satellite-based sea ice thickness changes in the Laptev Sea from 2002 to 2017: comparison to mooring observations, *The Cryosphere*, 14, 2189–2203, <https://doi.org/10.5194/tc-14-2189-2020>, 2020b.
- Belter, H. J., Krumpfen, T., Janout, M. A., Ross, E., and Haas, C.: Sea ice draft from upward-looking Acoustic Doppler Current Profilers (ADCPs): an adaptive approach, validated by Upward-Looking Sonar (ULS) data, in review at *Cold Regions Science and Technology*, 2020c.
- Bjoerk, G., Nohr, C., Gustafsson, B. G., and Lindberg, A. E. B.: Ice dynamics in the Bothnian Bay inferred from ADCP measurements, *Tellus*, 60, 178–188, <https://doi.org/10.1111/j.1600-0870.2007.00282.x>, 2008.
- Bourke, R. H. and Garret, R. P.: Sea ice thickness distribution in the Arctic Ocean, *Cold Regions Science and Technology*, 13, 259–280, [https://doi.org/10.1016/0165-232X\(87\)90007-3](https://doi.org/10.1016/0165-232X(87)90007-3), 1987.
- Budyko, M. I.: The effect of solar radiation variations on the climate of the Earth, *Tellus*, 21, 611–619, <https://doi.org/10.3402/tellusa.v21i5.10109>, 1969.
- Cavalieri, D. J. and Parkinson, C. I.: Arctic sea ice variability and trends, 1979–2010, *The Cryosphere*, 6, 881–889, <https://doi.org/10.5194/tc-6-881-2012>, 2012.
- Chapman, W. L. and Walsh, J. E.: Recent variations of Sea Ice and Air Temperature in High Latitudes, *Bulletin of the American Meteorological Society*, 74, 33–48, [https://doi.org/10.1175/1520-0477\(1993\)074<0033:RVOSIA>2.0.CO;2](https://doi.org/10.1175/1520-0477(1993)074<0033:RVOSIA>2.0.CO;2), 1993.
- CICE Consortium: Icepack version 1.1.0, <https://doi.org/10.5281/zenodo.1213462>, URL <https://buildmedia.readthedocs.org/media/pdf/cice-consortium-icepack/icepack1.1.1/cice-consortium-icepack.pdf>, 2020.

- Comiso, J. C. and Nishio, F.: Trends in the sea ice cover using enhanced and compatible AMSR-E, SSM/I, and SMMR data, *Journal of Geophysical Research*, 113, <https://doi.org/10.1029/2007JC004257>, 2008.
- Comiso, J. C., Meier, W. N., and Gersten, R.: Variability and trends in the Arctic Sea ice cover: Results from different techniques, *Journal of Geophysical Research: Oceans*, 122, 6883–6900, <https://doi.org/10.1002/2017jc012768>, 2017.
- Connor, L. N., Laxon, S. W., Ridout, A. L., Krabill, W. B., and McAdoo, D. C.: Comparison of Envisat radar and airborne laser altimeter measurements over Arctic sea ice, *Remote Sensing of Environment*, 113, 563–570, <https://doi.org/10.1016/j.rse.2008.10.015>, 2009.
- Cottier, F., Steele, M., and Nilsen, F.: Sea ice and Arctic Ocean oceanography, in: *Sea ice*, edited by Thomas, D. N., chap. 7, pp. 197–215, John Wiley and Sons, Ltd, Third edn., <https://doi.org/10.1002/9781118778371>, 2017.
- Curry, J. A., Schramm, J. L., and Ebert, E. E.: Sea Ice-Albedo Climate Feedback Mechanism, *Journal of Climate*, 8, 240–247, [https://doi.org/10.1175/1520-0442\(1995\)008<0240:SIACFM>2.0.CO;2](https://doi.org/10.1175/1520-0442(1995)008<0240:SIACFM>2.0.CO;2), 1995.
- Damm, E., Bauch, D., Krumpfen, T., Rabe, B., Korhonen, M., Vinogradova, E., and Uhlig, C.: The Transpolar Drift conveys methane from the Siberian Shelf to the central Arctic Ocean, *Scientific Reports*, 8, <https://doi.org/10.1038/s41598-018-22801-z>, 2018.
- Dee, D. P., Uppala, S. M., Simmons, A. J., Berrisford, P., Poli, P., Kobayashi, S., Andrae, U., Balmaseda, M. A., Balsamo, G., Bauer, P., Bechtold, P., Beljaars, A. C. M., van den Berg, L., Bidlot, J., Bormann, N., Delsol, C., Dragani, R., Fuentes, M., Geer, A. J., Haimberger, L., Healy, S. B., Hersbach, H., Holm, E. V., Isaksen, I., Kallberg, P., Koehler, M., Matricardi, M., McNally, A. P., Monge-Sanz, B. M., Morcrette, J.-J., Park, B.-K., Peubey, C., de Rosnay, P., Tavolato, C., Thepaut, J.-N., and Vitart, F.: The ERA-Interim reanalysis: configuration and performance of the data assimilation system, *Quarterly Journal of the Royal Meteorological Society*, 137, 553–597, <https://doi.org/10.1002/qj.828>, 2011.
- Dethleff, D., Rachold, V., Tintelnot, M., and Antonow, M.: Sea-ice transport of riverine particles from the Laptev Sea to Fram Strait based on clay mineral studies, *International Journal of Earth Sciences*, 89, 496–502, <https://doi.org/10.1007/s005310000109>, 2000.
- Eicken, H., Bluhm, B. A., Collins, R. E., Gradinger, R. R., Haas, C., Ingham, M., Mahoney, A., Nicolaus, M., and Perovich, D.: Field Techniques in Sea-Ice Research, in: *Cold Regions Science and Marine Technology*, in *Encyclopedia of Life Support Systems (EOLSS)*, edited by Shen, H., Auspices of the UNESCO, EOLSS Publisher, Paris, France, 2014.
- Ezraty, R., Girard-Ardhuin, F., Piolle, J.-F., Kaleschke, L., and Heygster, G.: Arctic and Antarctic Sea Ice Concentration and Arctic Sea Ice Drift Estimated from Special

- Sensor Microwave Data, Spatial and Physical Oceanography Laboratory IFREMER, Brest, France and University of Bremen, Germany, version 2.1 edn., 2007.
- Fukamachi, Y., Mizuta, G., Ohshima, K. I., Melling, H., Fissel, D., and Wakatsuchi, M.: Variability of sea-ice draft off Hokkaido in the Sea of Okhotsk revealed by a moored ice-profiling sonar in winter of 1999, *Geophysical Research Letters*, 30, <https://doi.org/10.1029/2002GL016197>, 2003.
- Fukamachi, Y., Simizu, D., Ohshima, K. I., Eicken, H., Mahoney, A. R., Iwamoto, K., Moriya, E., and Nihashi, S.: Sea-ice thickness in the coastal northeastern Chukchi Sea from moored ice-profiling sonar, *Journal of Glaciology*, 63, 888–898, <https://doi.org/10.1017/jog.2017.56>, 2017.
- German Arctic Office: Shipping in the Arctic, <https://www.arctic-office.de/en/publications/fact-sheets/>, URL https://www.arctic-office.de/fileadmin/user_upload/www.arctic-office.de/PDF_uploads/FactSheet_Shipping.pdf, 2019.
- Girard-Arduin, F. and Ezraty, R.: Enhanced Arctic Sea Ice Drift Estimation Merging Radiometer and Scatterometer Data, *IEEE Transactions on Geoscience and Remote Sensing*, 50, 2639–2648, <https://doi.org/10.1109/TGRS.2012.2184124>, 2012.
- Guerreiro, K., Fleury, S., Zakharova, E., Kouraev, A., Remy, F., and Maisongrande, P.: Comparison of CryoSat-2 and ENVISAT radar freeboard over Arctic sea ice: toward an improved ENVISAT freeboard retrieval, *The Cryosphere*, 11, 2059–2073, <https://doi.org/10.5194/tc-11-2059-2017>, 2017.
- Haas, C.: Evaluation of ship-based electromagnetic-inductive thickness measurements of summer sea-ice in the Bellinghausen and Amundsen Seas, Antarctica, *Cold Regions Science and Technology*, 27, 1–16, <https://doi.org/10013/epic.11731>, 1998.
- Haas, C.: Late-summer sea ice thickness variability in the Arctic Transpolar Drift 1991–2001 derived from ground-based electromagnetic sounding, *Geophysical Research Letters*, 31, <https://doi.org/10.1029/2003GL019394>, 2004.
- Haas, C.: Sea ice thickness distribution, in: *Sea ice*, edited by Thomas, D. N., chap. 2, pp. 42–64, John Wiley and Sons, Ltd, Third edn., <https://doi.org/10.1002/9781118778371>, 2017.
- Haas, C. and Druckenmiller, M.: Ice thickness and roughness measurements, in: *Field Techniques for Sea Ice Research*, edited by Eicken, H., pp. 49–116, University of Alaska Press., 2009.
- Haas, C., Gerland, S., Eicken, H., and Miller, H.: Comparison of sea-ice thickness measurements under summer and winter conditions in the Arctic using a small electromagnetic induction device, *Geophysics*, 62, 749–757, <https://doi.org/10013/epic.11729>, 1997.

- Haas, C., Pfaffling, A., Hendricks, S., Rabenstein, L., Etienne, J.-L., and Rigor, I. G.: Reduced ice thickness in Arctic Transpolar Drift favors rapid ice retreat, *Geophysical Research Letters*, 35, <https://doi.org/10.1029/2008GL034457>, 2008.
- Haas, C., Lobach, J., Hendricks, S., Rabenstein, L., and Pfaffling, A.: Helicopter-borne measurements of sea ice thickness, using a small and lightweight, digital EM system, *Journal of Applied Geophysics*, 67, 234–241, <https://doi.org/10.1016/j.jappgeo.2008.05.005>, 2009.
- Haas, C., Hendricks, S., Eicken, H., and Herber, A.: Synoptic airborne thickness surveys reveal state of Arctic sea ice cover, *Geophysical Research Letters*, 37, <https://doi.org/10.1029/2010GL042652>, 2010.
- Hakkinen, S., Proshutinsky, A., and Ashik, I.: Sea ice drift in the Arctic since the 1950s, *Geophysical Research Letters*, 35, <https://doi.org/10.1029/2008GL034791>, 2008.
- Hall, A.: The role of surface albedo feedback in climate, *Journal of Climate*, 17, 1550–1568, URL <https://escholarship.org/uc/item/0qd551rv>, 2004.
- Hansen, E., Gerland, S., Granskog, M. A., Pavlova, O., Renner, A. H. H., Haapala, J., Loyning, T. B., and Tschudi, M.: Thinning of Arctic sea ice observed on Fram Strait: 1990–2011, *Journal of Geophysical Research: Oceans*, 118, 5202–5221, <https://doi.org/10.1002/jgrc.20393>, 2013.
- Hansen, J., Ruedy, R., Sato, M., and Lo, K.: Global surface temperature change, *Review of Geophysics*, 48, <https://doi.org/10.1029/2010RG000345>, 2010.
- Hendricks, S.: Validierung von altimetrischen Meereisdickenmessungen mit einem helikopter-basierten elektromagnetischen Induktionsverfahren, PhD thesis, University of Bremen, <https://doi.org/10013/epic.33191.d001>, 2009.
- Hendricks, S. and Ricker, R.: C3S_312b_Lot3_CLS_2018SC2 – Product User Guide and Specification, Copernicus Climate Change Service, 2019a.
- Hendricks, S. and Ricker, R.: Product User Guide and Algorithm Specification: AWI CryoSat-2 Sea Ice Thickness (version 2.1), Alfred Wegener Institute, <https://doi.org/10013/epic.7dacf2fe-bead-4a1b-a266-c4fdd022877f>, 2019b.
- Hendricks, S., Paul, S., and Rinne, E.: ESA Sea Ice Climate Change Initiative (Sea_Ice_cci): Northern hemisphere sea ice thickness from the CryoSat-2 satellite on a monthly grid (L3C), v2.0 (Oct 2020)., DATA SET at Centre for Environmental Data Analysis: <http://dx.doi.org/10.5285/ff79d140824f42dd92b204b4f1e9e7c2>, 2018a.
- Hendricks, S., Paul, S., and Rinne, E.: ESA Sea Ice Climate Change Initiative (Sea_Ice_cci): Northern hemisphere sea ice thickness from CryoSat-2 on the satellite swath (L2P), v2.0., DATA SET at Centre for Environmental Data Analysis: <http://dx.doi.org/10.5285/5b6033bfb7f241e89132a83fdc3d5364>, 2018b.

- Hendricks, S., Paul, S., and Rinne, E.: ESA Sea Ice Climate Change Initiative (Sea_Ice_cci): Northern hemisphere sea ice thickness from the Envisat satellite on a monthly grid (L3C), v2.0 (Oct 2020)., DATA SET at Centre for Environmental Data Analysis: <http://dx.doi.org/10.5285/f4c34f4f0f1d4d0da06d771f6972f180>, 2018c.
- Hendricks, S., Paul, S., and Rinne, E.: ESA Sea Ice Climate Change Initiative (Sea_Ice_cci): Northern hemisphere sea ice thickness from Envisat on the satellite swath (L2P), v2.0., DATA SET at Centre for Environmental Data Analysis: <http://dx.doi.org/10.5285/54e2ee0803764b4e84c906da3f16d81b>, 2018d.
- Holland, M. M., Bitz, C. M., and Tremblay, B.: Future abrupt reductions in the summer Arctic sea ice, *Geophysical Research Letters*, 33, <https://doi.org/10.1029/2006GL028024>, 2006.
- Hunkeler, P., Hendricks, S., Hoppmann, M., Farquharson, C., Kalscheuer, T., Grab, M., Kaufmann, M. S., Rabenstein, L., and Gerdes, R.: Improved 1D inversions for sea ice thickness and conductivity from electromagnetic induction data: Inclusion of nonlinearities caused by passive bucking, *Geophysics*, 81, WA45–WA58, <https://doi.org/10.1190/GEO2015-0130.1>, 2016.
- Hunkeler, P. A., Hendricks, S., Hoppmann, M., Paul, S., and Gerdes, R.: Towards an estimation of sub-sea-ice platelet-layer volume with multi-frequency electromagnetic induction sounding, *Annals of Glaciology*, 56, <https://doi.org/10.3189/2015AoG69A705>, 2015.
- Hutchings, J. K.: Shipborne visual observations of Arctic sea ice, PANGAEA, <https://doi.org/10.1594/PANGAEA.889209>, 2018.
- Hyatt, J., Visbeck, M., Beardsley, R. C., and BrechnerOwens, W.: Estimating sea-ice coverage, draft, and velocity in Marguerite Bay (Antarctica) using a subsurface moored upward-looking acoustic Doppler current profiler (ADCP), *Deep-Sea Research II*, 55, 351–364, <https://doi.org/10.1016/j.dsr2.2007.11.004>, 2008.
- Itkin, P. and Krumpen, T.: Winter sea ice export from the Laptev Sea preconditions the local summer sea ice cover, *The Cryosphere*, 11, <https://doi.org/10.5194/tc-11-2383-2017>, 2017.
- Itkin, P., Spreen, G., Hvidegaard, S. M., Skourup, H., Wilkinson, J., Gerland, S., and Granskog, M.: Contribution of Deformation to Sea Ice Mass Balance: A Case Study From an N-ICE2015 Storm, *Geophysical Research Letters*, 45, 789–796, <https://doi.org/10.1002/2017GL076056>, 2018.
- Ivanov, V. V., Alexeev, V. A., Repina, I., Koldunov, N. V., and Smirnov, A.: Tracing Atlantic Water Signature in the Arctic Sea Ice Cover East of Svalbard, *Advances in Meteorology*, 2012, <https://doi.org/10.1155/2012/201818>, 2012.

- Jakobsson, M., Macnab, R., Mayer, L., Anderson, R., Edwards, M., Hatzky, J., Schenke, H. W., and Johnson, P.: An improved bathymetric portrayal of the Arctic Ocean: Implications for ocean modeling and geological, geophysical and oceanographic analyses, *Geophysical Research Letters*, 35, <https://doi.org/10.1029/2008GL033520>, 2008.
- Janout, M. A. and Lenn, Y.-D.: Semidiurnal Tides on the Laptev Sea Shelf with Implications for Shear and Vertical Mixing, *Journal of Physical Oceanography*, 44, 202–219, <https://doi.org/10.1175/JPO-D-12-0240.1>, 2014.
- Janout, M. A., Hoelemann, J., Waite, A. M., Krumpen, T., von Appen, W.-J., and Martynov, F.: Sea-ice retreat controls timing of summer plankton blooms in the Eastern Arctic Ocean, *Geophysical Research Letters*, 43, <https://doi.org/10.1002/2016GL071232>, 2016.
- JCGM: JCGM 100: Evaluation of measurement data - Guide to the expression of uncertainty in measurement (GUM1995), International Organization for Standardization, URL <https://www.iso.org/sites/JCGM/GUM/JCGM100/C045315e-html/C045315e.html?csnumber=50461>, 2008.
- Johannessen, O. M., Bengtsson, L., Miles, M. W., Kuzmina, S. I., Semenov, V. A., Alekseev, G. V., Nagurnyi, A. P., Zakharov, V. F., Bobylev, L. P., Pettersson, L. H., Hasselmann, K., and Cattle, H. P.: Arctic climate change: observed and modelled temperature and sea-ice variability, *Tellus A: Dynamic Meteorology and Oceanography*, 56, 328–341, <https://doi.org/10.3402/tellusa.v56i4.14418>, 2004.
- Jutila, A., King, J., Paden, J., Ricker, R., Hendricks, S., Polashenski, C., Helm, V., Binder, T., and Haas, C.: High-Resolution Snow Depth on Arctic Sea Ice From Low-Altitude Airborne Microwave Radar Data, in review at *IEEE Transactions on Geoscience and Remote Sensing*, 2020.
- Kaleschke, L., Maaß, N., Haas, C., Hendricks, S., Heygster, G., and Tonboe, R.: A sea-ice thickness retrieval model for 1.4 GHz radiometry and application to airborne measurements over low salinity sea-ice, *The Cryosphere*, 4, 583–592, <https://doi.org/10.5194/tc-4-583-2010>, 2010.
- Kaleschke, L., Tian-Kunze, X., Maaß, N., Mäkynen, M., and Drusch, M.: Sea ice thickness retrieval from SMOS brightness temperatures during the Arctic freeze-up period, *Geophysical Research Letters*, 39, <https://doi.org/10.1029/2012GL050916>, 2012.
- Kaleschke, L., Tian-Kunze, X., Maaß, N., Ricker, R., Hendricks, S., and Drusch, M.: Improved retrieval of sea ice thickness from SMOS and CryoSat-2, 2015 *IEEE International Geoscience and Remote Sensing Symposium (IGARSS)*, pp. 5232–5235, <https://doi.org/10.1109/IGARSS.2015.7327014>, 2015.
- Kanamitsu, M., Ebisuzaki, W., Woollen, J., Yang, S.-K., Hnilo, J. J., Fiorino, M., and Potter, G. L.: NCEP-DOE AMIP-II Reanalysis (R-2), *Bulletin of the American Meteorological Society*, 83, 1631–1643, <https://doi.org/10.1175/BAMS-83-11-1631>, 2002.

- Katlein, C., Arndt, S., Belter, H. J., Castellani, G., and Nicolaus, M.: Seasonal Evolution of Light Transmission Distributions Through Arctic Sea Ice, *Journal of Geophysical Research: Oceans*, 124, 5418–5435, <https://doi.org/10.1029/2018JC014833>, 2019.
- Keller, G. V. and Frischknecht, F. C.: *Electrical Methods in Geophysical Prospecting*, Pergamon Press, Oxford, 1966.
- Kern, M., Cullen, R., Berruti, B., Bouffard, J., Casal, T., Drinkwater, M. R., Gabriele, A., Lecuyot, A., Ludwig, M., Midthassel, R., Navas Traver, I., Parrinello, T., Ressler, G., Andersson, E., Martin-Puig, C., Andersen, O., Bartsch, A., Farrell, S., Fleury, S., Gascoin, S., Guillot, A., Humbert, A., Rinne, E., Shepherd, A., van den Broeke, M. R., and Yackel, J.: The Copernicus Polar Ice and Snow Topography Altimeter (CRISTAL) high-priority candidate mission, *The Cryosphere*, 14, 2235–2251, <https://doi.org/10.5194/tc-14-2235-2020>, 2020.
- Kern, S., Khvorostovsky, K., and Skourup, H.: D4.1 Product Validation and Intercomparison Report (PVIR-SIT) - SICCI-PVIR-SIT, Technical report, European Space Agency Sea Ice Climate Change Initiative, 2018.
- Kovacs, A. and Morey, R. M.: Sounding sea ice thickness using a portable electromagnetic induction instrument, *Geophysics*, 56, 1992–1998, <https://doi.org/10.1190/1.1443011>, 1991.
- Kovacs, A., Valleau, N. C., and Holladay, J. C.: Airborne electromagnetic sounding of sea-ice thickness and subice bathymetry, *Cold Regions Science and Technology*, 14, 289–311, URL <https://apps.dtic.mil/dtic/tr/fulltext/u2/a188939.pdf>, 1987.
- Krishfield, R. A. and Perovich, D. K.: Spatial and temporal variability of oceanic heat flux to the Arctic ice pack, *Journal of Geophysical Research*, 110, <https://doi.org/10.1029/2004JC002293>, 2005.
- Krishfield, R. A., Proshutinsky, A., Tateyama, K., Williams, W. J., Carmack, E. C., McLaughlin, F. A., and Timmermans, M.-L.: Deterioration of perennial sea ice in the Beaufort Gyre from 2003 to 2012 and its impact on the oceanic freshwater cycle, *Journal of Geophysical Research: Oceans*, 119, 1271–1305, <https://doi.org/10.1002/2013JC008999>, 2014.
- Krumpen, T.: TIFAX 2012 Summer Campaign - Sea ice thickness measurements with Polar 5 from Station Nord and Svalbard, Alfred Wegener Institute, <https://doi.org/10013/epic.6e9bb068-dd33-49ff-8b7b-6cc02ec201e7>, 2012.
- Krumpen, T.: AWI ICETrack: Antarctic and Arctic Sea Ice Monitoring and Tracking Tool, Technical report, Alfred Wegener Institute, <https://doi.org/10013/epic.51403>, 2017.
- Krumpen, T.: AWI ICETrack: Antarctic and Arctic Sea Ice Monitoring and Tracking Tool, Vers. 1.3, Technical report, Alfred Wegener Institute, <https://doi.org/10013/epic.9ee550b6-5966-4db6-a042-f4256810ec3f>, 2018.

- Krumpen, T. and Sellmann, M.: Campaign Report TIFAX 2016: Sea ice thickness measurements from Station Nord, Greenland, Alfred Wegener Institute, <https://doi.org/10013/epic.51537>, 2016.
- Krumpen, T. and Sokolov, V.: The Expedition AF122/1: Setting up the MOSAiC Distributed Network in October 2019 with Research Vessel AKADEMIK FEDOROV, *Berichte zur Polar-und Meeresforschung*, Alfred Wegener Institute for Polar and Marine Research, 744, 119, <https://doi.org/10013/epic.16bc0ab7-fe46-4fb5-ae69-3edc93a72356>, 2020.
- Krumpen, T., Gerdes, R., and Herber, A.: TIFAX 2011 Summer Campaign - Sea ice thickness measurements with Polar 5 from Station Nord and Svalbard, Alfred Wegener Institute, <https://doi.org/10013/epic.2165dad3-b55c-48c1-9c6d-ca9969391809>, 2011.
- Krumpen, T., Janout, M., Hodges, K. I., Gerdes, R., Girard-Arduin, F., Hoelemann, J., and Willmes, S.: Variability and trends in Laptev Sea ice outflow between 1992-2011, *The Cryosphere*, 7, 349–363, <https://doi.org/10.5194/tc-7-349-2013>, 2013.
- Krumpen, T., Gerdes, R., Haas, C., Hendricks, S., Herber, A., Selyuzhenok, V., Smedsrud, L., and Spreen, G.: Recent summer sea ice thickness surveys in Fram Strait and associated ice volume fluxes, *The Cryosphere*, 10, 523–534, <https://doi.org/10.5194/tc-10-523-2016>, 2016.
- Krumpen, T., Sellmann, M., and Rohde, J.: TIFAX 2017 Campaign Report: Sea ice thickness measurements with Polar 6 from Station Nord and Alert, Alfred Wegener Institute, <https://doi.org/10013/epic.51536>, 2017.
- Krumpen, T., Goessling, H., and Sellmann, M.: IceBird 2018 summer Campaign - Sea ice thickness measurements with Polar 6 from Station Nord and Alert, Alfred Wegener Institute, <https://doi.org/10013/epic.96923a78-d232-4bd8-82f4-337799d2fa07>, 2018.
- Krumpen, T., Belter, H. J., Boetius, A., Damm, E., Haas, C., Hendricks, S., Nicolaus, M., Noethig, E.-M., Paul, S., Peeken, I., Ricker, R., and Stein, R.: Arctic Warming interrupts the Transpolar Drift and affects long-range transport of sea ice and ice-rafted matter, *Nature Scientific Reports*, 9, <https://doi.org/10.1038/s41598-019-41456-y>, 2019.
- Krumpen, T., Birrien, F., Kauker, F., Rackow, T., v. Albedyll, L., Angelopoulos, M., Belter, H. J., Bessonov, V., Damm, E., Dethloff, K., Haapala, J., Haas, C., Hendricks, S., Hoelemann, J., Hoppmann, M., Kaleschke, L., Karcher, M., Kolabutin, N., Lenz, J., Morgenstern, A., Nicolaus, M., Nixdorf, U., Petrovsky, T., Rabe, B., Rabenstein, L., Rex, M., Ricker, R., Rohde, J., Shimanchuk, E., Singha, S., Smolyanitsky, V., Sokolov, V., Stanton, T., Timofeeva, A., and Tsamados, M.: The MOSAiC ice floe: sediment-laden survivor from the Siberian shelf, *The Cryosphere*, 14, 2173–2187, <https://doi.org/10.5194/tc-14-2173-2020>, 2020.
- Kurtz, N. T., Farrell, S. L., Studinger, M., Galin, N., Harbeck, J. P., Lindsay, R., Onana, V. D., Panzer, B., and Sonntag, J. G.: Sea ice thickness, freeboard, and snow

- depth products from Operation IceBridge airborne data, *The Cryosphere*, 7, 1035–1056, <https://doi.org/10.5194/tc-7-1035-2013>, 2013.
- Kurtz, N. T., Galin, N., and Studinger, M.: An improved CryoSat-2 sea ice freeboard retrieval algorithm through the use of waveform fitting, *The Cryosphere*, 8, 1217–1237, <https://doi.org/10.5194/tc-8-1217-2014>, 2014.
- Kwok, R.: Simulated effects of a snow layer on retrieval of CryoSat-2 sea ice freeboard, *Geophysical Research Letters*, 41, <https://doi.org/10.1002/2014GL060993>, 2014.
- Kwok, R.: Arctic sea ice thickness, volume, and multiyear ice coverage: losses and coupled variability (1958–2018), *Environmental Research Letters*, 13, <https://doi.org/10.1088/1748-9326/aae3ec>, 2018.
- Kwok, R. and Cunningham, G. F.: Variability of Arctic sea ice thickness and volume from CryoSat-2, *Philosophical Transactions of the Royal Society A*, 373, <https://doi.org/10.1098/rsta.2014.0157>, 2015.
- Kwok, R., and H. J. Zwally, G. F. C., and Yi, D.: Ice, Cloud, and land Elevation Satellite (ICESat) over Arctic sea ice: Retrieval of freeboard, *Journal of Geophysical Research: Oceans*, 112, <https://doi.org/10.1029/2006JC003978>, 2007.
- Kwok, R., Cunningham, G. F., Wensnahan, M., Rigor, I., Zwally, H. J., and Yi, D.: Thinning and volume loss of the Arctic Ocean sea ice cover: 2003–2008, *Journal of Geophysical Research: Oceans*, 114, <https://doi.org/10.1029/2009JC005312>, 2009.
- Kwok, R., Kurtz, N. T., Brucker, L., Ivanoff, A., Newman, T., Farrell, S. L., King, J., Howell, S., Webster, M. A., Paden, J., Leuschen, C., MacGregor, J. A., Richter-Menge, J., Harbeck, J., and Tschudi, M.: Intercomparison of snow depth retrievals over Arctic sea ice from radar data acquired by Operation IceBridge, *The Cryosphere*, 11, 2571–2593, <https://doi.org/10.5194/tc-11-2571-2017>, 2017.
- Larsen, J., Anisimov, O., Constable, A., Hollowed, A., Maynard, N., Prestrud, P., Prowse, T., and Stone, J.: Polar regions, in: *Climate Change 2014: Impacts, Adaptation, and Vulnerability. Part B: Regional Aspects. Contribution of Working Group II to the Fifth Assessment Report of the Intergovernmental Panel on Climate Change*, edited by Barros, V., Field, C., Dokken, D., Mastrandrea, M., Mach, K., Bilir, T., Chatterjee, M., Ebi, K., Estrada, Y., Genova, R., Girma, B., Kissel, E., Levy, A., MacCracken, S., Mastrandrea, P., and White, L., chap. 28, pp. 1567–1612, Cambridge University Press, Cambridge, United Kingdom and New York, NY, USA, 2014.
- Lavergne, T.: Validation and Monitoring of the OSI SAF Low Resolution Sea Ice Drift Product (v5), Technical report, The EUMETSAT Network of Satellite Application Facility, <https://doi.org/10.13140/RG.2.1.4155.5449>, 2016.
- Lavergne, T., Sorensen, A. M., Kern, S., Tonboe, R., Notz, D., Aaboe, S., Bell, L., Dybkjaer, G., Eastwood, S., Gabarro, C., Heygster, G., Killie, M. A., Kreiner, M. B., Lavelle, J., Saldo, R., Sandven, S., and Pedersen, L. T.: Version 2 of the EUMETSAT

- OSI SAF and ESA CCI sea-ice concentration climate data records, *The Cryosphere*, 13, 49–78, <https://doi.org/10.5194/tc-13-49-2019>, 2019.
- Laxon, S. W., Giles, K. A., Ridout, A. L., Wingham, D. J., Willatt, R., Cullen, R., Kwok, R., Schweiger, A., Zhang, J., Haas, C., Handricks, S., Krishfield, R., Kurz, N., Farrell, S., and Davidson, M.: CryoSat-2 estimates of Arctic sea ice thickness and volume, *Geophysical Research Letters*, 40, 732–737, <https://doi.org/10.1002/grl.50193>, 2013.
- Leppäranta, M.: *The Drift of Sea Ice*, Springer-Verlag, Berlin, Heidelberg, Germany, second edn., <https://doi.org/10.1007/978-3-642-4683-4>, 2011.
- Lin, L. and Zhao, J.: Estimation of Oceanic Heat Flux Under Sea Ice in the Arctic Ocean, *Journal of Ocean University of China*, 18, 605–614, <https://doi.org/10.1007/s11802-019-3877-7>, 2019.
- Markus, T., Stroeve, J. C., and Miller, J.: Recent changes in Arctic sea ice melt onset, freezeup, and melt season length, *Journal of Geophysical Research: Oceans*, 114, <https://doi.org/10.1029/2009JC005436>, 2009.
- Maykut, G. A.: Large-scale heat exchange and ice production in the central Arctic, *Journal of Geophysical Research*, 87, 7971–7984, <https://doi.org/10.1029/JC087iC10p07971>, 1982.
- Maykut, G. A. and McPhee, M. G.: Solar heating of the Arctic mixed layer, *Journal of Geophysical Research: Oceans*, 100, 24 691–24 703, <https://doi.org/10.1029/95JC02554>, 1995.
- Maykut, G. A. and Untersteiner, N.: Some results from a time-dependent thermodynamic model of sea ice, *Journal of Geophysical Research*, 76, <https://doi.org/10.1029/JC076i006p01550>, 1971.
- McPhee, M. G.: The sea ice-ocean boundary, in: *Sea Ice*, edited by Thomas, D. N., chap. 5, pp. 138–159, John Wiley and Sons, Ltd, Third edn., 2017.
- Meier, W. and Haas, C.: Changes in the physical state of sea ice, in: *Arctic Climate Issues 2011: Changes in Arctic Snow, Water, Ice and Permafrost. SWIPA 2011 Overview Report.*, chap. 9, Arctic Monitoring and Assessment Programme, Oslo, 2012.
- Melling, H. and Riedel, D. A.: The underside topography of sea ice over the continental shelf of the Beaufort Sea in the winter of 1990, *Journal of Geophysical Research*, 100, 13 641–13 653, <https://doi.org/10.1029/95JC00309>, 1995.
- Merkouriadi, I., Cheng, B., Graham, R. M., Rösel, A., and Granskog, M. A.: Critical Role of Snow on Sea Ice Growth in the Atlantic Sector of the Arctic Ocean, *Geophysical Research Letters*, 44, 10 479–10 485, <https://doi.org/10.1002/2017GL075494>, 2017.
- Multala, J., Hautaniemi, H., Oksama, M., Leppäranta, M., Haapala, J., Herlevi, A., Riska, K., and Lensu, M.: An airborne electromagnetic system on a fixed wing aircraft for sea ice thickness mapping, *Cold Regions Science and Technology*, 24, 355–373, [https://doi.org/10.1016/S0165-232X\(96\)00006-7](https://doi.org/10.1016/S0165-232X(96)00006-7), 1996.

- Nandan, V., Geldsetzer, T., Yackel, J., Mahmud, M., Scharien, R., Howell, S., King, J., Ricker, R., and Else, B.: Effect of Snow Salinity on CryoSat-2 Arctic First-Year Sea Ice Freeboard Measurements, *Geophysical Research Letters*, 44, 10 419–10 426, <https://doi.org/10.1002/2017GL074506>, 2017.
- Nansen, F.: *Fram over Polhavet, Den norske polarfærd 1893-1896*, Aschehoug, Kristiania, 1897.
- Nicolaus, M., Katlein, C., Maslanik, J., and Hendricks, S.: Changes in Arctic sea ice result in increasing light transmittance and absorption, *Geophysical Research Letters*, 39, <https://doi.org/10.1029/2012GL053738>, 2012.
- NPI: Thickness of sea ice measured in the Fram Strait. Environmental monitoring of Svalbard and Jan Mayen (MOSJ), Norwegian Polar Institute, URL <http://www.mosj.no/en/climate/ocean/sea-ice-thickness-arctic-ocean-fram-strait.html>, 2018.
- Onarheim, I. H., Smedsrud, L. H., Ingvaldsen, R. B., and Nilsen, F.: Loss of sea ice during winter north of Svalbard, *Tellus A: Dynamic Meteorology and Oceanography*, 66, <https://doi.org/10.3402/tellusa.v66.23933>, 2014.
- Onarheim, I. H., Eldevik, T., Smedsrud, L. H., and Stroeve, J. C.: Seasonal and Regional Manifestation of Arctic Sea Ice Loss, *Journal of Climate*, 31, 4917–4932, <https://doi.org/10.1175/JCLI-D-17-0427.1>, 2018.
- Overland, J., Dunlea, E., Box, J. E., Corell, R., Forsius, M., Kattsov, V., Olsen, M. S., Pawlak, J., Reiersen, L.-O., and Wang, M.: The urgency of Arctic change, *Polar Science*, 21, 6–13, <https://doi.org/10.1016/j.polar.2018.11.008>, 2019.
- Overland, J. E. and Wang, M.: When will the summer Arctic be nearly sea ice free?, *Geophysical Research Letters*, 40, 2097–2101, <https://doi.org/10.1002/grl.50316>, 2013.
- Parkinson, C. L., Cavalieri, D. J., Gloersen, P., Zwally, H. J., and Comiso, J. C.: Arctic sea ice extents, areas, and trends, 1978-1996, *Journal of Geophysical Research*, 104, 20 837–20 856, <https://doi.org/10.1029/1999JC900082>, 1999.
- Paul, S., Hendricks, S., Ricker, R., Kern, S., and Rinne, E.: Empirical parametrization of Envisat freeboard retrieval of Arctic and Antarctic sea ice based on CryoSat-2: progress in the ESA Climate Change Initiative, *The Cryosphere*, 12, 2437–2460, <https://doi.org/10.5194/tc-12-2437-2018>, 2018.
- Peeken, I., Primpke, S., Beyer, B., Guetermann, J., Katlein, C., Krumpfen, T., Bergmann, M., Hehemann, L., and Gerdt, G.: Arctic sea ice is an important temporal sink and means of transport for microplastic, *Nature Communications*, 9, <https://doi.org/10.1038/s41467-018-03825-5>, 2018.
- Perovich, D. K. and Richter-Menge, J. A.: Loss of Sea Ice in the Arctic, *The Annual Review of Marine Science*, pp. 417–441, <https://doi.org/10.1146/annurev.marine.010908.163805>, 2009.

- Perovich, D. K., Light, B., Eicken, H., Jones, K. F., Runciman, K., and Nghiem, S. V.: Increasing solar heating of the Arctic Ocean and adjacent seas, 1979-2005: Attribution and role in the ice-albedo feedback, *Geophysical Research Letters*, 34, <https://doi.org/10.1029/2007GL031480>, 2007.
- Petrich, C. and Eicken, H.: Overview of sea ice growth and properties, in: *Sea ice*, edited by Thomas, D. N., chap. 1, pp. 1–41, John Wiley and Sons, Ltd, Third edn., <https://doi.org/10.1002/9781118778371>, 2017.
- Petty, A. A., Kurtz, N. T., Kwok, R., Markus, T., and Neumann, T. A.: Winter Arctic Sea Ice Thickness From ICESAT-2 Freeboards, *Journal of Geophysical Research: Oceans*, 125, <https://doi.org/10.1029/2019JC015764>, 2020.
- Pfaffling, A., Haas, C., and Reid, J. E.: A direct helicopter EM sea ice thickness inversion, assessed with synthetic and field data, *Geophysics*, 72, <https://doi.org/10.1190/1.2732551>, 2007.
- Pfirman, S., Haxby, W., Eicken, H., Jeffries, M., and Bauch, D.: Drifting Arctic sea ice archives changes in ocean surface conditions, *Geophysical Research Letters*, 31, <https://doi.org/10.1029/2004GL020666>, 2004.
- Pinker, R. T., Niu, X., and Ma, Y.: Solar heating of the Arctic Ocean in the context of ice-albedo feedback, *Journal of Geophysical Research: Oceans*, 119, <https://doi.org/10.1002/2014JC010232>, 2014.
- Pithan, F. and Mauritsen, T.: Arctic amplification dominated by temperature feedbacks in contemporary climate models, *Nature Geoscience*, 7, 181–184, <https://doi.org/10.1038/ngeo2071>, 2014.
- Polyakov, I. V., Pnyushkov, A. V., Alkire, M. B., Ashik, I. M., Baumann, T. M., Carmack, E. C., Goszczko, I., Guthrie, J., Ivanov, V. V., Kanzow, T., Krishfield, R., Kwok, R., Sundfjord, A., Morison, J., Rember, R., and Yulin, A.: Greater role for Atlantic inflows on sea-ice loss in the Eurasian Basin of the Arctic Ocean, *Science*, 356, 285–291, <https://doi.org/10.1126/science.aai8204>, 2017.
- Polyakov, I. V., Rippeth, T. P., Fer, I., Alkire, M. B., Baumann, T. M., Carmack, E. C., Ingvaldsen, R., Ivanov, V. V., Janout, M., Padman, S. L. L., Pnyushkov, A. V., and Rember, R.: Weakening of Cold Halocline Layer Exposes Sea Ice to Oceanic Heat in the Eastern Arctic Ocean, *Journal of Climate*, 33, 8107–8123, <https://doi.org/10.1175/JCLI-D-19-0976.1>, 2020.
- Provost, C., Sennechael, N., Miguët, J., Itkin, P., Rösel, A., Koenig, Z., Villaceros-Robineau, N., and Granskog, M.: Observations of flooding and snow-ice formation in a thinner Arctic sea-ice regime during the N-ICE2015 campaign: Influence of basal melt and storms, *Journal of Geophysical Research: Oceans*, 122, 7115–7134, <https://doi.org/10.1002/2016JC012011>, 2017.

- Rabenstein, L., Hendricks, S., Martin, T., Pfaffhuber, A., and Haas, C.: Thickness and surface-properties of different sea-ice regimes within the Arctic Trans Polar Drift: Data from summers 2001, 2004 and 2007, *Journal of Geophysical Research*, 115, <https://doi.org/10.1029/2009JC005846>, 2010.
- Rahmstorf, S.: Thermohaline circulation: The current climate, *Nature*, 421, <https://doi.org/10.1038/421699a>, 2003.
- Rampal, P., Weiss, J., and Marsan, D.: Positive trend in the mean speed and deformation rate of Arctic sea ice, 1979-2007, *Journal of Geophysical Research*, 114, <https://doi.org/10.1029/2008JC005066>, 2009.
- Reimnitz, E., Dethleff, D., and Nuernberg, D.: Contrasts in Arctic shelf sea-ice regimes and some implications: Beaufort Sea versus Laptev Sea, *Marine Geology*, 119, 215–225, [https://doi.org/10.1016/0025-3227\(94\)90182-1](https://doi.org/10.1016/0025-3227(94)90182-1), 1994.
- Renner, A. H. H., Gerland, S., Haas, C., Spreen, G., Beckers, J. F., Hansen, E., Nicolaus, M., and Goodwin, H.: Evidence of Arctic sea ice thinning from direct observations, *Geophysical Research Letters*, 41, 5029–5036, <https://doi.org/10.1002/2014GL060369>, 2014.
- Ricker, R., Hendricks, S., Helm, V., Skourup, H., and Davidson, M.: Sensitivity of CryoSat-2 Arctic sea-ice freeboard and thickness on radar-waveform interpretation, *The Cryosphere*, 8, 1607–1622, <https://doi.org/10.5194/tc-8-1607-2014>, 2014.
- Ricker, R., Hendricks, S., Kaleschke, L., Tian-Kunze, X., King, J., and Haas, C.: A weekly Arctic sea-ice thickness data record from merged CryoSat-2 and SMOS satellite data, *The Cryosphere*, 11, 1607–1623, <https://doi.org/10.5194/tc-11-1607-2017>, 2017.
- Rigor, I. G. and Conoly, R. L.: Sea-ice production and transport of pollutants in the Laptev Sea, 1979-1993, *Science of The Total Environment*, 202, 89–110, [https://doi.org/10.1016/S0048-9697\(97\)00107-1](https://doi.org/10.1016/S0048-9697(97)00107-1), 1997.
- Rigor, I. G., Wallace, J. M., and Colony, R. L.: Response of Sea Ice to the Arctic Oscillation, *Journal of Climate*, 15, 2648–2663, [https://doi.org/10.1175/1520-0442\(2002\)015<2648:ROSITT>2.0.CO;2](https://doi.org/10.1175/1520-0442(2002)015<2648:ROSITT>2.0.CO;2), 2002.
- Ross, E., Clarke, M., Fissel, D. B., Chave, R. A. J., Johnston, P., Buermans, J., and Lemon, D.: Testing of Ice Profiler Sonar (IPS) Targets Using a Logarithmic Detector, ASL Environmental Science Inc., URL <https://aslenv.com/reports/IPS-Oceans-2016.pdf>, 2016.
- Rothrock, D. A. and Wensnahan, M.: The accuracy of sea ice drafts measured from U.S. Navy submarines, *Journal of Atmospheric and Oceanic Technology*, <https://doi.org/10.1175/JTECH2097.1>, 2007.
- Sallila, H., Farrell, S. L., McCurry, J., and Rinne, E.: Assessment of contemporary satellite sea ice thickness products for Arctic sea ice, *The Cryosphere*, 13, 1187–1213, <https://doi.org/10.5194/tc-13-1187-2019>, 2019.

- Screen, J. and Simmonds, I.: The central role of diminishing sea ice in recent Arctic temperature amplification, *Nature*, 464, 1334–1337, <https://doi.org/10.1038/nature09051>, 2010.
- Shcherbina, A. Y., Rudnick, D. L., and Talley, L. D.: Ice-Draft Profiling from Bottom-Mounted ADCP Data, *American Meteorological Society*, 22, 1249–1266, <https://doi.org/10.1175/JTECH1776.1>, 2005.
- Smedsrud, L. H., Esau, I., Ingvaldsen, R. B., Eldevik, T., Haugan, P. M., Li, C., Lien, V. S., Olsen, A., Omar, A. M., Ottera, O. H., Risebrobakken, B., Sandø, A. B., Semenov, V. A., and Sorokina, S. A.: The role of the Barents Sea in the Arctic climate system, *Review of Geophysics*, 51, 415–449, <https://doi.org/10.1002/rog.20017>, 2013.
- Spren, G. and Kern, S.: Methods of satellite remote sensing of sea ice, in: *Sea ice*, edited by Thomas, D. N., chap. 9, pp. 239–260, John Wiley and Sons, Ltd, Third edn., <https://doi.org/10.1002/9781118778371>, 2017.
- Spren, G., Kaleschke, L., and Heygster, G.: Sea ice remote sensing using AMSR-E 89 GHz channels, *Journal of Geophysical Research*, 113, <https://doi.org/10.1029/2005JC003384>, 2008.
- Spren, G., Kwok, R., and Menemenlis, D.: Trends in Arctic sea ice drift and role of wind forcing: 1992-2009, *Geophysical Research Letters*, 38, <https://doi.org/10.1029/2011GL048970>, 2011.
- Starkenbug, D., Metzger, S., Fochesatto, G. J., Alfieri, J. G., Gens, R., Prakash, A., and Cristobal, J.: Assessment of Despiking Methods for Turbulence Data in Micrometeorology, *Journal of Atmospheric and Oceanic Technology*, 33, 2001–2013, <https://doi.org/10.1175/JTECH-D-15-0154.1>, 2016.
- Stroeve, J. and Notz, D.: Changing state of Arctic sea ice across all seasons, *Environmental Research Letters*, 13, 103 001, <https://doi.org/10.1088/1748-9326/aade56>, 2018.
- Stroeve, J. C., Kattsov, V., Barrett, A., Pavlova, T., Holland, M., and Meier, W. N.: Trends in Arctic sea ice extent from CMIP5, CMIP3 and observations, *Geophysical Research Letters*, 39, <https://doi.org/10.1029/2012GL052676>, 2012.
- Sturm, M. and Holmgren, J.: An Automatic Snow Depth Probe for Field Validation Campaigns, *Water Resources Research*, 54, 9695–9701, <https://doi.org/10.1029/2018WR023559>, 2018.
- Sumata, H., Lavergne, T., Girard-Ardhuin, F., Kimura, N., Tschudi, M. A., Kauker, F., Karcher, M., and Gerdes, R.: An Intercomparison of Arctic ice drift products to deduce uncertainty estimates, *Journal of Geophysical Research: Oceans*, 119, 4887–4921, <https://doi.org/10.1002/2013JC009724>, 2014.
- Sumata, H., Kauker, F., Karcher, M., and Gerdes, R.: Simultaneous Parameter Optimization of an Arctic Sea Ice-Ocean Model by a Genetic Algorithm, *Monthly Weather Review*, 147, 1899–1926, <https://doi.org/10.1175/MWR-D-18-0360.1>, 2019.

- Teledyne RDI: Acoustic Doppler Current Profiler - Principles of Operation - A Practical Primer, Technical report, Teledyne RD Instruments, URL <http://www.comm-tec.com/Docs/Manuali/RDI/BBPRIME.pdf>, 2011.
- Teledyne RDI: WorkHorse - Sentinel, Monitor, Mariner Operation Manual, Teledyne RD Instruments, URL http://www.comm-tec.com/Docs/Manuali/RDI/WH_CG_Mar14.pdf, 2014.
- Thompson, D. W. J. and Wallace, J. M.: The Arctic oscillation signature in the wintertime geopotential height and temperature fields, *Geophysical Research Letters*, 25, 1297–1300, <https://doi.org/10.1029/98GL00950>, 1998.
- Thorndike, A. S.: A toy model linking atmospheric thermal radiation and sea ice growth, *Journal of Geophysical Research: Oceans*, 97, 9401–9410, <https://doi.org/10.1029/92JC00695>, 1992.
- Thorndike, A. S., Rothrock, D. A., Maykut, G. A., and Colony, R.: The thickness distribution of sea ice, *Journal of Geophysical Research*, 80, <https://doi.org/10.1029/JC080i033p04501>, 1975.
- Tian-Kunze, X., Kaleschke, L., Maass, N., Maekynen, M., Serra, N., Drusch, M., and Krumpfen, T.: SMOS-derived thin sea ice thickness: algorithm baseline, product specifications and initial verification, *The Cryosphere*, 8, 997–1018, <https://doi.org/10.5194/tc-8-997-2014>, 2014.
- Tilling, R. L., Ridout, A., and Shepherd, A.: Estimating Arctic sea ice thickness and volume using CryoSat-2 radar altimeter data, *Advances in Space Research*, 62, 1203–1225, <https://doi.org/10.1016/j.asr.2017.10.051>, 2018.
- Timokhov, L. A.: Regional characteristics of the Laptev and the East Siberian seas: climate, topography, ice phases, thermohaline regime, circulation, *Berichte zur Polarforschung*, 114, 15–32, URL <http://epic.awi.de/26322/1/BerPolarforsch1994144.pdf>, 1994.
- Tschudi, M., Meier, W. N., Stewart, J. S., Fowler, C., and Maslanik, J.: Polar Pathfinder Daily 25 km EASE-Grid Sea Ice Motion Vectors, Version 4., NASA National Snow and Ice Data Center Distributed Active Archive Center, <https://doi.org/10.5067/INAWUWO7QH7B>, 2019.
- Urrego-Blanco, J. R., Urban, N. M., Hunke, E. C., Turner, A. K., and Jeffery, N.: Uncertainty quantification and global sensitivity analysis of the Los Alamos sea ice model, *Journal of Geophysical Research: Oceans*, 121, 2709–2732, <https://doi.org/10.1002/2015JC011558>, 2016.
- Vihma, T., Tisler, P., and Uotila, P.: Atmospheric forcing on the drift of Arctic sea ice in 1989–2009, *Geophysical Research Letters*, 39, <https://doi.org/10.1029/2011GL050118>, 2012.

- Vinje, T. and Finnekasa, O.: The ice transport through Fram Strait, vol. 186, Norsk Polarinstitut Skrifter, URL <https://books.google.de/books?id=0dL5Y3IyGXEC>, 1986.
- Vinje, T., Nordlund, N., and Kvambekk, A.: Monitoring ice thickness in Fram Strait, *Journal of Geophysical Research*, 103, 10 437–10 449, <https://doi.org/10.1029/97JC03360>, 1998.
- Visbeck, M. and Fischer, J.: Sea Surface Conditions Remotely Sensed by Upward-looking ADCPs, *American Meteorological Society*, 12, 141–149, [https://doi.org/10.1175/1520-0426\(1995\)012<0141:SSCRSB>2.0.CO;2](https://doi.org/10.1175/1520-0426(1995)012<0141:SSCRSB>2.0.CO;2), 1995.
- von Albedyll, L., Haas, C., and Dierking, W.: Linking sea ice deformation to ice thickness redistribution using high-resolution satellite and airborne observations, <https://doi.org/10.5194/tc-2020-303>, in review, published as a preprint in *The Cryosphere Discussions*, 2020.
- Wang, M. and Overland, J. E.: A sea ice free summer Arctic within 30 years?, *Geophysical Research Letters*, 36, <https://doi.org/10.1029/2009GL037820>, 2009.
- Warren, S. G., Rigor, I. G., and Untersteiner, N.: Snow Depth on Arctic Sea Ice, *Journal of Climate*, 12, 1814–1829, [https://doi.org/10.1175/1520-0442\(1999\)012<1814:SDOASI>2.0.CO;2](https://doi.org/10.1175/1520-0442(1999)012<1814:SDOASI>2.0.CO;2), 1999.
- WHOI: Upward-Looking Sonar data at BGEF Moorings from 2003 through 2013, Woods Hole Oceanographic Institution, URL <https://www.whoi.edu/page/preview.do?pid=66559>, 2014.
- Wingham, D., Francis, C., Baker, S., Bouzinac, C., Brockley, D., Cullen, R., de Chateau-Thierry, P., Laxon, S., Mallow, U., Mavrocordatos, C., Phalippou, L., Ratier, G., Rey, L., Rostan, F., Viau, P., and Wallis, D.: CryoSat: A mission to determine the fluctuations in Earth’s land and marine ice fields, *Advances in Space Research*, 37, 841–871, <https://doi.org/10.1016/j.asr.2005.07.027>, 2006.
- Zhang, J., Rothrock, D., and Steele, M.: Recent Changes in Arctic Sea Ice: the Interplay between Ice Dynamics and Thermodynamics, *Journal of Climate*, 13, 3099–3114, [https://doi.org/10.1175/1520-0442\(2000\)013<3099:RCIASI>2.0.CO;2](https://doi.org/10.1175/1520-0442(2000)013<3099:RCIASI>2.0.CO;2), 2000.

Acknowledgements

First and foremost, I want to thank Thomas Krumpfen for being an outstanding supervisor and supporter throughout these last years. I have learned so much from you professionally, but also as a person. You have always treated me as an equal and gave me confidence when I needed it most. I could not have wished for a better supervisor! I will never forget it, thank you!

I am also thankful to Prof. Dr. Christian Haas, who took me on as his PhD student, agreed to be the first reviewer of my dissertation, and gave critical and constructive comments whenever they were needed. You also gave me the freedom to develop this project for myself, for which I am extremely grateful.

Prof. Dr. Torsten Kanzow is very much acknowledged for agreeing to be the second reviewer of this dissertation.

Thank you to the other members of my PhD committee: Stefan Hendricks, for answering so many of my questions, supporting me during the writing of papers, and ultimately letting me use your office for the final stages of the dissertation; and Markus Janout, for sharing your expertise on moorings and the eastern Arctic, and the great collaboration during the 2018 cruise to the Laptev Sea.

Special thanks to my colleagues and even more importantly my friends Jan Rohde, Robert Ricker, and Arttu Jutila for distracting me, proofreading my manuscripts (and most likely finding every single comma that was missing), for sharing offices and cabins, and most of all making this an extremely fun time.

A profound thank you to all my former and current colleagues. I would like to thank Luisa von Albedyll, Nicolas Le Paih, Niels Fuchs, Nele Lamping, Stefanie Arndt, Marcel Nicolaus, Stephan Paul, Anja Nicolaus, Damien Ringeisen, Philipp Anhaus, Verena Merk, Florent Birrien, Daniela Krampe, Julia Regnery, Christian Katlein, Ilkka Matero, Frank Kauker, Michael Karcher, Kathrin Riemann-Kampe, Martin Schiller, Dirk Kalmbach, and Lilian Schubert, in particular. I was extremely comfortable at AWI and I have you to thank for it!

I am thankful for the great people who supported the expeditions I was fortunate enough to join: the Russian ship and helicopter crews on RV Akademik Tryoshnikov, RV Akademik Fedorov, the flight crews of Polar 5 and 6, and the numerous people involved in the organisation and planning of these campaigns.

I am very grateful for the financial support and the great opportunities for further education provided by the POLMAR graduate school.

Thank you to the QUARCCS and CATS communities.

This dissertation was funded by the Federal Ministry for Education and Research and the AWI.

Lastly, I want to express my deepest gratitude to my family, especially to my three wonderful sisters, to Pia, and to Ines! Finally, my parents, this is for you! Thank you!

Hans JAKOB Belter

Curriculum Vitae

Klußmannstraße 3d
D-27570 Bremerhaven
☎ +49 471 4831-2840
✉ jakob.belter@awi.de

In Person

Nationality German
Date of Birth 03.04.1990
Place of Birth Halle/Saale, Germany

Education

Academic

since Sep 2017 **PhD Student**, *University of Bremen, Alfred Wegener Institute, Helmholtz Centre for Polar and Marine Research, Germany.*

Dissertation: "Observing sea ice thickness variability in the Laptev Sea and the implications for the Transpolar Drift system"

Member of POLMAR, *Helmholtz Graduate School for Polar and Marine Research.*

2014– 2017 **Master of Science**, *Climate Physics*,
Christian Albrechts University Kiel, Germany.
Exchange (Jan-Mar 2016), University Centre in Svalbard, Longyearbyen/Norway
Master thesis: "Impact of water properties on the vertical distribution of light under sea ice"

2010– 2014 **Bachelor of Science**, *Physics of the Earth System*,
Christian Albrechts University Kiel, Germany.
ERASMUS (Aug-Dec 2013), University Centre in Svalbard, Longyearbyen/Norway
Bachelor thesis: "A link between Arctic sea ice and surface air temperature variability over the northern continents: empirical and model analysis"

School

2000– 2008 **University Qualification**, *Elisabeth-Gymnasium, Halle/Saale, Germany.*

1996– 2000 **Elementary School**, *Talamt/Glauchau, Halle/Saale, Germany.*

Experience

Field Campaigns

2020 **Flight campaign to the Arctic Ocean**, *IceBird MOSAiC Summer*,
Research aircraft Polar 6.

Responsibilities: Co-PI, flight planning, airborne sea ice thickness surveys (EM-Bird), deployment of autonomous measurement systems.

2019 **Expedition to the Arctic Ocean**, *MOSAiC support (Leg 1a)*,
Research Vessel Akademik Fedorov.

Responsibilities: Deployment of autonomous measurement systems, ground-based snow depth and ice thickness surveys, sea ice observations.

2018 **Expedition to the Arctic Ocean, ARCTICA2018 (CATS/T-ICE/NABOS)**,
Research Vessel Akademik Tryoshnikov.

Responsibilities: Principle investigator 'Sea Ice Physics', deployment of autonomous measurement systems, ground-based snow depth and ice thickness surveys, sea ice observations, ice navigation support.

2015 **Expedition to the Arctic Ocean, PS92/ARK-29/1 (TRANSSIZ)**,
Research Vessel Polarstern.

Responsibilities: Research Assistant 'Sea Ice Physics', under-ice ROV operations, ground-based snow depth and ice thickness surveys, airborne sea ice thickness measurements, sea ice observations.

2013 **Expedition to Fram Strait, Arctic**, Research Vessel Haakon Mosby.

Responsibilities: Oceanographic measurements.

2012 **Expedition to the Baltic Sea, AL404**, Research Vessel F. S. Alkor.

Responsibilities: Geophysical measurements.

Vocational

Nov– Dec 2016 **Research Assistant, Alfred Wegener Institute, Helmholtz Centre for Polar and Marine Research**, Research Group: Sea Ice Physics, Bremerhaven.

Responsibilities: Remotely Operated Vehicle (ROV) data processing and software development

2011– 2013 **Research Assistant, Geomar Helmholtz Centre for Ocean Research**, FB2 Marine Biogeochemistry, Kiel.

Responsibilities: Sample preparation and chemical processing for U/Th dating in clean laboratory

2009– 2010 **Community Service,**

Sheltered work centre for persons with disabilities (HBW), Halle/Saale.

Responsibilities: Car service for the laundry facility

Internships

Sep– Oct 2014 **Alfred Wegener Institute, Helmholtz Centre for Polar and Marine Research**,
Research Group: Sea Ice Physics, Bremerhaven.

Responsibilities: Snow buoy data processing

Jul– Aug 2012 **ETH Zuerich, Work experience placement,**

Research Group: Trace Element and Micro Analysis, Zuerich.

Responsibilities: Laser Ablation-ICP-MS analysis of stalagmite SOP-20

Jul– Aug 2010 **GRS Gemresearch Swisslab AG**, Bangkok, Thailand.

Supervisor: Dr. Adolf Peretti

May 2010 **IFM Geomar Leibniz Institute of Marine Sciences**,
FB2 Marine Biogeochemistry, Kiel.

Apr 2007 **IFM Geomar Leibniz Institute of Marine Sciences**,
FB2 Marine Biogeochemistry, Kiel.

Jan 2006 **University Clinic Kroellwitz, Social Internship,**

Department for Vascular Surgery, Halle/Saale.

Education/Summer schools

2018 **ESA Advanced Training on Cryosphere Remote Sensing 2018**,
Longyearbyen, Norway.

2017 **Ice Profiling Sonar Processing Training**, ASL Environmental Sciences Inc., Saanichton, BC, Canada.

2004 **English summer school**, Bexhill on Sea, United Kingdom.

Skills

Computer

Scientific Advanced: MATLAB; Intermediate: ARCGIS; Basic: UNIX
Typography L^AT_EX, Microsoft Office
OS Linux/Unix, Windows, Mac OS X

Additional

2018 Sea Survival STCW A-VI/1-1, valid until 2023

2007 German drivers license (class B), international drivers license

Languages

German **Native**.

English **Fluent**, *speaking, reading, writing*, Certificate of Proficiency, European Level (CEFR): C2.

Publications

Peer-reviewed

2020 **Belter, H. J.**, T. Krumpfen, S. Hendricks, J. Hoelemann, M. A. Janout, R. Ricker and C. Haas, 2020. Satellite-based sea ice thickness changes in the Laptev Sea from 2002 to 2017: comparison to mooring observations. *The Cryosphere*, 14, 2189-2203, <https://doi.org/10.5194/tc-14-2189-2020>

Krumpfen, T., F. Birrien, F. Kauker, T. Rackow, L. von Albedyll, M. Angelopoulos, **H. J. Belter**, et al., 2020. The MOSAiC ice floe: sediment-laden survivor from the Siberian shelf. *The Cryosphere*, 14, 2173-2187, <https://doi.org/10.5194/tc-14-2173-2020>

2019 Krumpfen, T., **H. J. Belter**, A. Boetius, E. Damm, C. Haas, S. Hendricks, M. Nicolaus, E.-M. Noethig, S. Paul, I. Peeken, R. Ricker and R. Stein, 2019. Arctic warming interrupts the Transpolar Drift and affects long-range transport of sea ice and ice-rafted matter. *Scientific Reports*, 9, 5459, doi:10.1038/s41598-019-41456-y

Katlein, C., S. Arndt, **H. J. Belter**, G. Castellani and M. Nicolaus, 2019. Seasonal Evolution of Light Transmission Distributions Through Arctic Sea Ice. *Journal of Geophysical Research: Oceans*, 124, 5418-5435, <https://doi.org/10.1029/2018JC014833>

2017 Katlein, C., M. Schiller, **H. J. Belter**, V. Coppolaro, D. Wenslandt and M. Nicolaus, 2017: A New Remotely Operated Sensor Platform for Interdisciplinary Observations under Sea Ice. *Frontiers in Marine Science - Ocean Observation*, doi: 10.3389/fmars.2017.00281

In review

2020 **Belter, H. J.**, T. Krumpfen, M. A. Janout, E. Ross and C. Haas. Sea ice draft from upward-looking Acoustic Doppler Current Profilers: an adaptive approach, validated by Upward-Looking Sonar data. **In review** at *Cold Regions Science and Technology*

Belter, H. J., T. Krumpfen, L. von Albedyll, T. A. Alekseeva, S. V. Frolov, S. Hendricks, A. Herber, I. Polyakov, I. Raphael, R. Ricker, S. S. Serovetnikov, M. Webster and C. Haas. Interannual variability in Transpolar Drift ice thickness and potential impact of Atlantification. **Pre-print in review** at *The Cryosphere Discuss.*, <https://doi.org/10.5194/tc-2020-305>

Lei, R., M. Hoppmann, B. Cheng, G. Zuo, D. Gui, Q. Cai, **H. J. Belter** and W. Yang. Seasonal changes in sea ice kinematics and deformation in the Pacific Sector of the Arctic Ocean in 2018/2019. **Pre-print in review** at *The Cryosphere Discuss.*, <https://doi.org/10.5194/tc-2020-211>

Conferences and Workshops

2019 Krumpfen, T., **H. J. Belter**, A. Boetius, E. Damm, C. Haas, S. Hendricks, M. Nicolaus, E.-M. Noethig, S. Paul, I. Peeken, R. Ricker and R. Stein, 2019. Arctic warming interrupts the Transpolar Drift and affects long-range transport of sea ice and ice-rafted matter. *IGS Sea Ice Symposium, Winnipeg. Talk*

Belter, H. J., T. Krumpfen, M. A. Janout, R. Ricker, S. Hendricks and C. Haas, 2019: 13 years of sea ice draft observations in the Laptev Sea from moored ADCPs and Upward-Looking Sonar: changes, variability and comparison to Earth Observation data. *IGS Sea Ice Symposium, Winnipeg. Poster*

2018 **Belter, H. J.**, T. Krumpfen, R. Ricker, S. Hendricks, S. Paul, M. Janout, E. Ross and C. Haas, 2018: A new time series of sonar-based sea ice draft records from the Siberian Shelf. *POLAR 2018 SCAR/IASC Open Science Conference, Davos. Talk*

Statement/Erklärung

I hereby declare that I have written this dissertation on my own and that I have used no other than the properly cited and mentioned sources and aids.
Finally, I affirm that I have never written a dissertation before and that this work has not been submitted anywhere else.

Hiermit erkläre ich, dass ich diese Doktorarbeit selbstständig und nur mit Hilfe der hier deutlich gekennzeichneten Referenzen und Hilfsmittel angefertigt habe.
Weiter bestätige ich, dass ich mich bisher keinem anderen Promotionsverfahren unterzogen habe und dass ich diese Arbeit noch nicht für einen Abschluss an anderer Stelle eingereicht habe.



Bremerhaven, November 17, 2020

Hans JAKOB Belter